International Ocean Atlas and Information Series, Volume 14

NOAA Atlas NESDIS 78

doi:10.7289/V5Q52MK5

Atlas of Climatic Changes in Nine Large Marine Ecosystems of the Northern Hemisphere (1827-2013)

Silver Spring, MD
December 2014

U.S. DEPARTMENT OF COMMERCE
National Oceanic and Atmospheric Administration
National Environmental Satellite, Data, and Information Service

National Oceanographic Data Center

Additional copies of this publication, as well as information about NODC data holdings and services, are available upon request directly from NODC.

National Oceanographic Data Center User Services Team
NOAA/NESDIS E/OC1
SSMC-3, 4th Floor
1315 East-West Highway
Silver Spring, MD 20910-3282

Telephone: (301) 713-3277

Fax: (301) 713-3300

E-mail: nodc.services@noaa.gov

NODC home page: http://www.nodc.noaa.gov/

This publication should be cited as:
Matishov, G.G., Berdnikov, S.V., Zhichkin, A.P., Dzhenyuk, S.L., Smolyar, I.V., Kulygin, V.V., Yaitskaya, N.A., Povazhniy, V.V., Sheverdyaev, I.V., Kumpan, S.V., Tret'yakova, I.A., Tsygankova, A.E., D'yakov, N.N., Fomin, V.V., Klochkov, D.N., Shatohin B. M., Plotnikov, V.V., Vakul'skaya, N.M., Luchin, V.A., Kruts, A.A. (2014). Atlas of Climatic Changes in Nine Large Marine Ecosystems of the Northern Hemisphere (1827-2013). Matishov, G.G., Sherman, K., Levitus, S. (Eds.), NOAA Atlas NESDIS 78, 131 pp. doi:10.7289/V5Q52MK5

The present work is implemented within the framework of:

- "Global Oceanographic Data Archaeology and Rescue" (GODAR) and "World Ocean Database" projects endorsed by the Intergovernmental Oceanographic Commission (IOC) UNESCO

- Memorandum of Understanding between the National Oceanic and Atmospheric Administration of the Department of Commerce of the United States of America and the Russian Academy of Sciences of the Russian Federation on Cooperation in the Area of the World Oceans and Polar Regions.

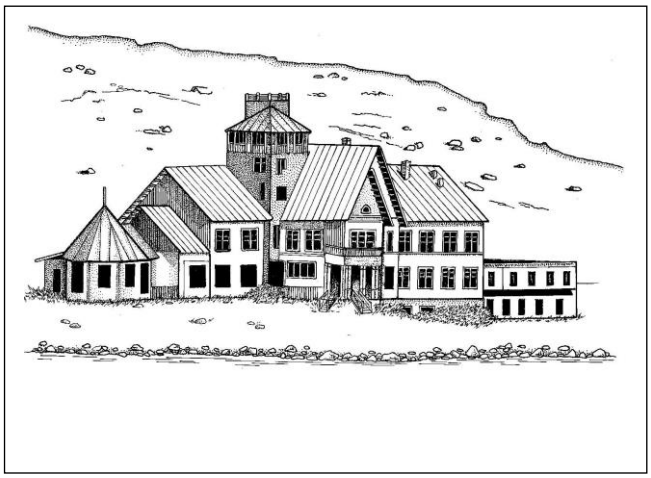

Main building, Biological Station of the Barents Sea. *Artist T. Chernenko.*

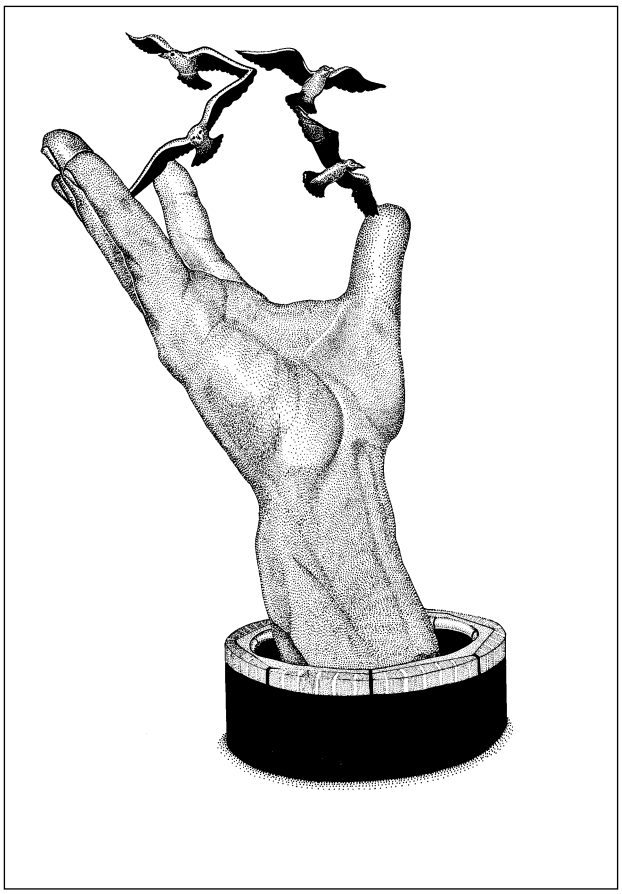

Sculpture outside the National Oceanic and Atmospheric Administration building, Silver Spring, Maryland. *Artist T. Chernenko.*

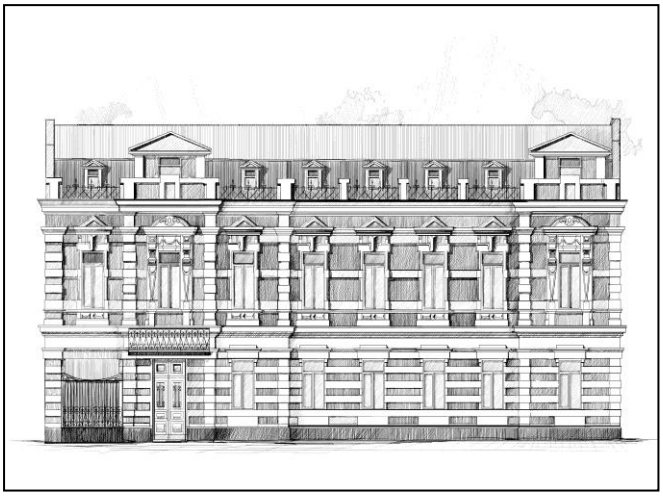

Headquarters of the South Scientific Center, Rostov-Don, Russia. *Artist Y. Yakavleva.*

Abstract

The present Atlas of nine Large Marine Ecosystems (LMEs) is a result of long-term international co-operation of the scientists from Russia, Ukraine, and the USA within the frameworks of national research programmes, focusing on climate change, and international data management projects (GODAR UNESCO and IOC UNESCO).

The Atlas encompasses LMEs of the Eastern Arctic Seas: Barents Sea LME (including the White Sea subarea), Kara Sea LME, Laptev Sea LME, East Siberian Sea LME, Chukchi Sea LME, Western and Eastern Bering Sea LMEs - and LME of the southern European Russian Seas: the Black Sea LME (including the Sea of Azov subarea) and the Caspian Sea LME, and contains the primary oceanographic data, covering the period of 1827 to 2013, and is accessible at the NODC/NOAA webpage.

Apart from the primary oceanographic data, the Atlas contains the results of processing to trace and determine the climatic variability of hydrological processes in the Arctic and in the southern region, seasonal climatic charts of vertical distribution of water temperature and salinity for the key hydrological transects in the Barents Sea, Black Sea, Sea of Azov, and Caspian Sea, as well as time series of water temperature and salinity anomalies for every month of each year or for a specified period.

The Atlas presents long-term data on the ice conditions of the Barents Sea LME and charts of fishery dynamics, information about long-term variability of ice conditions of the Barents, Bering, Caspian Seas LMEs, and Sea of Azov subarea.

DATABASE

Region 1. Eastern Arctic Seas LMEs

(Large Marine Ecosystems (LMEs) of the Eastern Arctic)
Time period: 1827-2013
Total number of stations: 418,916
Total number of plankton samples: 5,471

Barents Sea LME and the White Sea subarea:	238,286 stations (1870-2013)
Kara Sea LME:	38,445 stations (1870-2013)
Laptev Sea LME:	6,570 stations (1878-2009)
East Siberian Sea LME:	3,459 stations (1878-2008)
Chukchi Sea LME:	50,858 stations (1849-2012)
East and West Bering Sea LME:	81,298 stations (1827-2012)

Region 2. Black Sea, Sea of Azov subarea, and Caspian Sea LMEs

(Large Marine Ecosystems (LMEs) of the Black Sea (including the Sea of Azov subarea), and the Caspian Sea)
Time period: 1884-2012
Total number of stations: 196,778
Total number of plankton samples: 1,411

Black Sea LME:	86,836 stations (1884-2012)
Sea of Azov subarea:	66,609 stations (1891-2012)
Caspian Sea LME:	43,333 stations (1897-2011)

The Atlas and associated data are for international distribution without restriction in accordance with the principles of the World Data Center System of the International Council of Scientific Unions and the UNESCO Intergovernmental Oceanographic Commission.

Editors and Authors (by organization)

Matishov, G.G., Academician, Chairperson of the Southern Scientific Centre of the Russian Academy of Sciences (Rostov-on-Don, Russia), Director of Murmansk Marine Biological Institute of the Kola Scientific Centre of the Russian Academy of Sciences, Murmansk, Russia.

Sherman, K., Director NOAA's Large Marine Ecosystem Program Northeast Fisheries Science Center, Narragansett Laboratory, Narragansett, Rhode Island, USA

Levitus, S., former Director, World Ocean Data Center, Silver Spring and Director, Ocean Climate Laboratory NODC/NOAA, Silver Spring, USA. Currently at Department of Atmospheric and Oceanic Science, University of Maryland, College Park, MD, USA.

Smolyar, I.V. , Ocean Climate Laboratory NODC/NOAA, Silver Spring, USA.

Berdnikov, S.V., Povazhniy, V.V., Sheverdyaev, I.V., Tsygankova, A.E, Southern Scientific Centre of the Russian Academy of Sciences, Rostov-Don, Russia.

Kulygin, V.V., Yaitskaya, N.A., Kumpan, S.V., Tret'yakova, I.A., Institute of Arid Zones of the Southern Scientific Centre of the Russian Academy of Sciences, Rostov-Don, Russia.

Dzhenyuk, S.L., Zhichkin, A.P., Murmansk Marine Biological Institute of the Kola Scientific Centre of the Russian Academy of Sciences, Murmansk, Russia.

D'yakov, N.N., Fomin, V.V., Marine Department of the Ukrainian Hydro-Meteorological Research Institute of the Ministry of Emergency Situations and the National Academy of Sciences of Ukraine, Sevastopol, Ukraine.

Klochkov, D.N., Shatohin B. N. Scientific and Industrial Company *Morskaya Informatika*, Murmansk, Russia

Plotnikov, V.V., Vakul'skaya, N.M., Luchin, V.A., **V., I Il'ichev** Pacific Oceanological Institute of the Far Eastern Branch of the Russian Academy of Sciences, Vladivostok, Russia.

Kruts, A.K., Far Eastern Regional Hydro-Meteorological Research Institute, Vladivostok, Russia.

Preface

Large Marine Ecosystems (LMEs) are regions of ocean space of 200,000 km^2 or greater that encompass coastal waters from river basins and estuaries seaward to the break or slope of the continental shelf, or the leading ocean frontal boundary of principal coastal currents. LMEs are defined by ecological criteria including bathymetry, hydrography, marine productivity, and trophically linked populations. LMEs annually produce 80 percent of the World's marine fish catch. They are at present under stress from overfishing, pollution, nutrient over-enrichment, acidification, climate change, and loss of biodiversity and important habitat areas. These stressors are impacting sustainable development of an estimated 12 trillion dollars in goods and services contributed annually by LMEs to the global economy.

Since the mid-1990s, LMEs have been designated by a growing number of coastal countries in Africa, Asia, Latin America and Eastern Europe as place-based assessment and management areas for introducing an ecosystem-based approach to recover, develop, and sustain marine resources. The LME approach to the assessment and management of marine resources is based on the operationalization of five modules, with suites of indicators for monitoring and assessing changing conditions in ecosystem productivity, fish and fisheries, pollution and ecosystem health, socioeconomics, and governance. The approach is part of an emerging effort by the scientific community to relate the scale of place-based ecosystem assessment and management of marine resources to policy making, and to tighten the linkages among basic science and applied science, and the management of ocean resources within the natural boundaries of LMEs.

During the present period of climate change and the variable responses of marine populations from marine plankton to fish, marine mammals and sea birds to the effects of accelerated warming reported in the world's LMEs, scientists of Russian Academy of Sciences Southern Scientific Center, Institute of Arctic Zones (SSC-RAS) and the Murmansk Marine Biological Institute (KSC-RAS) have joined with scientists of the National Oceanic and Atmospheric Administration, National Oceanographic Data Center and National Marine Fisheries Service in providing an extraordinary atlas of key biological and physical time series data spanning 186 years from 1827 to 2013.

The Atlas provides an exceptionally long record of biological and physical time-series data and indices extracted from archival sources in Russia, Ukraine, and the United States. Included in the Atlas are time-series for the eastern Arctic Seas LMEs, including the Barents Sea LME (and the White Sea subarea), Kara Sea, Laptev Sea, East Siberian Sea, Chukchi Sea, and the West Bering Sea and East Bering Sea LMEs. Included also are time-series for the Black Sea (and the Sea of Azov subarea) and the Caspian Sea LMEs.

Given that climate change is occurring throughout the northern hemisphere, the Atlas of Climate Change in 9 Large Marine Ecosystems of the Northern Hemisphere (1827-2013) should prove to be most welcome and timely to those natural and social scientists and marine resource managers supporting the global movement toward sustainable development of the world's LMEs.

Kenneth Sherman, Director
NOAA's Large Marine Ecosystem Program
Northeast Fisheries Science Center,
Narragansett Laboratory,
Narragansett, Rhode Island, USA

Acknowledgements

The present publication has been implemented by employees of the Russian Academy of Sciences jointly with colleagues from the Ocean Climate Laboratory of the National Oceanographic Data Centre NOAA (USA), Programmes of Basic Research of the Presidium of the Russian Academy of Sciences «Basic Problems of Poly-Ethnic Macro-Region Modernization under the Conditions of Tension Growth» and «Basic Problems of Oceanology: Physics, Geology, Biology, and Ecology», of the Department of Earth Sciences of the Russian Academy of Sciences «Geographical Grounds for Sustainable Development of the Russian Federation and its Regions», Federal Targeted Programme of Russia «The World Ocean».

Due to the support from the UNESCO Intergovernmental Oceanographic Commission (IOC UNESCO), the GODAR Project (Global Oceanographic Data Archaeology and Rescue) and the World Ocean Database Project, vast data material has been rescued.

Significant help when searching for and obtaining the books, papers, graphic material, containing the primary oceanographic data, was provided by the employees of the NOAA Central Library, as well as of the libraries of Rostov-on-Don (Sharapova, T.A., Kolesnikova, E.M., Men'shikh, O.A., Bondarenko, S.A.).

We are grateful to the employees of the IAZ SSC RAS (Matishov, D.G., Arkhipova, O.E., Dashkevich, L.V., Likhtanskaya, N.V., and Sorokina, V.V.), of the MMBI KSC RAS (Makarevich, P.R., Moiseev, D.V.), of the Marine Department of UkrNIGMI (Levitskaya, O.V., Fomina, I.N., Timoshenko, T.Yu, and Martynova, E.S.) for their assistance when developing the database.

Considerable assistance, when searching for and comparing the historical navigational charts of the Northern Bering Sea, was provided by the NOAA employees: from the National Geodetic Survey - J. Blackwell, Director, M. Aslaksen, Chief of Staff, D. Graham, cartographer, I. Blat, cartographer; from the National Ocean Service/Office of Coast Survey – M. Westington, geographer; from the Central Library - J. Cloud, Ph.D.

Our special gratitude goes to the employees of SSC RAS and IAZ SSC RAS (Aleshina, N.V., Aleshina, E.G., Aksenov, D.S., Vikrishchuk, A.V., Verbitskiy, R.E., Glushchenko, G.Yu., Grigorenko, K.S., Eliseeva, O.I., Ermolov, V.V., Ermolaeva, E.V., Ivanov, V.A., Kovaleva, G.V., Kreneva, K.V., Luzhnyak, O.L., Oleinikov, E.P., Ponomarenko, E.P., Saprygin, V.V., Soier, V.G., Filatova, T.B., Shishkina, A.V., Yasakova, O.N.) and of MMBI KSC RAS (Berchenko, I.V., Deryabin, A.A., Dvoretskiy, V.G., Druzhkova, E.I., Kuznetsov, A.V., Oleinik, A.A., Shumilov, A.A.), who collected the primary data in marine expeditions and cruises and at hydrochemical and biological laboratories in 2000-2013.

We are also grateful to the Head of the Department of Rosgidromet (The Federal Service of Russia for Hydrometeorology and Monitoring of the Environment) in the Southern Federal District and Northern Caucasus Federal District of Russia Bazelyuk, A.A. for the possibility provided to get acquainted with the historical data on the ice conditions of the Sea of Azov LME and the Caspian Sea LME.

We express our gratitude to Roman Mikhalyuk for his help with Russian-English translation.

Contents

Introduction

The late 20th century to the early 21st century is characterized as an epoch of global climatic change affecting diverse aspects of human activity in many countries. With this in mind and under such conditions, conclusions on the trends of climate change are important both from the scientific and practical points of view. Climate change forecasts are a significant element of economic infrastructure development and planning. Climate change is significant for countries that have access to the seas since the coastal areas are distinguished by highly developed economic infrastructure. These coastal areas are sensitive and subject to extreme weather and climatic phenomena.

Climate change studies require international cooperation in terms of environmental data collection and analysis. Understanding the mechanisms of climate change and modeling prognoses at various spatial and temporal scales are the focus of these data collection and analyses efforts. The objective of this Atlas was to unite the efforts of specialists from Russia, United States, and Ukraine to form and develop an oceanographic database. The goal was to create a database that is accessible and openly available to the international community. In so doing, climatic changes over vast marine areas of the Northern Hemisphere can be documented.

The Atlas covers nine Large Marine Ecosystems (LME) of the Barents Sea LME (and the White Sea subarea), Kara Sea LME, Laptev Sea LME, East Siberian Sea LME, Chukchi Sea LME, and the Bering Sea (both East and West LMEs) in the north and the Black Sea LME, the Sea of Azov subarea, and Caspian Sea LME in the south.

Apart from the primary oceanographic data, this Atlas contains the results of data collection on climatic variability of hydrological processes in the Arctic and in the Caspian Sea LME and Sea of Azov subarea and Black Seas LME. Vertical mean climatic distributions of salinity and water temperature have been constructed for the hydrological transects of the Barents Sea LME, Black Sea LME, Sea of Azov subarea, and the Caspian Sea LME by month of each year. Anomalies were also recorded during the same time period.

Long-term data on the Barents Sea LME ice conditions, fishery charts, variability of ice conditions in the Sea of Azov subarea and the Caspian Sea LME are presented for the first time.

The cooperation between specialists from Russia (SSC RAS in Rostov-on-Don) and Ukraine (Marine Department of the UkrNIGMI in Sevastopol) resulted in the significant enlargement of the Sea of Azov database (up to 67,000 sea stations).

The Atlas contains observations made by expeditions in 2001-2013 by MMBI KSC RAS (1,290 stations in the Barents and Kara Seas LMEs) and SSC RAS (7,169 stations in the Sea of Azov subarea, Black Sea LME, and the Caspian Sea LME).

A total of 863 stations have been added to the Barents Sea plankton database. The Sea of Azov plankton database (1,411 samples) has become a component of the Atlas for the first time.

The first chapter contains general oceanographic characteristics, key references, discussions on data storage, procedures of quality control for historical and contemporary data, and the methodology.

The second and third chapters give descriptions of the databases for the Arctic and Southern Regions, respectively. Specific features of station distributions are considered for each sea (presented in the database). Samples of construction of time series of water temperature and salinity, ice conditions, and fishery are given for the Barents Sea LME and the southern seas. In the case of the East and West Bering Sea LMEs, ice conditions for the period 1960-2012, interannual variability for the period 1955-2012, and assessments of changes of the coastline based on the comparison of navigation charts are considered.

1. Oceanographic database

1.1. Data sources

The data for the present Atlas come from the following main sources:

- Climatic Atlases, published by NOAA (Matishov et al. 1998, Matishov et al. 2000, Matishov et al. 2004, Matishov et al. 2006, Matishov et al. 2008, Luchin et al. 2010).

- Database of the National Oceanographic Data Center and the World Data Center for Oceanography, Silver Spring, NOAA, USA (http://www.nodc.noaa.gov/OC5/WOD/pr_wod.html);

- Database of the Unified (Russian) State System of Information about the Situation in the World Ocean (ESIMO), http://data.oceaninfo.ru.

Part of the data for the period of 2001-2013 was obtained from the cruise reports of SSC RAS and MMBI KSC RAS.

Materials and data used in climate change studies in large marine ecosystems for the last 140 years were registered in the libraries of the Norwegian Polar Institute (Tromsø, Norway), Dartmouth College (Hanover, USA), University of Alaska Fairbanks (Fairbanks, USA), Museum of Natural History (New York, USA), Russian Academy of Sciences (Saint-Petersburg, Russia), as well as public libraries of Murmansk, Rostov-on-Don, Moscow, and Saint-Petersburg.

Historical data on the ice conditions of the Sea of Azov subarea and the Caspian Sea LME were provided by the Department of Rosgidromet (Federal Service of Russia for Hydrometeorology and Monitoring of the Environment) in the Southern Federal District and Northern Caucasus Federal District of Russia; the observations by SSC RAS specialists in the Don Delta were also used.

The ice charts of the National Snow and Ice Data Center (USA) (http://nsidc.org) for 1977-1996 and the general ice charts of the Arctic Ocean from the Ice Centre (The Centre of Ice and Hydrometeorological Information) of the Arctic and Antarctic Research Institute (AARI) (Russia) (http://www.aari.ru) for 1997-2010 are the data sources for the Barents Sea LME ice conditions.

The primary data on Russian fisheries in the Barents Sea LME for the period of 1985 to 2010 were provided by employees of the Scientific and Industrial Company «Morskaya Informatika (Marine Informatics)» (Murmansk, Russia).

1.2. Data formats

The NODC "WODselect csv format", accepted at NOAA, with a comma used as a separator, is used for the presentation of primary data in the electronic version. The reading of data in this format does not require any specialized software.

The format is composed of fields (sections) entitled the **GENERAL FIELDS** presented in Table 1.1. Every station starts with the key word **CAST** in the first column and its description is divided into several fields (sections). Below the description of the main fields (sections) such as **CAST, METADATA, BIOLOGY METADATA, VARIABLES,** and **BIOLOGY** is given (see Tables 1.2-1.4)**.**

A more detailed description is provided at the NODC website: http://www.nodc.noaa.gov/OC5/SELECT/dbsearch/csv_info.html. Special codes are used in the tables, which are also presented at the website: http://www.nodc.noaa.gov/OC5/WOD13/wod_codes.html.

Table 1.1. General fields:

Starting Indicator	Ending Indicator	Content
CAST	next section start	Station position, date, and cruise identification
METADATA	next section start	Country, NODC accession#, ship/platform, project, institution, meteorology, and other measurement related information
VARIABLES	END OF VARIABLES SECTION	Profile measurements (if present)
BIOLOGY METADATA	BIOLOGY	Plankton sampling information (if present)
BIOLOGY	END OF BIOLOGY SECTION	Plankton measurements (if present)

Table 1.2. Cast / metadata / biology metadata:

Column #1	Column #2	Column #3	Column #4	Column #5
KEY WORD	Specific measured variable (empty if general metadata)	Value	Units or code type	Text description

Example: "CAST" section

CAST		7550947	WOD Unique Station	WOD code
NODC Cruise ID		GE_9629		NODC code
Latitude		-11.3338	Decimal degrees	

Example: "METADATA" section

Country		GE	ISO code	GERMANY
Ship/platform		7977	WOD code	METEOR

Dataset	Temperature	4	WOD code	CTD: TYPE UNKNOWN

Example: "BIOLOGY METADATA" section

Water_volume		23.4	m^3(cubic meters)	
Mesh_size		54	um (micrometers)	
Gear_code		101	WOD code	

Table 1.3. Variables (profile data):
F - individual level WOD flag O - individual level originator's flag

VARIABLE	**Depth**	**F**	**O**	**Variable 1**	**F**	**O**	**...**	**Variable n_v**	**F**	**O**
UNITS	m			variable 1 units			...	variable n_v units		
Prof-Flag (entire profile)		(WOD code)			(WOD code)		...		(WOD code)	
depth level 1	orig. depth value at level 1	depth WOD flag at level 1	depth origs. flag at level 1	variable 1 value at level 1	variable 1 WOD flag at level 1	variable 1 origs. flag at level 1	...	variable $n_v$value at level 1	variable n_vWOD flag at level 1	variable n_v origs. flag at level 1
depth level 2	orig. depth value at level 2	depth WOD flag atlevel 2	depth origs. flag at level 2	variable 1 value at level 2	variable 1 WOD flag at level 2	variable 1 origs. flag at level 2	...	variable $n_v$value at level 2	variable n_v WOD flag at level 2	variable n_v origs. flag at level 2
...	...	...	...	...	...	...	...	...	...	...
depth level n_z	orig. depth value at level n_z	depth WOD flag at level n_z	depth origs. flag at level n_z	variable 1 value at level n_z	variable 1WOD flag at level n_z	variable 1 origs. Flag at level n_z	...	variable n_v value at level n_z	variable n_v WOD flag at level n_z	variable n_v origs. flag at level n_z
Example: "VARIABLES" section										
VARIABLES	Depth	F	O	Temperature	F	O	...	Oxygen	F	O
UNITS	m			degrees C			...	ml/l		
Prof-Flag		0			0		...		0	2
1	12.23	0	2	25.4467	0	2	...	4.575	0	2
2	30.72	0	2	25.4405	0	2	...	4.584	0	2
3	50.80	0	2	19.9403	0	2	...	4.784	0	2
...	...	...	...	...	...	...	...	...	...	...
15	993.99	0	2	4.1416	0	2	...	---.---	0	2

Missing values are indicated with a "--.--" at the appropriate depth level(s)

Table 1.4. Biology:
Fixed position, blank field if value not present

Column #	Column name	Column description	Example
1	BIOLOGY	count of biology information set	1
2	Upper Z	upper range of sampling depths (in meters)	0
3	Lower Z	lower range of sampling depths (in meters)	200
4	Value Type	type of value present in column 5	Taxon count, Wet Mass, etc.
5	ORIGINAL VALUE	value of original measurement	(value)
6	F	originator's flag (if provided)	WOD code
7	Orig Unit	units of original measurement	#/m2, mg/haul
8	WOD CBV value	value after calculation to standard units of "#/m3", "mg/m3" or "ml/m3"	(value)
9	F	World Ocean Database CBV flag	WOD code
10	_unit	CBV standard units	#/m3, mg/m3, or ml/m3
11	_meth	calculation method	WOD code
12	WOD PGC	World Ocean Database Plankton Grouping Code	4212000 (= zooplankton, crustacean, copepod)
13	ITIS TSN/Name	ITIS Taxonomic Serial Number/Name	85272 (= *Calanus finmarchicus*)
14	mod	any taxonomic modifier	WOD code (sp., spp., ...)
15	sex	any sex indicators	WOD code (male, female)
16	lif	any life stage indicators	WOD code (egg, larva, copepodite, ...)
17	trp	any trophic indicators	WOD code (parasitic, autotrophic, ...)
18	rlm	any realm indicators	WOD code (benthic, pelagic, endobiotic, ...)
19	ftr	taxon shape	WOD code
20	spm	count method	WOD code (special dyes or lighting)
21	min size	minimum size	WOD code or mm
22	max size	maximum size	WOD code or mm
23	ind length	taxon length	microns
24	ind width	taxon width	microns
25	ind rad	taxon radius	microns
26	tsv	observation-specific sampled volume	used for multi-net samplers

1.3. Data access

The data and supplementary materials in this report can be accessed through WODSelect retrieval system from the NODC public website at
http://www.nodc.noaa.gov/OC5/SELECT/dbsearch/dbsearch.html.
The data can be read and plotted in the Ocean Data View software http://odv.awi.de/.

1.4. Data quality control

Data quality control was in accordance with the procedures accepted by the Ocean Climate Laboratory NODC (Ingleby and Huddleston 2007, Boyer et al. 2009).

To create this Atlas and the Climatic Atlases of the Sea of Azov of 2006 and 2008, general approaches to data quality were applied (Matishov et al. 2005; Matishov et al. 2009, Matishov et al. 2009, Matishov 2010, Moiseev et al. 2012).

Quality control procedures include:

- An automated quality control of data performed by computer software developed for this purpose;
- A stage of subjective analysis made by a specialist.

The procedure is iterative since corrections are subject to subsequent automated and subjective checks.

The automated process of quality control includes the searches for and consideration of possible errors in data. The result is a report that contains information about the registered errors and warnings.

All checks may be divided into several groups:

- Control over data formats;
- Check of spatial-temporal location;
- Check of vertical structure of changes;
- Check of measurement values;
- Search for duplicates.

The first group of quality control include date and time checks (e.g., date of station and duration of cruise, order of data collection by station). Data collected from stations and cruises is also checked for missing data.

The second group of quality control verifies the accuracy of coordinates and time stamps (e.g. date, time):

- The temporal interval between two consecutively visited stations to the vessel's maximum speed;
- Shift of coordinates of stations onto land;
- Verification of depth at station in relation to known bathymetry;
- Verification of a vessel's route to determine sudden and sharp changes of directions (e.g. zigzags).

The third group of quality control verifies:

- Duplication of data;
- Negative data values;
- Valid bathymetry data points;

- Check of correlation of profiles' values to station's depth (in case there is the depth value at the station);
-Valid gradients of hydrological and hydrochemical parameters.

The fourth group of quality control verifies parameters associated with allowable and known ranges (e.g. water areas, time of the year, and time of the day). Density inversion and freezing temperatures are verified against measurements of water temperature and salinity. With respect to instrument validation, significance of measured values was verified. Also, comparative data associations were made when appropriate. For example, water salinity was checked against chlorine values.

To carry out the visual control over the spatial location, all stations are marked on the chart by geo-informational system using "ArcGIS Desktop 9.*".

All oceanographic data used for the development of atlases within the International Ocean Atlas and Information Series are available without restrictions via the Internet portal, supported by the NOAA National Oceanographic Data Centre.

1.5. Data processing methods

Data processing was conducted as follows
- Inventory of data;
- Statistical analysis, assessment, and validation of data
- Construction of station distribution by grids, areas, and transects;
- Averaging of data to determine the climatic norm (standard pattern);
- Construction of vertical distribution of water temperature and salinity at the transects;
- Calculation of anomalies.

Several types of data inventories were performed:
- Construction of station distribution charts for each month by year;
- Construction of station distribution charts by month for the entire observation period;
- Construction of station distribution charts by month for the entire observation period for oceanographic transects (for the Barents Sea and the southern seas).

Statistical analysis was performed on the relevant data. Regularities of changes of annual climatic cycles of temperature and salinity were determined and limits of allowable values of the indicated parameters were set. If the measured value was outside the allowable limits, the data point was flagged. This flagged data point was not used when the climatic fields were calculated using time series of temperature and salinity.

2. Region 1. Large Marine Ecosystems of the Eastern Arctic

Climatic changes in the Arctic are characterized by the greatest differences and lead to significant consequences for ecosystems and maritime activities. The Arctic region was formed

in the post-glacial period, which lasted for more than 10,000 years. The natural anomalies that are deviations of the statistically reliable standards and patterns may be discussed only in relation to this post-glacial period. The warmest period in history was the period of the Atlantic optimum – around 6 thousand years ago (Matishov and Pavlova 1990). Cyclic changes of climate and ice cover conditions were registered during the last centuries. Among them 'the little glaciation period' of the middle of the last millennium was characterised by cooling in Europe, worsening of ice conditions in the Western Arctic seas, and the destruction of settlements of Europeans in Greenland.

Approximately 150 years ago, the Dutch conducted surveys near the Novaya Zemlya, which laid the foundation of research with respect to climate fluctuations in the Arctic. Knowledge about the Eastern Arctic region broadened considerably at the end of the 19th century and beginning of the 20th century due to numerous efforts of outstanding researchers and explorers (Figure 2.1).

A network of meteorological stations and regular ice surveys were deployed in the Arctic seas at the end of the 19th century. Based on the data received, information databases were developed, allowing conclusions to be drawn regarding the trends of the last century. Among climatic indicators, the changes in water temperature and ice cover are important for practical reasons. The state/status of bioresources and conditions of fishery, as well as possibilities of shelf oil and gas resource development depend the changes. The ice conditions determine the navigation possibilities along the Northern Sea Route (NSR).

A generally accepted index of climate regime changes is a series of water temperature observations (1898-present) at the Kola Transect in the Barents Sea (along 33°30' E). One major anomaly was "the warming of the Arctic" in the 1920-1930s. This phenomenon resulted in an increase in air temperature near coastal areas and islands as well as a reduction of ice cover in the Arctic seas (Frolov et al., 1997). There were no regular data collection systems on ice conditions of the seas at the time, however, regular cruises along the NSR took place before the appearance of effective icebreakers. For example, the expedition of 1914–1915 by the ice-breaking steamers *Taimyr* and the *Vaigach* failed to navigate the NSR during one navigation period.

Figure 2.1. Prominent explorers of the Arctic of the 19th – early 20th centuries.

In 1878, Nils Nordenskjold on board the *Vega* covered almost the entire Northern Sea Route from Stockholm to the Bering Strait in one summer period.

The end of the 20th century was characterized by warming events, which significantly impacted the state of atmosphere, ocean, sea and terrestrial ice in the northern polar area (Levitus et al. 2005, Levitus et al. 2009, Matishov et al. 2011, Matishov et al. 2012, Frolov et al., 1997 ; Alekseev et al., 2010).

The reasons for climatic fluctuations in various areas of the Arctic are different. The most significant factors in the Barents Sea are the transfers in the atmosphere (zonally and meridionally) and the inflow of warm Atlantic waters. The intensity depends on the global oceanic circulation and the Gulf Stream current. In the case of the Eastern Arctic seas, changes in water discharge and thermal advection of the great Siberian Rivers are most influential. The increased discharge causes a freshening of the surface layer of seas, which fastens the formation of ice cover. At the same time, the increased freshwater runoff contributes to early ice melt due to its higher content of heat.

The databases and graphics of marine environment observations presented in the Atlas provide grounds for reliable prognoses of possible climatic trends.

The second part of the Atlas considers large marine ecosystems (LMEs) of the Eastern Arctic, covering the Barents Sea LME and White Sea subarea, the Kara Sea LME, the Laptev Sea LME, the East Siberian Sea LME, and the Chukchi Sea LME. This section also includes the East and West Bering Sea LMEs (Figure 2.2).

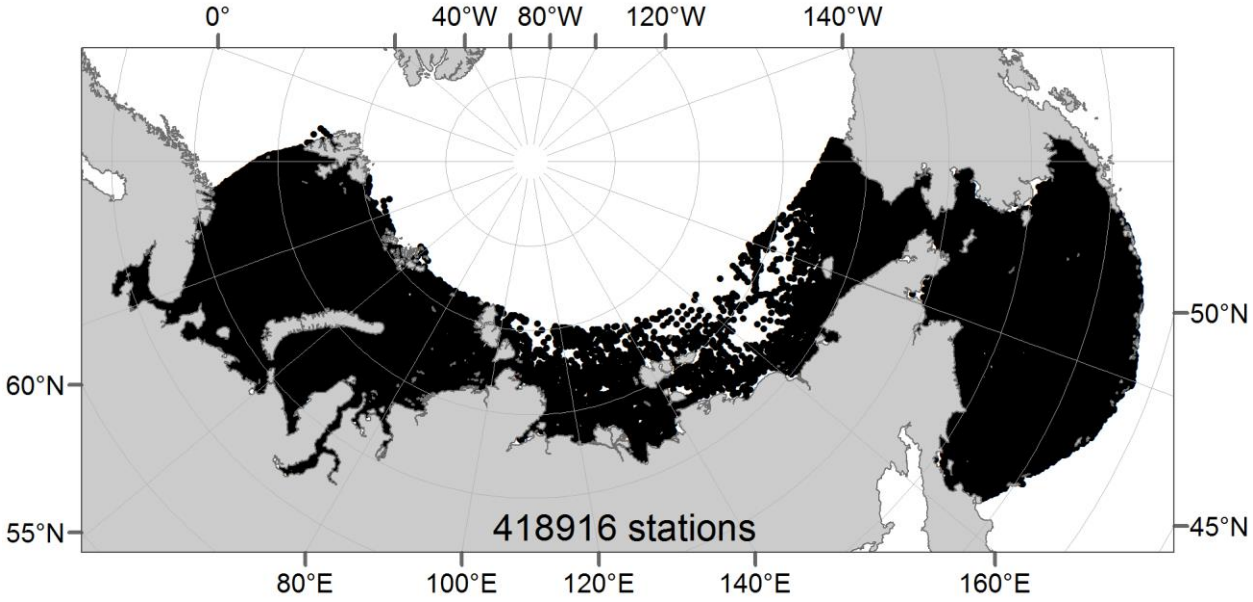

Figure 2.2. Distribution of stations in the Eastern Arctic seas in 1827-2013.

The northern Arctic component of the database in this Atlas includes data from 418,916 stations. Their distribution by seas is given in Table 2.1 by years and months (see Figure 2.3).

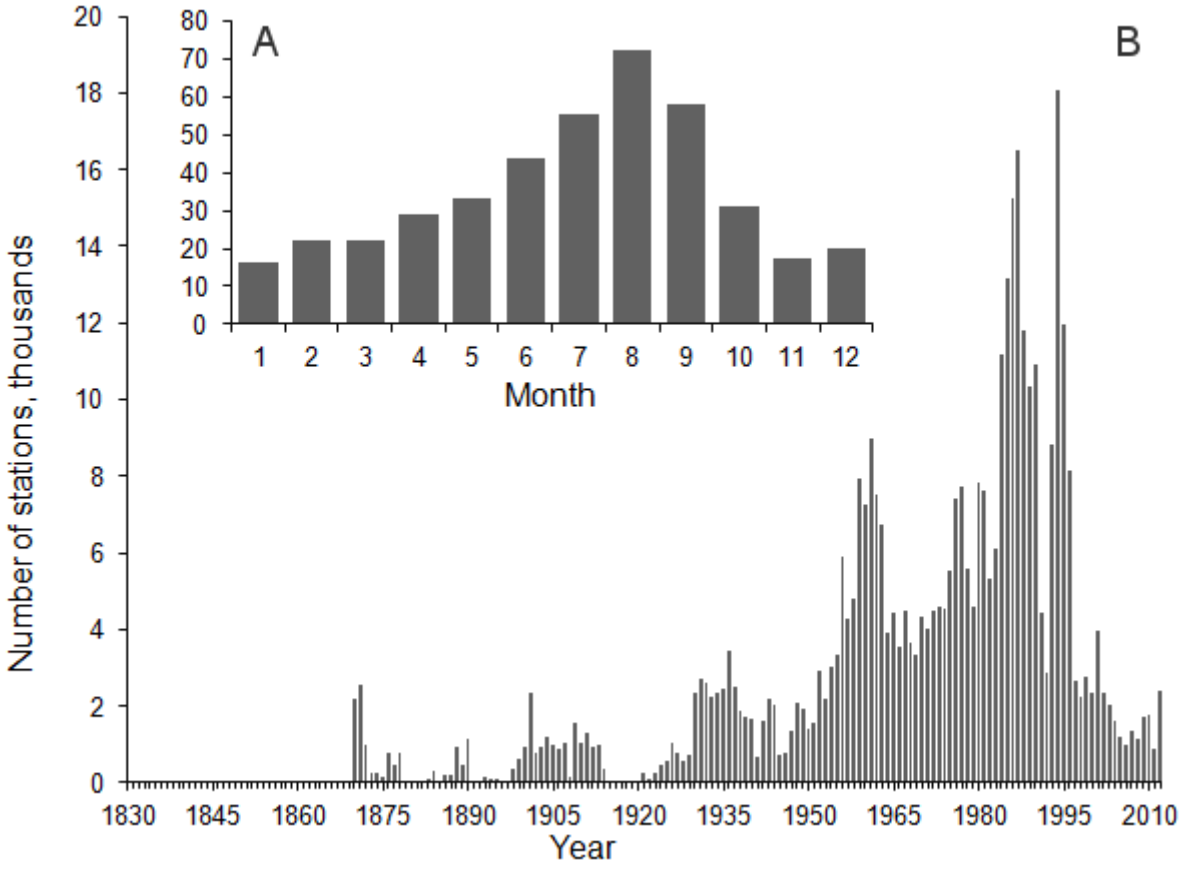

Figure 2.3. Distribution of stations by months (A) and years (B) in the Eastern Arctic seas database (1827-2013).

Table 2.1. Distribution of stations by the Eastern Arctic Large Marine Ecosystems

Large Marine Ecosystems	Number of stations	Period
Barents Sea (including the White Sea subarea)	238,286	1870-2013
Kara Sea	38,445	1870-2013
Laptev Sea	6,570	1878-2009
East Siberian Sea	3,459	1878-2008
Chukchi Sea	50,858	1849-2012
Bering Sea	81,298	1827-2012
Total	418,916	

For a long time, the non-freezing seas of the Western Arctic were the arena for marine expeditions due to their importance in fisheries. Ice-covered seas – from the Kara Sea LME to the Chukchi Sea LME – have always been of interest but were accessible by navigation for a short period of time, usually from July to September. Biological processes of the winter stillness were weakly studied until recently, and it was considered that they have minimal influence on bioproductivity and species diversity.

MMBI KSC RAS has conducted a range of marine and coastal expeditions and cruises. It is also responsible for the organization of research stations in the Arctic. MMBI KSC RAS activities along the Northern Sea Route on board nuclear icebreakers have become a new stage of studies in areas that are otherwise difficult to access.

The first MMBI KSC RAS expedition along the Northern Sea Route took place in February – March 1996 on board the *Taimyr* and *Vaigach* nuclear icebreakers. Its main task was to assess the possibilities of using cruises of passing vessels for research. The results of the expedition confirmed that it was possible to collect unique scientific material during ice shipping seasons. Consequently, research on cruises became a permanent component of the Institute expeditions.

Since then the Institute conducts two to four expeditions on an annual basis. From 1996-2013, 61 cruises were carried out with scientific data collected at 2,379 stations (Figure 2.4).

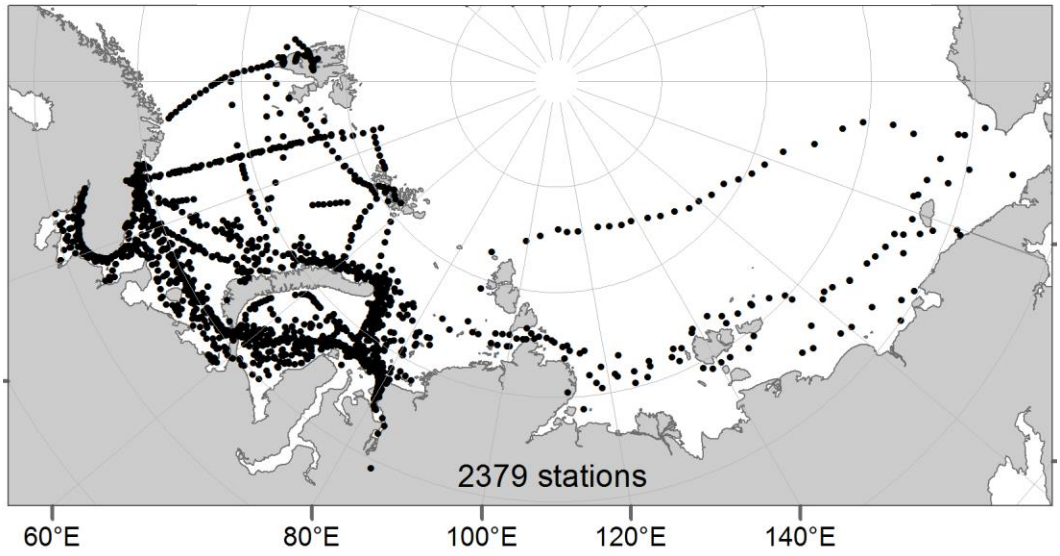

Figure 2.4. Sampling stations in the MMBI KSC RAS expeditions of 1996-2013, including the ones along the Northern Sea Route on board the nuclear icebreakers of the Murmansk Shipping Company.

2.1. The Barents Sea LME (including the White Sea subarea)

The studies of the environment and ecosystems of the Barents and White Sea subarea have been conducted for longer than a century. In the Barents Sea, a scientific and fishery expedition was headed by N.M. Knipovich in 1899. In the White Sea, a biological station on the Solovetsky Islands was established in 1883.

During 1970-80s, large-scale monitoring was undertaken of the Barents and White Sea subarea. These efforts included regular deep-water surveys at standard transects, State-wide System of Environment Pollution Observation and Control (OGSNK) studies, observations from the network of coastal stations, and aerial surveys.

Historically, studies of the Barents Sea were focused on collecting temperature conditions. Data on water temperature are of primary importance for fisheries. Hydro-physical characterristics in ice thickness depend on water temperature since the variability of salinity in the Barents Sea pelagic zone is relatively low. Data from thermohaline surveys are frequently used in calculations of water circulation.

Oceanographic database and inventory

The Barents Sea LME and White Seas subarea oceanographic database contains 238,286 stations for the period 1870 – 2013. The White Sea subarea contains 24,156 stations (Figure 2.5).

The distribution of stations by years and months is presented in Figure 2.6.

Only stations located within the boundaries of the Barents Sea LME and White Sea subarea are considered here, versus the Climatic Atlas of the Arctic Seas that considers stations outside the boundaries as well (Matishov et al. 2004). For Barents Sea LME and White Sea subarea, 9,572 new stations have been established after 2000 and have been added to the database. Of the new stations, 1,504 stations were established during the MMBI KSC RAS expeditions (Figure 2.7).

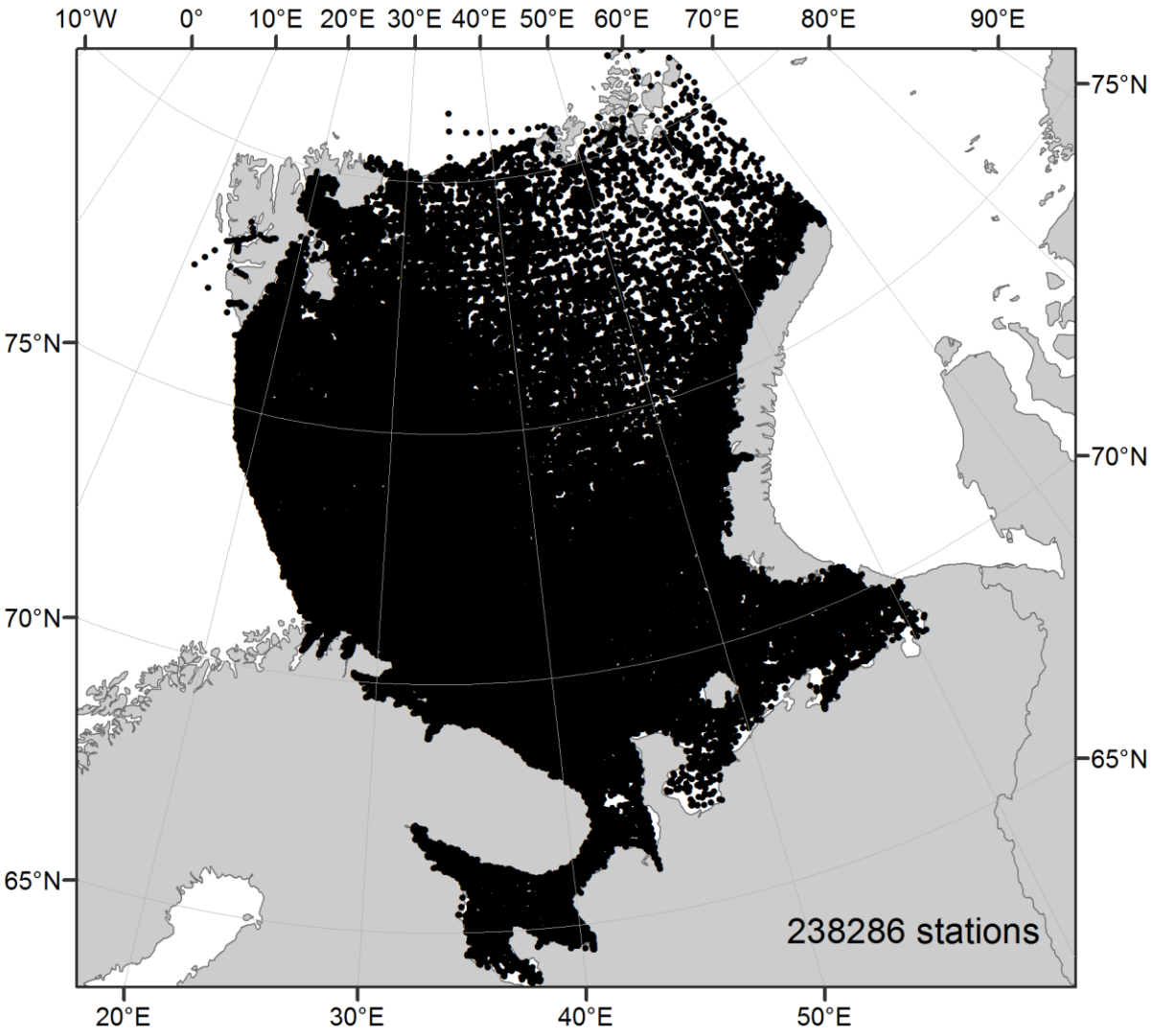

Figure 2.5. Distribution of stations over the Barents Sea LME and White Seas subareas (1870-2013).

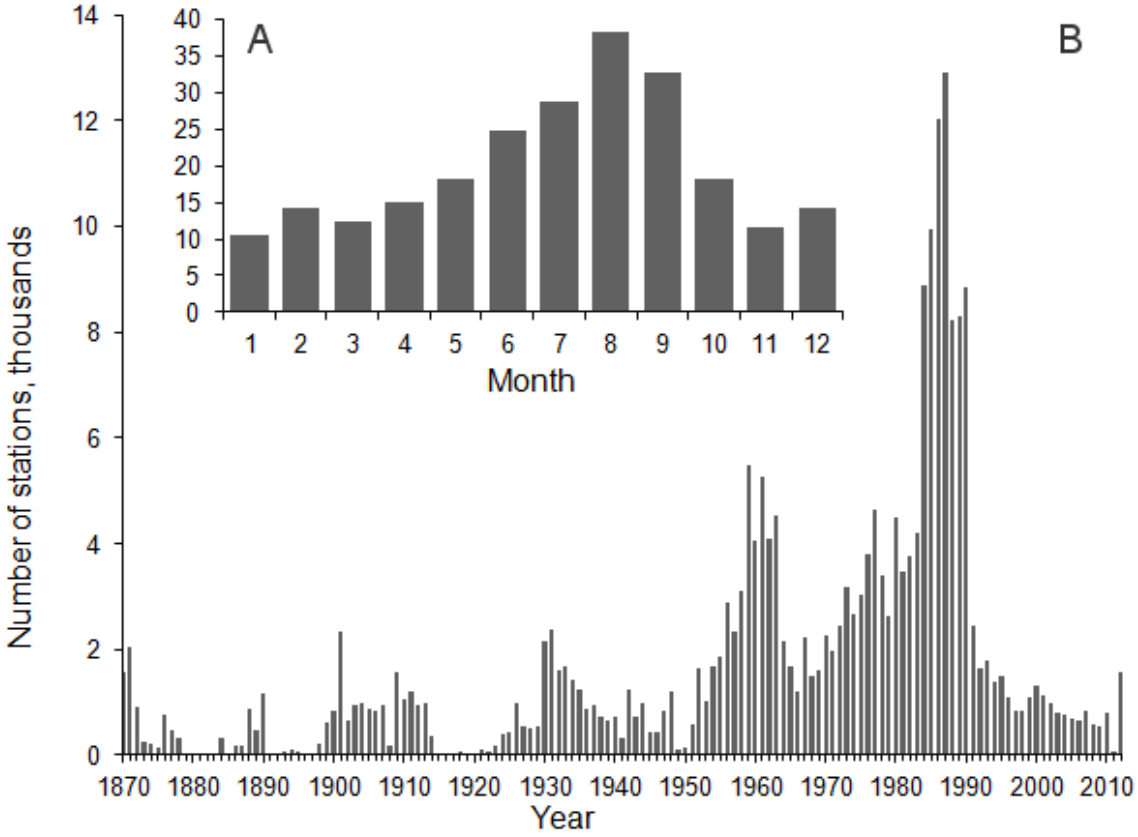

Figure 2.6. Distribution of stations by months (A) and years (B) in the Barents Sea LME and White Sea subarea database (1870-2013)

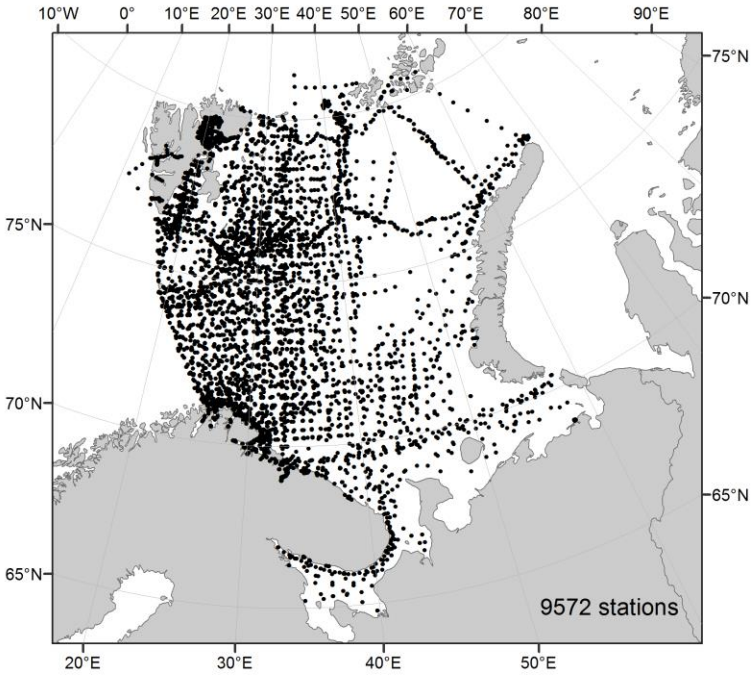

Figure 2.7. Stations in the Barents Sea LME and White Seas subarea database, 2001-2013.

Surveys in the deep waters of the Barents Sea LME have been conducted for a long period of time. Transect VI of the Kola Meridian/Transect (Figure 2.8) is of particular interest, and data is collected every month on an annual basis. With this long-standing dataset, trends regarding the variability of oceanographic processes are noted (Levitus et al. 2009, Matishov et al. 2009).

The White Sea, due to its small size and ease of accessibility, is evenly covered by a net of surveys. Until recently, these surveys were performed systematically. Surveys were not performed during the ice season. Hydrological conditions of winter are relatively stable and only slightly impact the maritime activity.

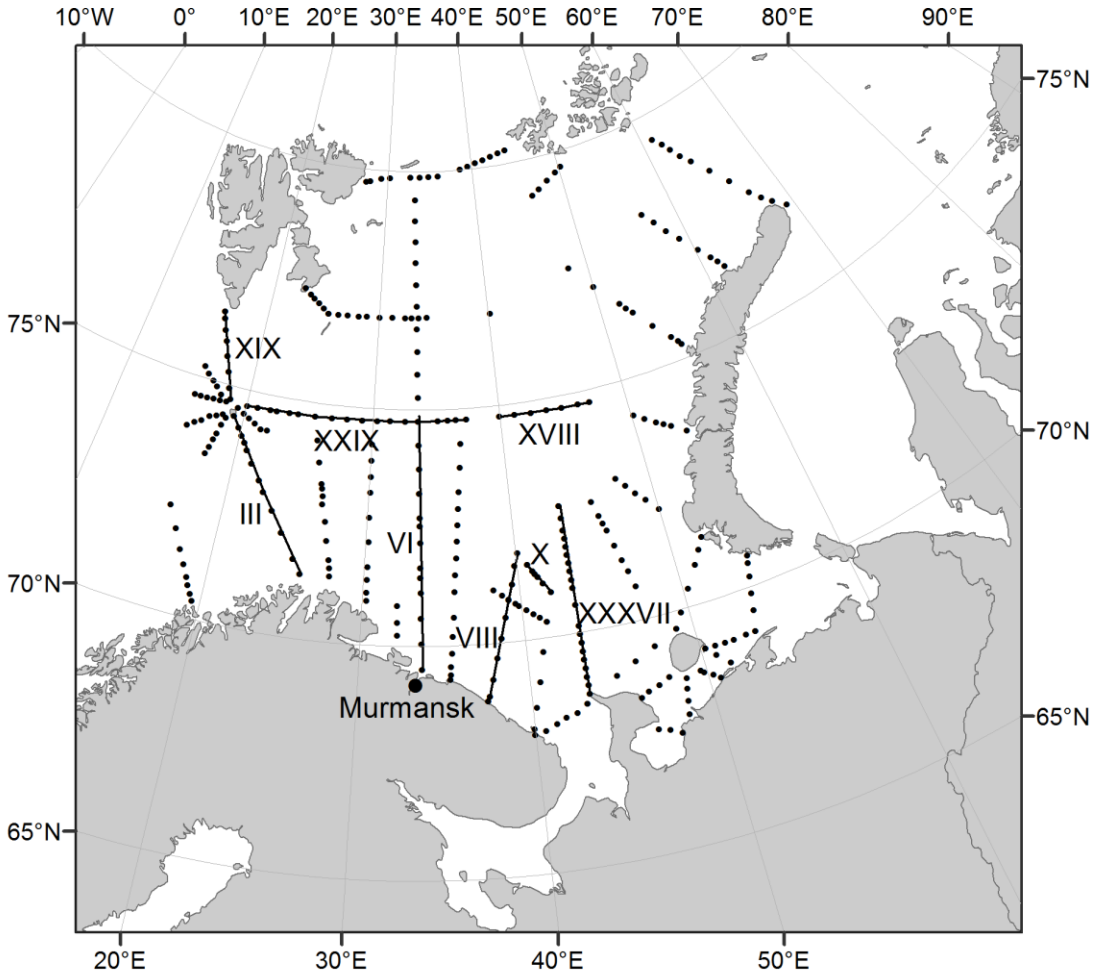

Figure 2.8. Observation network of the Barents Sea LME.

To analyze the climatic variability of hydrological characteristics of the Barents Sea LME, the following two transects are considered in the Atlas:

- The Kola Transect, along 33°30'E, from Murmansk to Belyi Island and comprising Transect VI (the Kola Meridian) and to 80°N (Figure 2.9);

- Medvezhinsky Transect, along parallel 74°30' N, from Bear Island to the Novaya Zemlya and uniting oceanographic transects XXIX and XVIII (Figure 2.10).

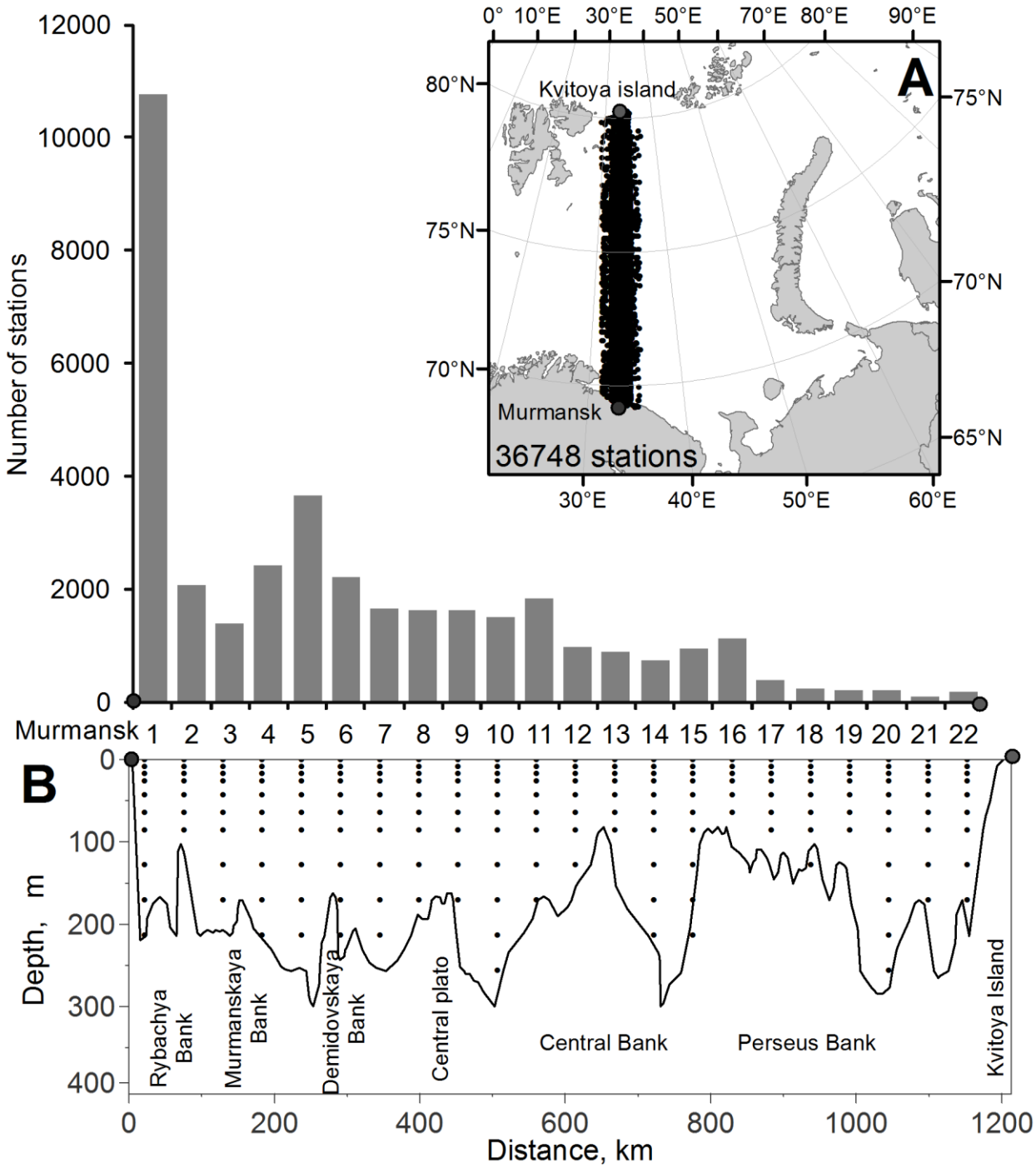

Figure 2.9. Distribution of stations in the 80-km buffer zone (A) and bottom relief (B) along the Kola Transect.

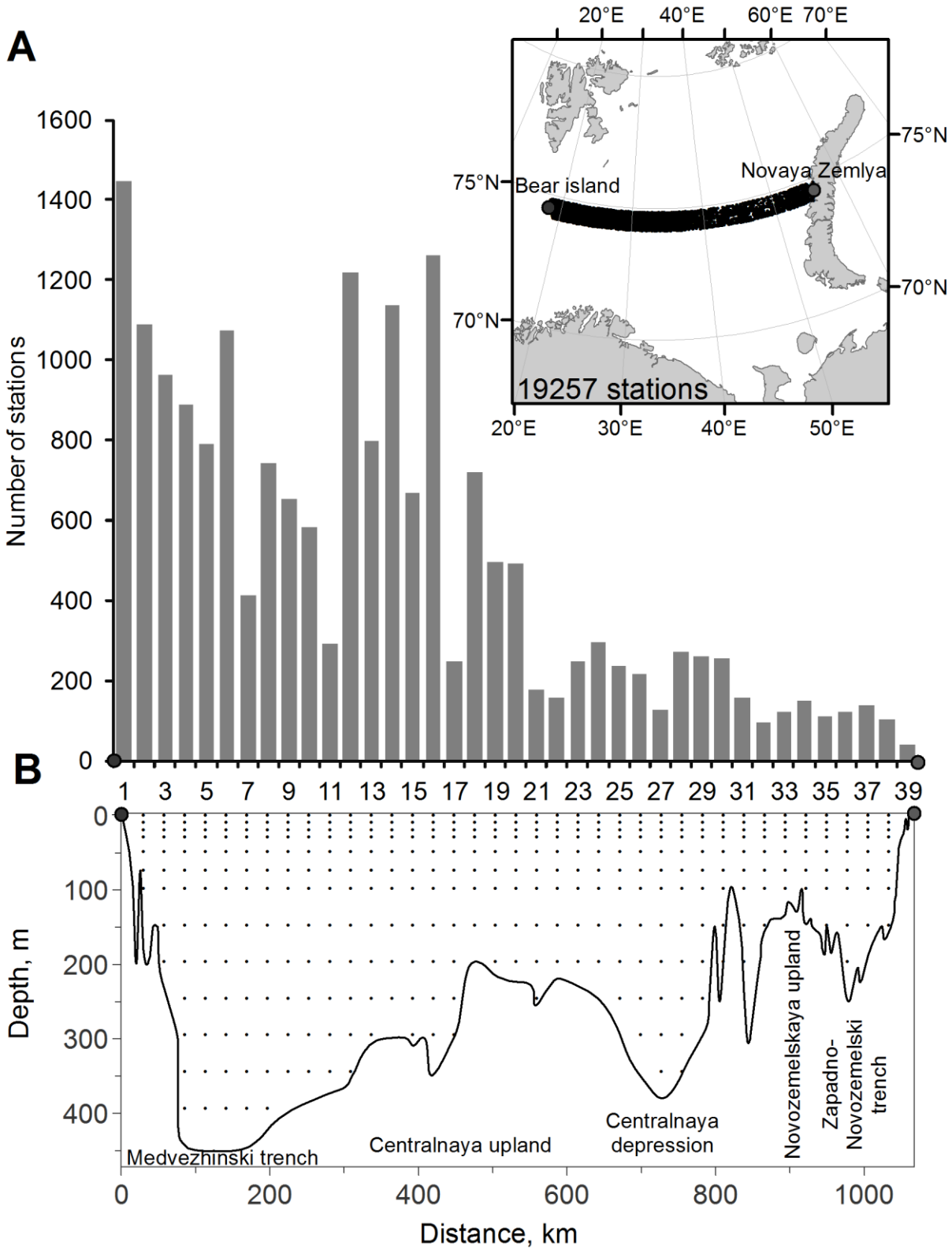

Figure 2.10. Distribution of stations in the 80-km buffer zone (A) and bottom relief (B) along the Medvezhinsky Transect.

Data from a number of stations located in the 40-km buffer zone from each side of every transect is used in calculations of climatic standards, patterns, and anomalies. The total number of such stations is 36,748 in the Kola Transect and 19,257 in the Medvezhinsky Transect. The Barents Sea LME and White Sea subarea database includesthe parameters listed in (Table 2.2).

Table 2.2. List of indices included in the Barents Sea and White Sea database.

Parameter		Units of measurement		Number of measurements
Name	**Code**	**Name**	**Sign**	
Temperature	TEMP	Degree Celsius	C	4,956,658
Pressure	PRESS	Decibar	DBAR	2,163,027
Conductivity	COND	Siemens/m	SIEMENS/M	1,854,343
Salinity	SAL	Units of practical scale of salinity	PSS	4,207,207
Absolute content of dissolved oxygen	OXY	Ml/l	ML/L	120,320
pH	PH	-	-	67,796
Alkalinity	ALK	Milligram-equivalent/l	MEQ/L	34,721
Nitrates	NO3	Micromole/l	UMOL/L	35,610
Phosphates	PO4	Micromole/l	UMOL/L	70, 334
Silicates	SIO4	Micromole/l	UMOL/L	42,645
Chlorophyll	CHL	Mkg/l	UG/L	2,011

Plankton database

The Barents Sea LME plankton database includes phytoplankton (Figure 2.11, Table 2.3) and zooplankton samples (Figure 2.12, Table 2.4). The total number of stations with phytoplankton samples is 617 and 246 with zooplankton.

Table 2.3. Distribution of stations with phytoplankton samples in the Barents Sea LME, White Sea subarea, and the Kara Sea LME (1999-2011).

	Jan	**Feb**	**Mar**	**Apr**	**May**	**Jun**	**Jul**	**Aug**	**Sep**	**Oct**	**Nov**	**Dec**	**Total**
1999	-	-	-	-	-	-	7	-	-	36	4	3	50
2000	2	4	16	3	4	3	4	3	2	3	5	7	56
2001	5	6	-	2	6	1	-	-	-	-	-	-	20
2002	6	22	2	6	1	-	-	-	-	13	16	-	66
2003	-	2	3	8	24	-	14	28	9	3	11	34	136
2004	1	7	-	1	4	1	23	2	16	-	-	5	60
2005	3	8	11	16	3	1	8	2	11	1	3	22	89
2006	-	3	2	3	-	1	8	7	11	8	-	-	43
2007	-	-	13	2	4	1	1	30	20	11	-	2	84
2008	-	-	-	-	-	-	3	-	-	-	-	-	3
2009	-	-	-	-	-	-	-	-	-	-	-	-	0
2010	-	-	-	-	-	1	-	-	3	5	-	-	9
2011	-	-	-	-	-	-	-	1	-	-	-	-	1
Total	**17**	**52**	**47**	**41**	**46**	**9**	**68**	**73**	**72**	**80**	**39**	**73**	**617**

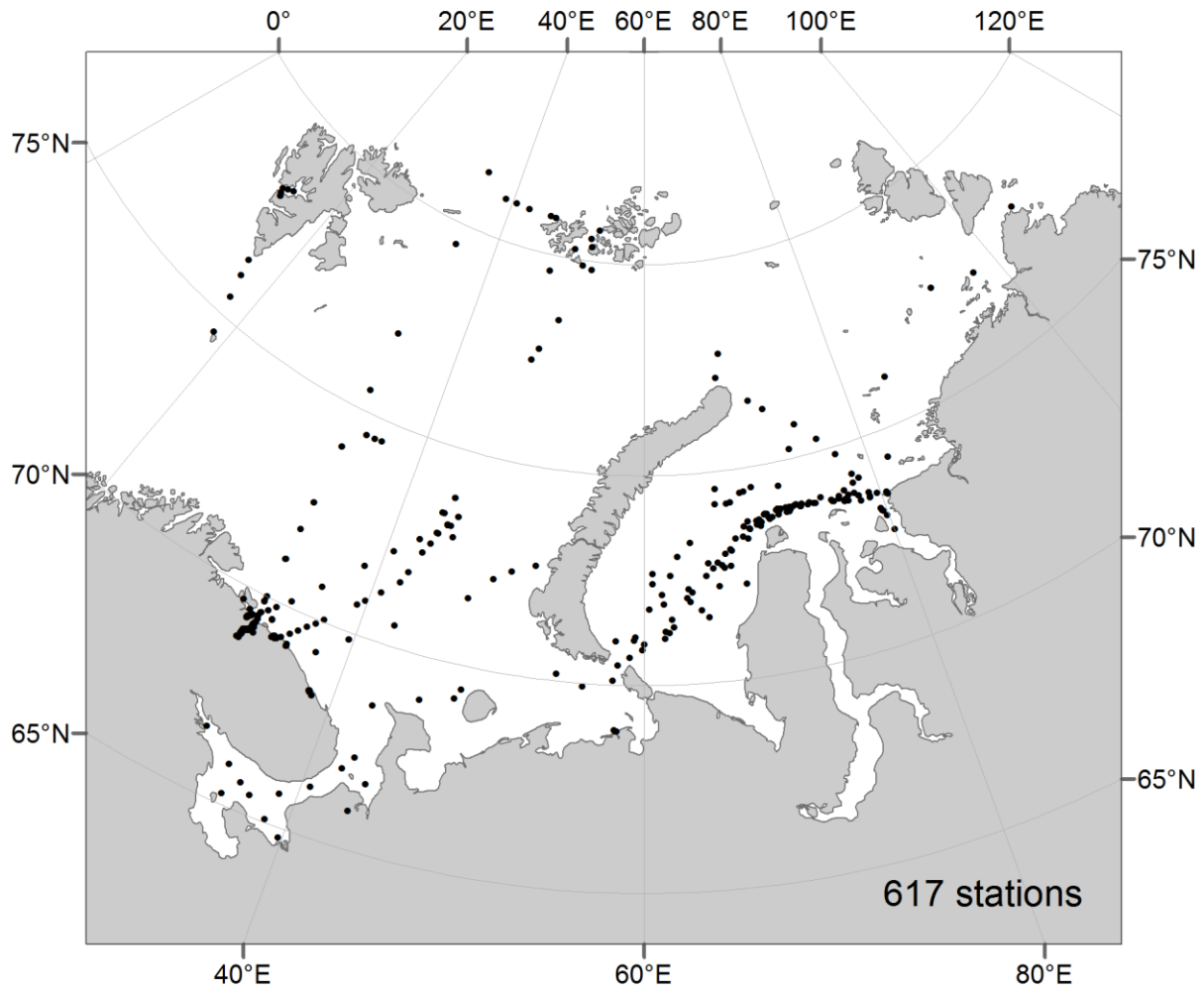

Figure 2.11. Distribution of stations with phytoplankton samples in the Barents, White, and Kara Seas LMEs (1999-2011).

Table 2.4. Distribution of zooplankton samples with the Barents Sea LME (2001-2010).

	Jan	**Feb**	**Mar**	**Apr**	**May**	**Jun**	**Jul**	**Aug**	**Sep**	**Oct**	**Nov**	**Dec**	**Total**
2001	-	-	-	-	-	-	59	-	-	-	-	-	59
2004	-	-	-	-	-	-	9	-	-	-	-	-	9
2005	-	-	-	-	-	-	10	-	9	-	-	-	19
2006	-	-	-	-	-	1	12	38	11	7	-	-	70
2007	-	-	-	-	-	-	-	16	27	-	-	-	43
2008	-	-	-	-	-	-	15	8	-	-	-	-	23
2009	-	-	-	-	-	-	-	6	-	-	-	-	6
2010	-	-	-	-	-	-	-	-	8	9	-	-	17
Total	**-**	**-**	**-**	**-**	**-**	**1**	**105**	**68**	**55**	**16**	**-**	**-**	**246**

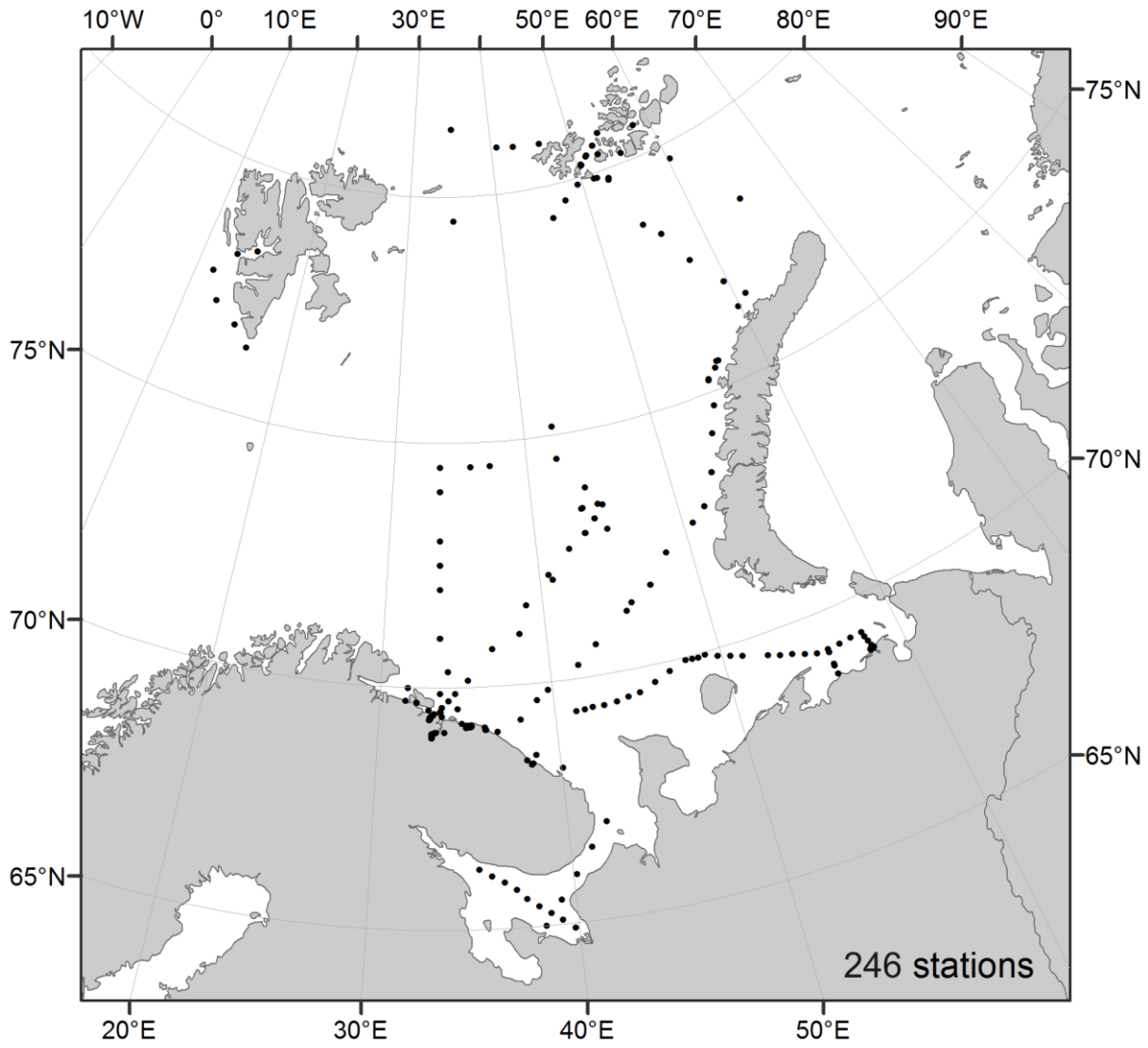

Figure 2.12. Distribution of stations with the Barents Sea LME zooplankton samples (2001-2010).

Time series of water temperature and salinity

Vertical distributions of temperature and salinity, averaged for the period of 1870-2013 (climatic standards/patterns) have been constructed for the Kola and Medvezhinsky Transects. Their location by the vertical corresponds to standard horizons of 0, 10, 20, 30, 50, 75, 100, 150, 200, 250, and 300 m. The grid size for the Kola Transect was 0.5^{o}N x 0.5^{o}E. The grid size for Medvezhinsky was 0.25^{o}N x 0.5^{o}E.

Sample charts with climatic standard of water temperature (Figure 2.13) and of temperature anomaly in September 2003 (Figure 2.14) are given for the Kola Transect.

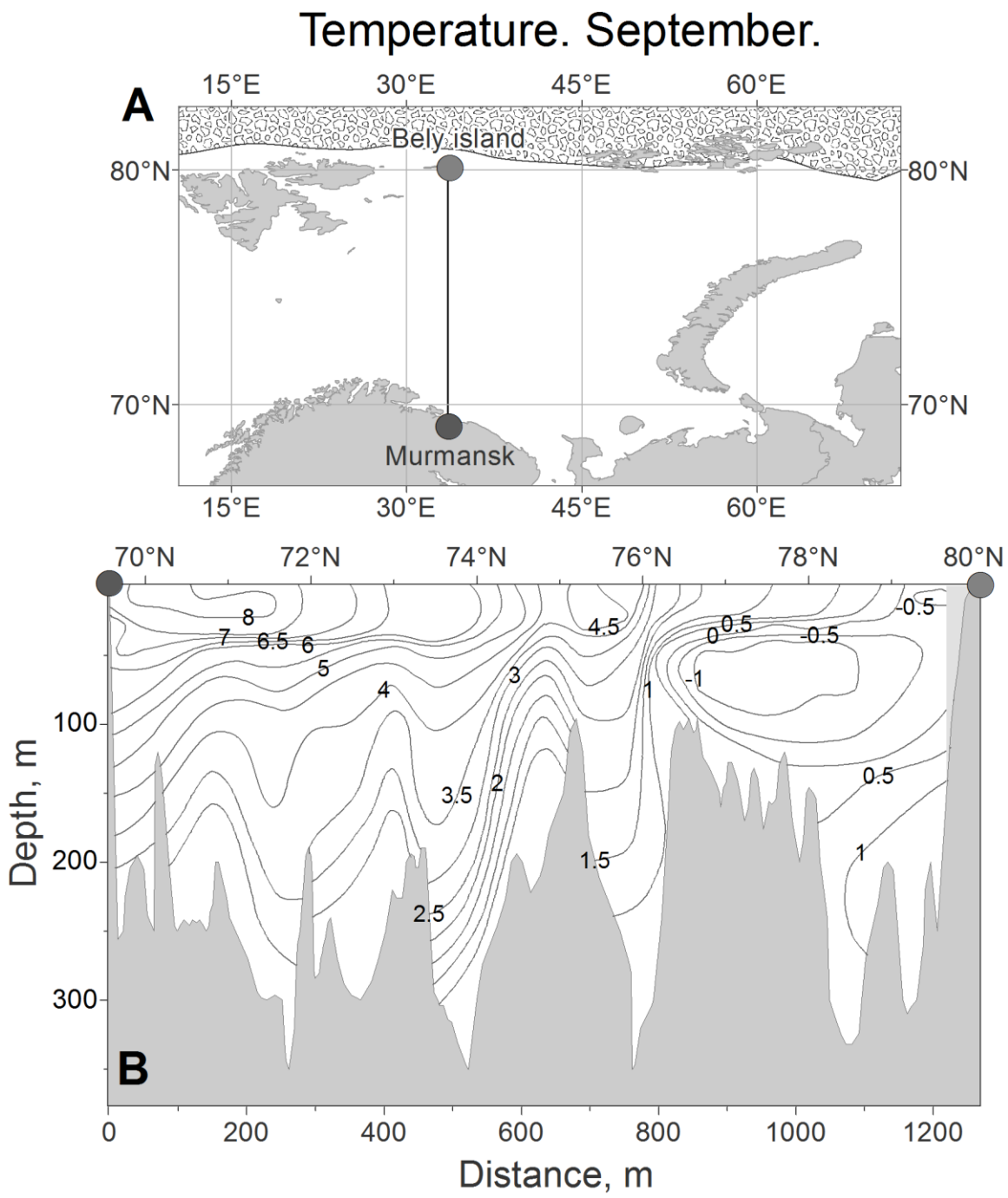

Figure 2.13. A sample of construction of the mean long-term vertical distribution of water temperature (^{o}C) for the Kola Transect (A) in September 2003 (B).

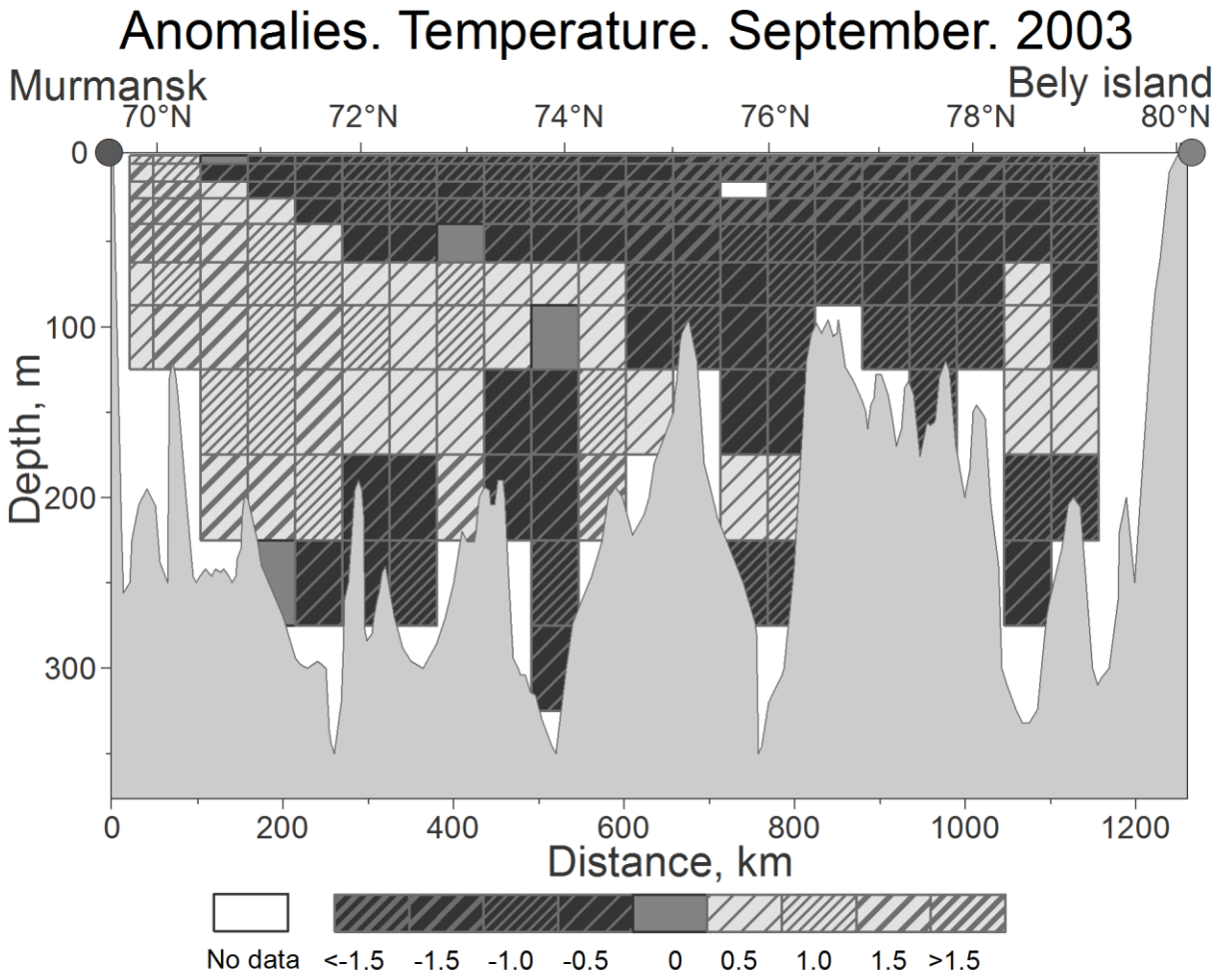

Figure 2.14. An example of calculated water temperature anomaly (^{o}C) in the Kola Transect area in September 2003.

Time series of ice conditions

The Barents Sea has floating and drifting ice, but it is never fully ice covered due to the inflow of warm Atlantic waters (Hydrometeorology, 1990; Mironov, 2004). Ice observations in the Barents Sea have been conducted for a long period of time (Figure 2.15).

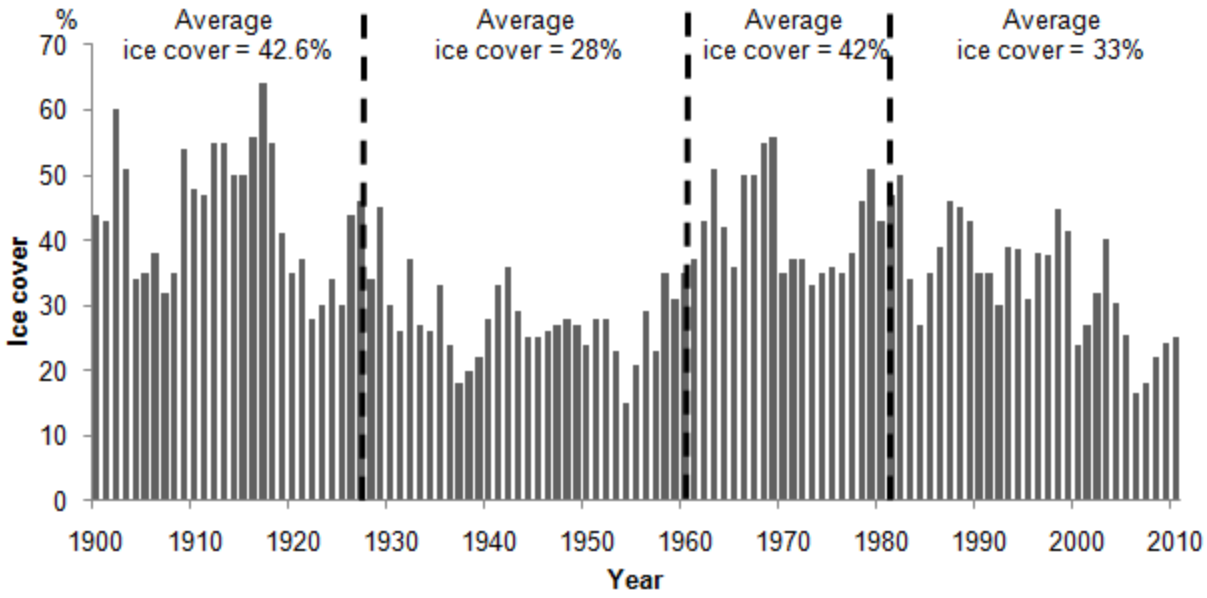

Figure 2.15. Dynamics of the Barents Sea ice conditions in 1900-2010.

This time series is based on published reference data for the period of 1900-1959 (Privalsky 1985), as well as a database at MMBI KSC RAS. This database contains time series of monthly values of the total ice area for 1960–1976 (results of a joint study by MMBI KSC RAS, Russia and the University of Alaska Fairbanks,USA) (Matishov et al. 2000) and 408 monthly charts for the period of 1977-2010. These charts are the result of digitizing of charts from the National Snow and Ice Data Centre (USA) for 1977-1996, and the general ice charts of the Arctic Ocean from the Centre of Ice and Hydrometeorological Information of the AARI for 1997-2011.

Two long periods of increased and decreased ice concentration in the Barents Sea can be distinguished for the period of 1899-2010.

For the first three decades of the last century, apart from some years (1904, 1907, and 1922-1925), the ice conditions exceeded the standard pattern (were heavier when compared to the standard pattern). During the following three decades (1930-1961), the reduction of the total ice area in the Barents Sea was registered with the minimum values being in 1954-56. Only some years of the period (1932, 1941, 1942, and 1958) were characterized by increased ice concentrations (heavier ice conditions).

The next period of the increased ice concentration and heavier ice conditions lasted from 1962 to 1982. However, the mean ice concentrations during those years were less than in 1899-1929.

The results of observations demonstrate that ice conditions fluctuated in the Barents Sea during the last half of the century. Overall, two long periods may be indicated before the early 1990s: a cold period (heavier ice conditions) followed by a warm period (the dominance of light ice conditions). The ecosystem of the Barents Sea LME in the first decade of the 21st century is

characterized by a high content of heat in water and low ice concentrations (light ice conditions). At the same time, gradual reduction of the total ice area took place in 2006 (Matishov et al. 2007). This resulted in easier conditions for shipping, as well as longer feeding migrations of commercial fish species (Zhichkin 2009, Matishov et al. 2011). Starting with 2007, an increasing trend of the total ice area has been observed.

Fishery time series

The ichthyofauna of the Barents Sea is composed of more than 180 fish species and subspecies (Karamushko 2008). The main commercial fish species are bottom species such as cod, haddock, and pelagic species such as capelin and Polar/Arctic cod.

A database has been developed and formed at MMBI KSC RAS (Matishov, Zhichkin, 2008). Charts of monthly catches of cod, haddock, capelin, and Arctic/Polar cod by the Russian vessels in the Barents Sea LME for the period of 1977-2010 have been constructed.

The data of daily records of fishing vessels of various types were used as the primary and initial material for mapping; the number of the vessels in the Barents Sea LME ranged during the year from 40-50 to 70-80 per month, and in some years (especially in summer months) exceeded 100. Daily records and information from research vessels of the fishing survey (from 2 to 5 vessels every month during a year searching for commercial concentrations of bottom fish species) were also used. The database contains information on the fishing grid area, number and type of vessels, and volume of the catch/fish caught.

Distribution charts of fishing vessels provide a visual of the fishing geography, commercial concentrations of fish species and their migration routes (Figure 2.16).

During the years with cold hydrological conditions (1977-1982) cod migrated mostly in an eastern direction (Figure 2.16A). However, the commercial concentrations of cod during those years did not go outside the Murmansk shallow water areas and the western slope of the Severo-Kaninskaya/North Kanin fishing grounds/bank.

The schoolings did not reach the coastal waters of the Novaya Zemlya nor the slopes of the Gusinaya fishing grounds/bank since their migrations are restrained by cold water. Fishing activities were thus concentrated in the southern and southwestern areas of the sea. At the same time, the migration of cod to the North was rather weak (Zhichkin 2009).

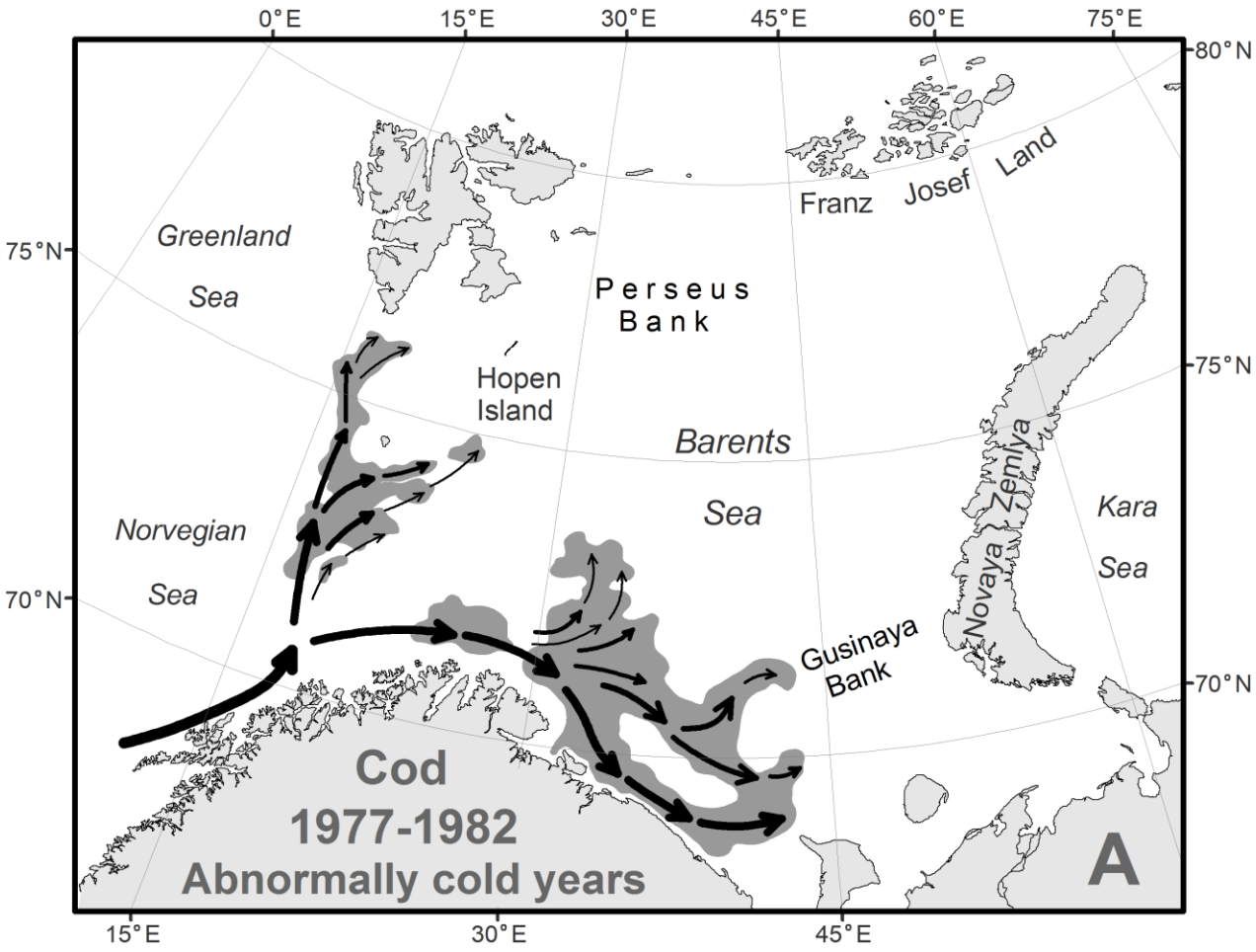

Figure 2.16. Migration and distribution pattern of commercial concentrations of cod in the Barents Sea LME in abnormally cold (A) and abnormally warm (B) years.

As a warm phase in climatic fluctuations began in the early 1990s, the redistribution of the migration routes and flows of cod took place. The fishing area enlarged both in the eastern and northern directions (Matishov et al., 2010). In the East, the concentrations of cod in September-October reached the coastal waters of the Novaya Zemlya between 70-74°N.L., though the main migration flow directed north up to 79°N.L. (the area of Nadezhda, the Perseus Uplands) (Figure 2.16B).

Analysis of distribution charts of commercial concentrations of haddock for the last 25 years indicates that haddock, similar to cod, reacts to the change of heat state/content of water masses. During the warming periods, haddock can be found anywhere in the Barents Sea. During the cooling periods, the geographical range of haddock is reduced. As a result of the Barents Sea warming during the last two decades, the geographical ranges of haddock are broadened to the east and north.

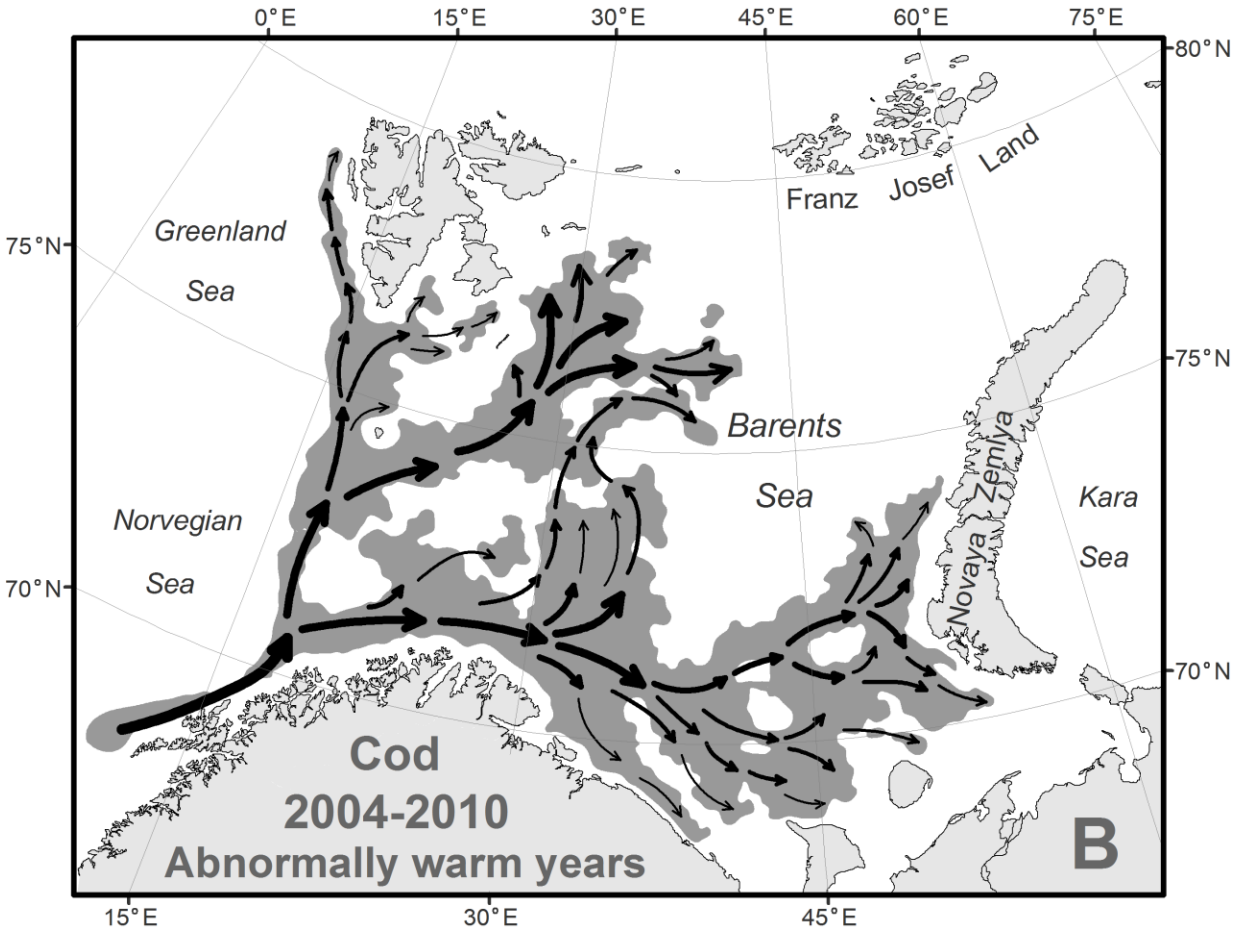

Continuation of Figure 2.16.

During the initial warm phase of climatic fluctuations in the 1990s, the concentrations of haddock were registered on the slopes of the Severo-Kaninskaya/North Kanin and Gusinaya fishing grounds. These are areas where haddock had limited distribution as noted in early catch records. During the first decade of the 21st century, the total volume of the haddock catch of the entire sea gradually increased and reached its maximum value in 2007-08. However, a local cooling event occurred in 1997-98, which briefly paused the commercial increases of haddock.

In 2001 an extension of fishing areas occurred in a northern direction toward the Spitsbergen Archipelago (Svalbard), which led to an increase in rationing of the catch. In 2008-09, the commercial fishery recovered due to an increase in heat content in sea waters in the areas of the Western and Northern Spitsbergen between 79 and 80°N.L. (Figure 2.17).

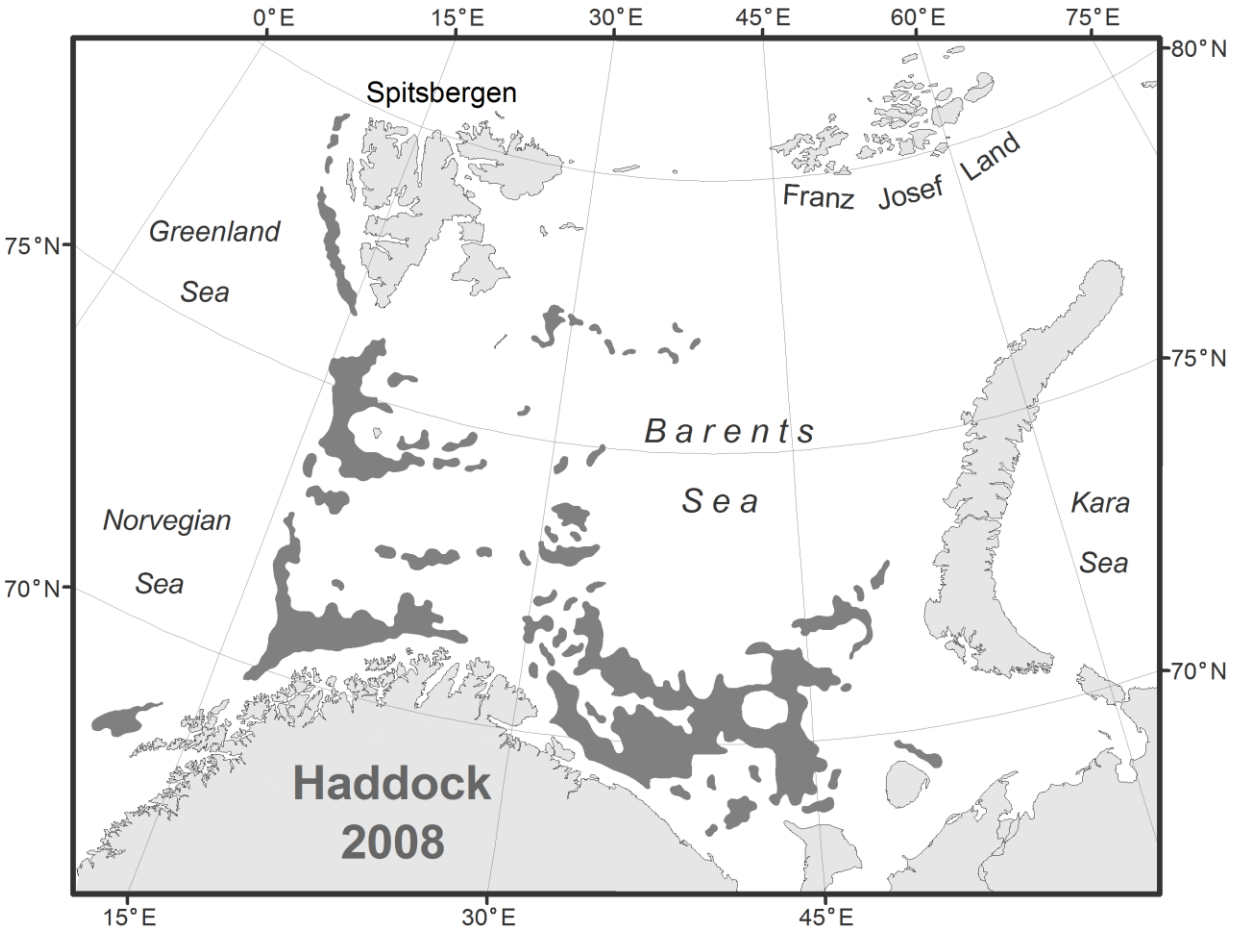

Figure 2.17. Distribution of commercial concentrations of haddock during the warm period of 2008.

Analysis of capelin concentrations for the period of 1977-2010 indicates that fishing areas are not permanent and change from year to year depending on the heat content/thermal conditions of the Barents Sea. In cold years, the main part of capelin fishing was in the north-western and northern areas, whereas in warm years considerable amounts of fish were concentrated in the eastern areas of the sea. For example, during the abnormally cold period of 1980-1981 main concentrations of capelin were found in the areas of Nadezhda, Central Uplands, the Perseus Uplands, and Sudkap trough (Figure 2.18A).

During the warm period of 1992, the concentrations of capelin moved east, and the main fishing areas in September-December were the Novaya Zemlya fishing grounds/bank, the south-eastern part of the Perseus Uplands, and the area of the Admiral Teistvo Peninsula (Figure 2.18B).

Negative anomalies of water temperature in the layer of 0-200 m are likely responsible for a shift in spawning areas of capelin to the west toward the coast of Norway. For example, the main spawning during the cold period of 1980-81 was near the Varanger Peninsula and in the area of Söre/Søre and Fuley fishing grounds/banks. In contrast, the positive temperature

anomalies of water masses contribute to higher migration concentrations of capelin to the coast of the Kola Peninsula. This was observed again during the warm years of the last decade (Matishov and Zhichkin, 2013).

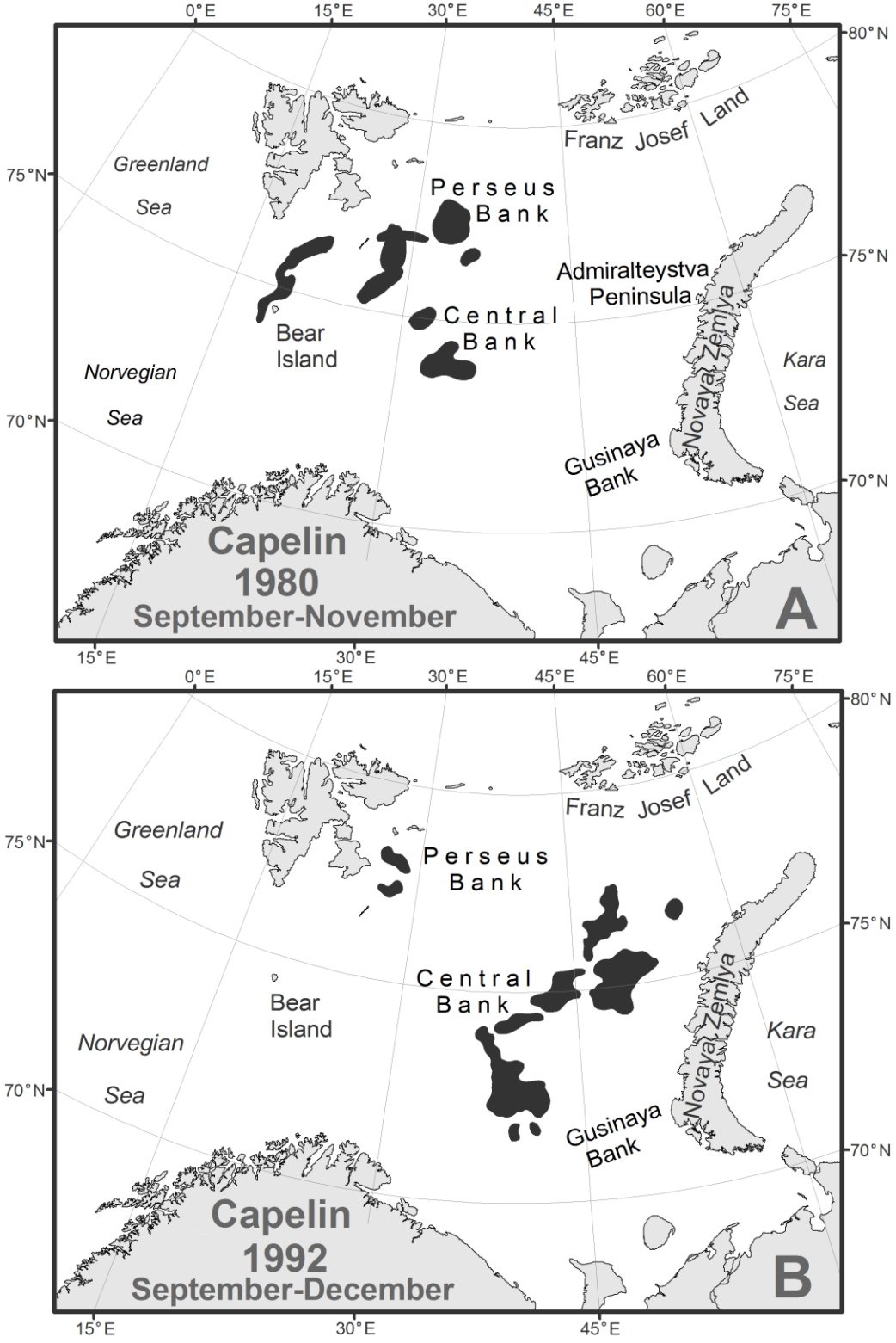

Figure 2.18. Distribution of feeding concentrations of capelin in the Barents Sea LME during the cold period in 1980 (A) and the warm period in1992 (B).

The distribution of commercial concentrations of Polar/Arctic cod is closely linked with water temperature variability. The colder the Barents Sea LME water is in the autumn-winter months, the further west and south of the Novaya Zemlya coast Arctic/Polar cod migrates. For example, during the cold period of 1998 Arctic/Polar cod fishing was on the southern slope of the Gusinaya fishing grounds/bank and near Kolguev Island. During the warm period in 2007, fishing activities occurred in the coastal waters of the Novaya Zemlya (the area of the Admiralty/Admiralteistva Peninsula) and the area adjoining the Kara Strait/Kara Gates (Figure 2.19).

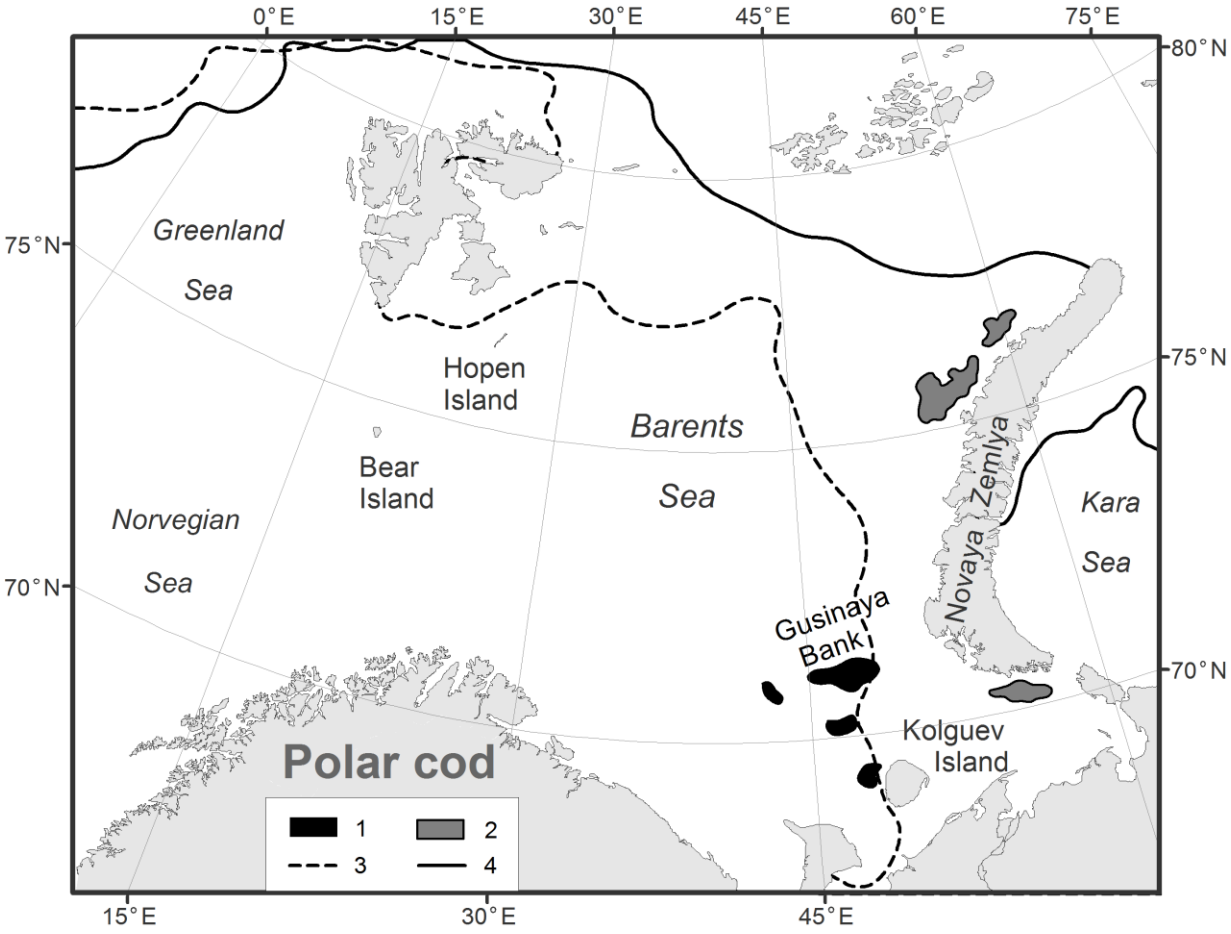

Figure 2.19. Fishing areas for Arctic cod in November during the cold period in1998 and the warm period in 2007. 1 – fishing areas in 1998; 2 – fishing areas in 2007; 3 – ice edge in November 1998; 4 – ice edge in November 2007.

2.2. The Kara Sea LME

Oceanographic database and inventory

The Kara Sea LME oceanographic database contains 38 445 stations covering the period of 1870 to 2013 (Figure 2.20).

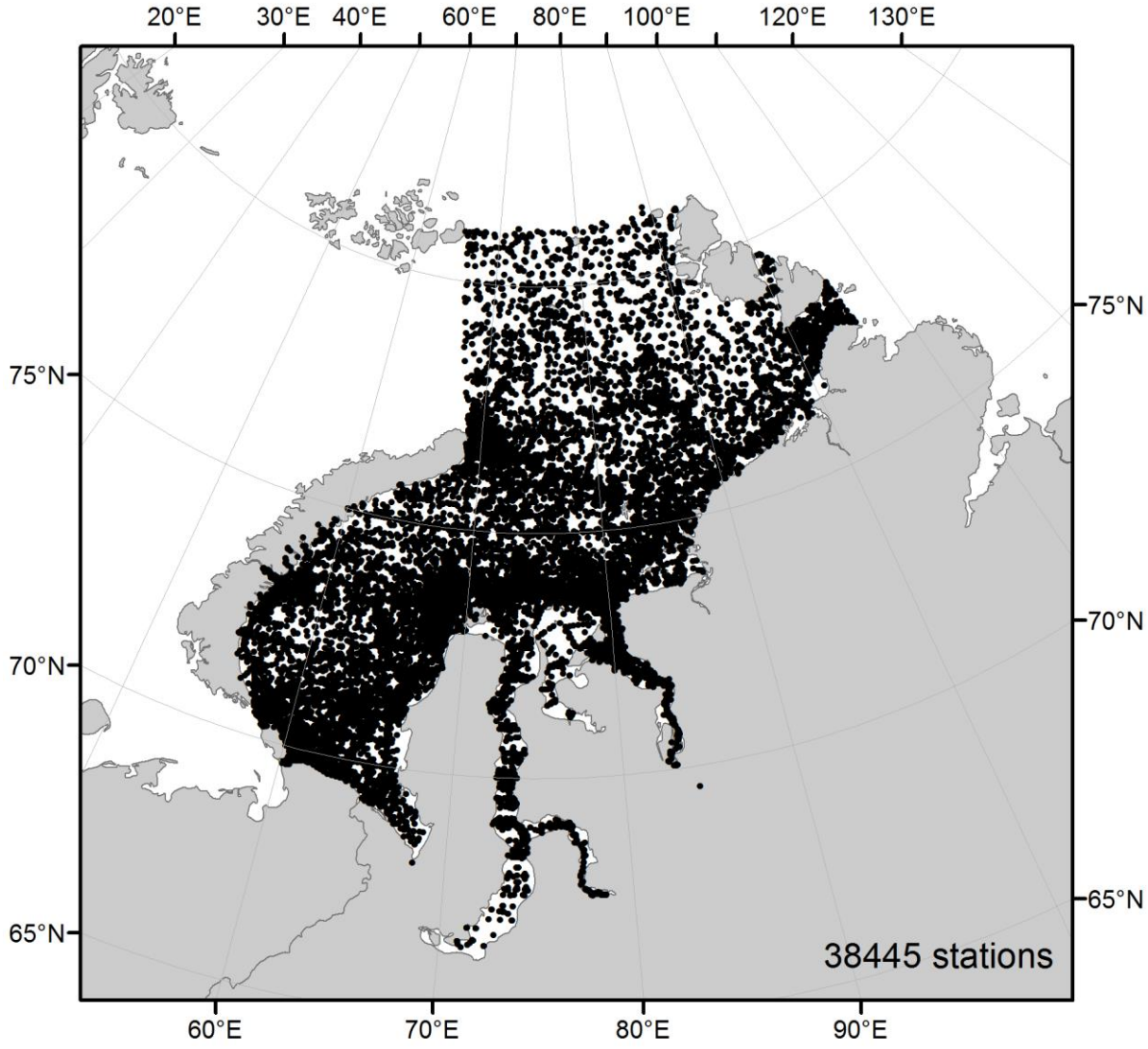

Figure 2.20. Distribution of stations over the Kara Sea LME (1870-2013).

The distribution of stations by years and months is presented in Figure 2.21.

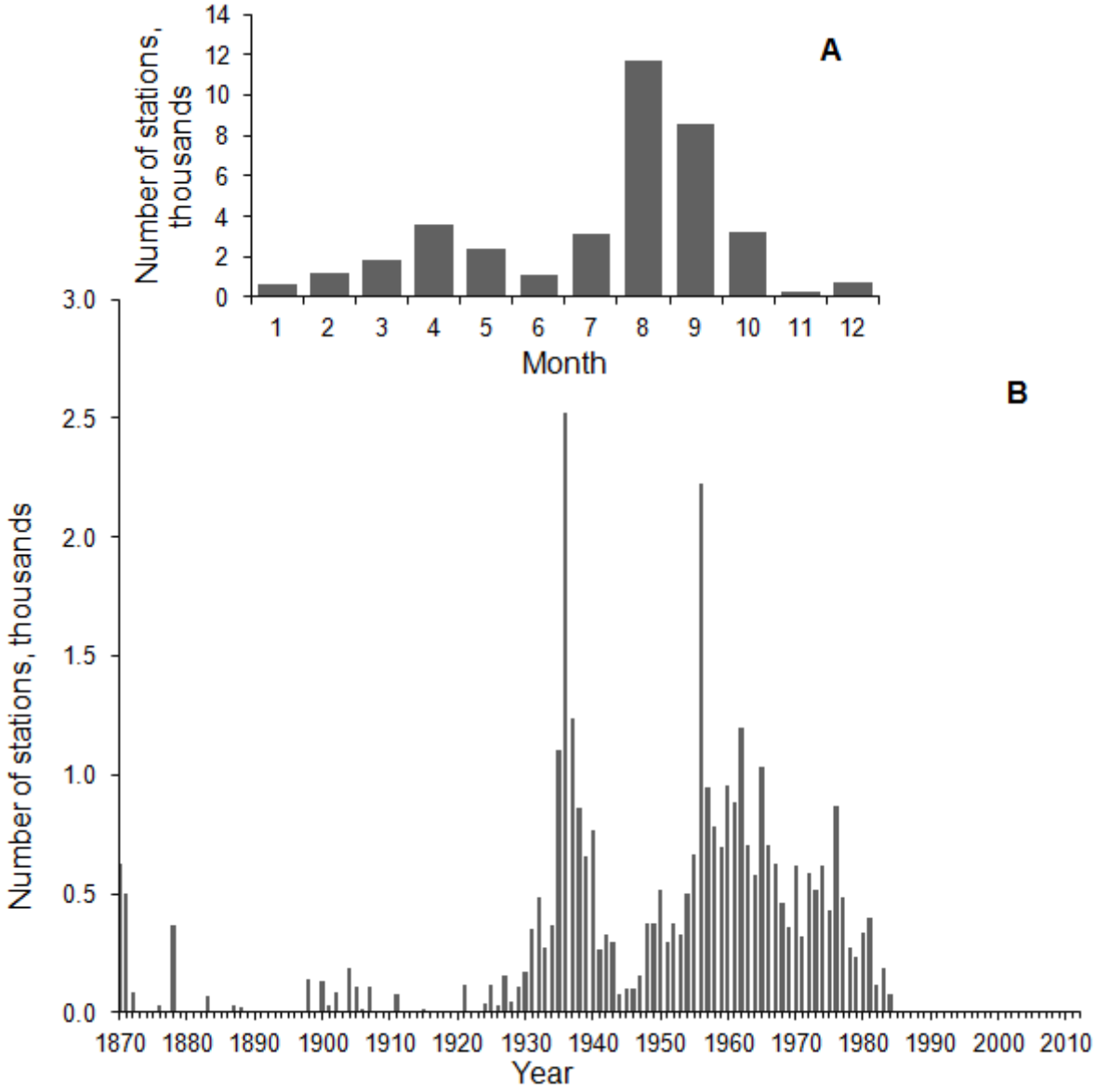

Figure 2.21. Distribution of stations by months (A) and years (B) in the Kara Sea LME database (1870-2013).

The database has been expanded with the addition of 516 stations created after 2000 (Figure 2.22).

The Kara Sea database includes the parameters listed in (Table 2.5).

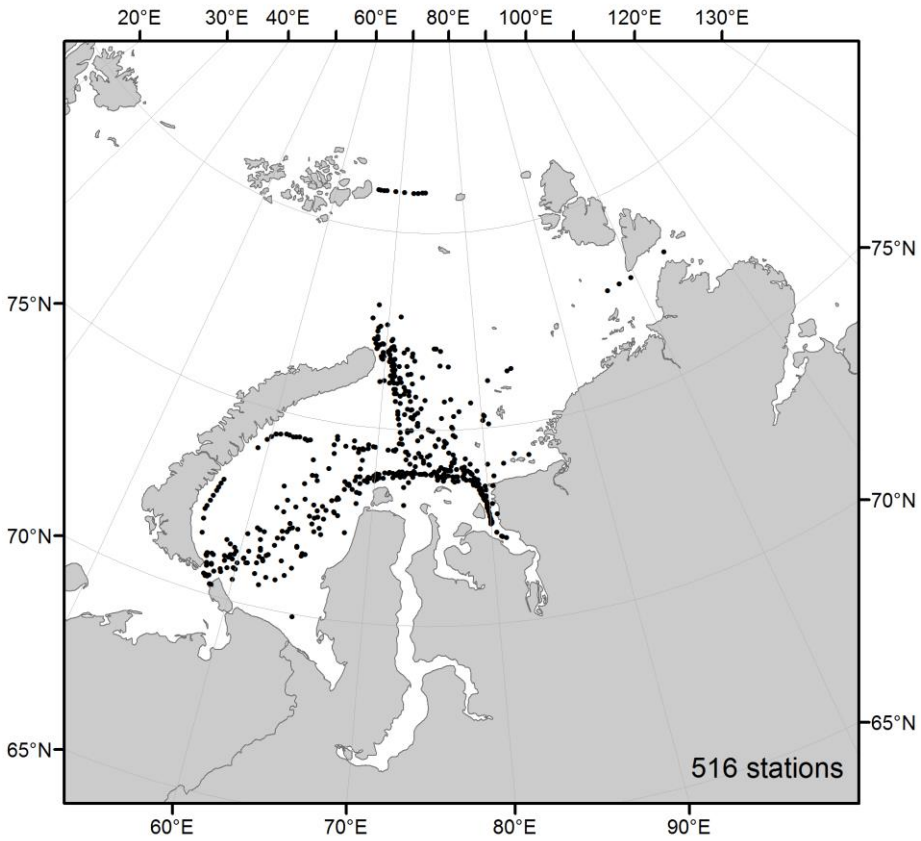

Figure 2.22. Stations in the Kara Sea LME database, made in 2001-2013.

Table 2.5. List of indices included in the Kara Sea LME database

Parameter		**Units of measurement**		**Number of measurements**
Name	**Sign**	**Name**	**Sign**	
Temperature	TEMP	Degree Celsius	C	344,632
Pressure	PRESS	Decibar	DBAR	100,482
Conductivity	COND	Siemens/m	SIEMENS/M	1,627
Salinity	SAL	Units of practical scale of salinity	PSS	306,184
Absolute content of dissolved oxygen	OXY	Ml/l	ML/L	52,916
pH	PH	-	-	28,237
Alkalinity	ALK	Milligram-equivalent/l	MEQ/L	15,224
Nitrates	NO3	Micromole/l	UMOL/L	4,517
Phosphates	PO4	Micromole/l	UMOL/L	17,603
Silicates	SIO4	Micromole/l	UMOL/L	26,852
Chlorophyll	CHL	Mkg/l	UG/L	52

2.3. The Laptev Sea LME

Oceanographic database and inventory

The Laptev Sea LME oceanographic database contains 6 570 stations covering the period of 1878 - 2009 (Figure 2.23).

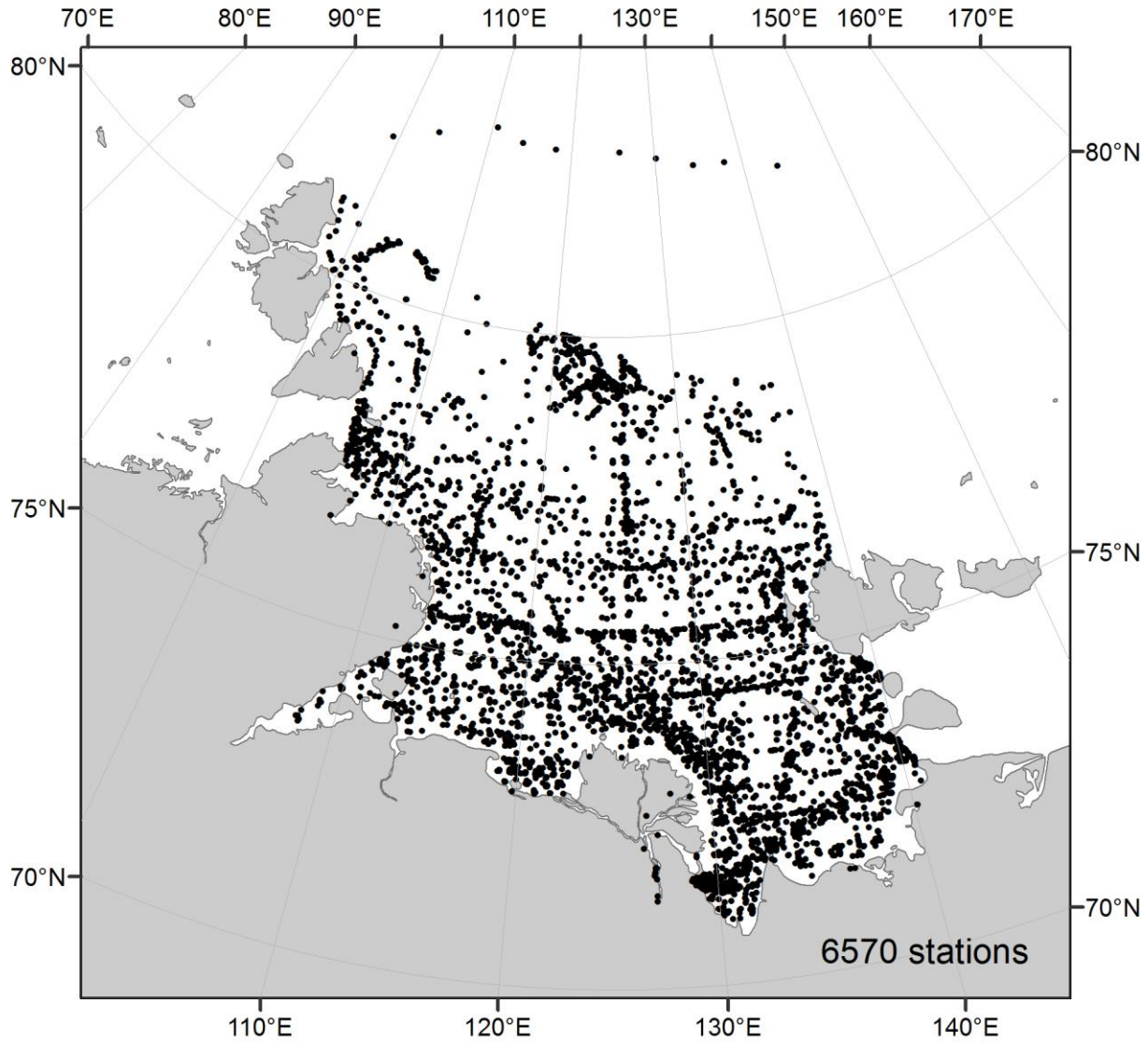

Figure 2.23. Distribution of stations over the Laptev Sea LME (1878-2009).

The distribution of stations by years and months is provided in Figure 2.24.

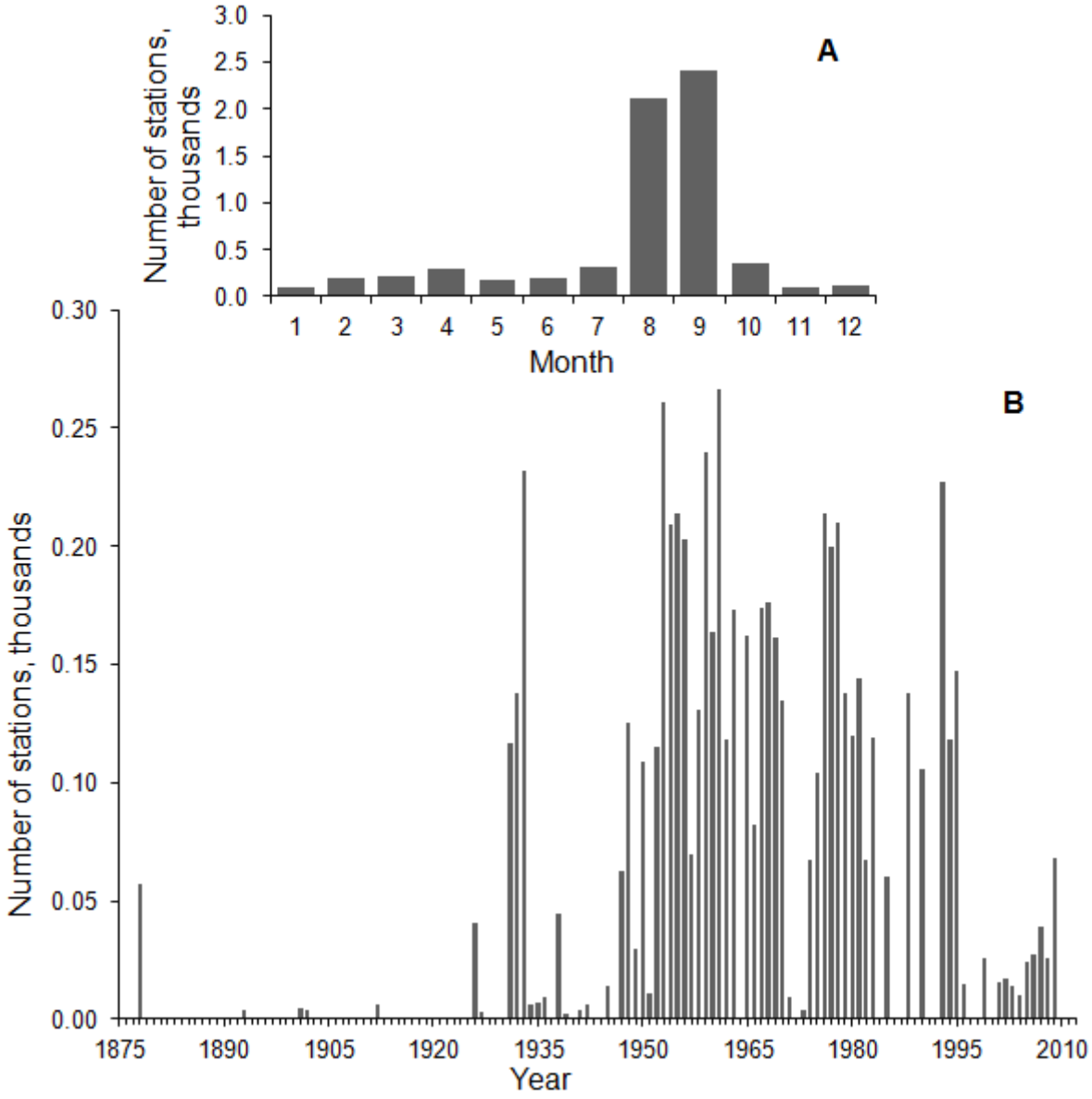

Figure 2.24. Distribution of stations by months (A) and years (B) in the Laptev Sea LME database (1878-2009).

Comparing to the previous versions of the Climatic Atlas of the Arctic Seas (Matishov et al. 2004), the database was expanded to include 241 new stations created after 2000 (Figure 2.25).

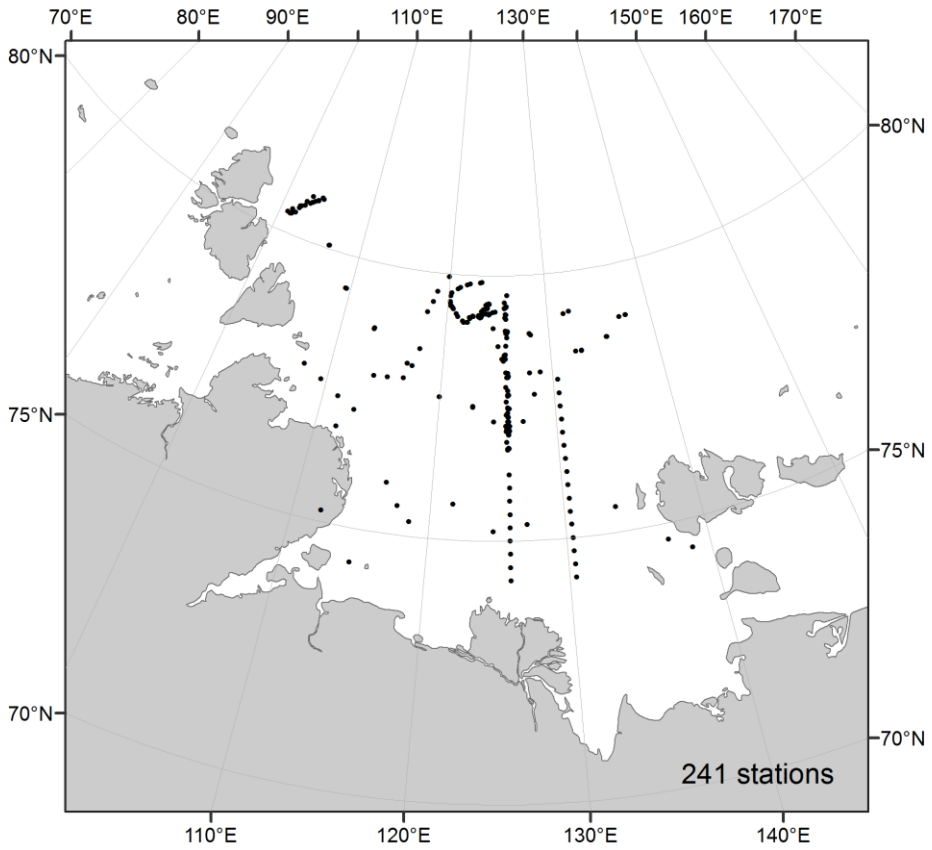

Figure 2.25. Stations in the Laptev Sea LME database, 2001-2009.

The Laptev Sea database includesthe parameters listed in (Table 2.6).

Table 2.6. List of indices included in the Laptev Sea LME database.

Parameter		**Units of measurement**		**Number of measurements**
Name	**Sign**	**Name**	**Sign**	
Temperature	TEMP	Degree Celsius	C	816,933
Pressure	PRESS	Decibar	DBAR	465,541
Conductivity	COND	Siemens/m	SIEMENS/M	50
Salinity	SAL	Units of practical scale of salinity	PSS	808,478
Absolute content of dissolved oxygen	OXY	Ml/l	ML/L	5,101
pH	PH	-	-	4,030
Alkalinity	ALK	Milligram-equivalent/l	MEQ/L	1,203
Nitrates	NO3	Micromole/l	UMOL/L	1,917
Phosphates	PO4	Micromole/l	UMOL/L	3,461
Silicates	SIO4	Micromole/l	UMOL/L	3,723

2.4. The East Siberian Sea LME

Oceanographic database and inventory

The East Siberian LME oceanographic database contains 3,459 stations from 1878 to 2008 (Figure 2.26).

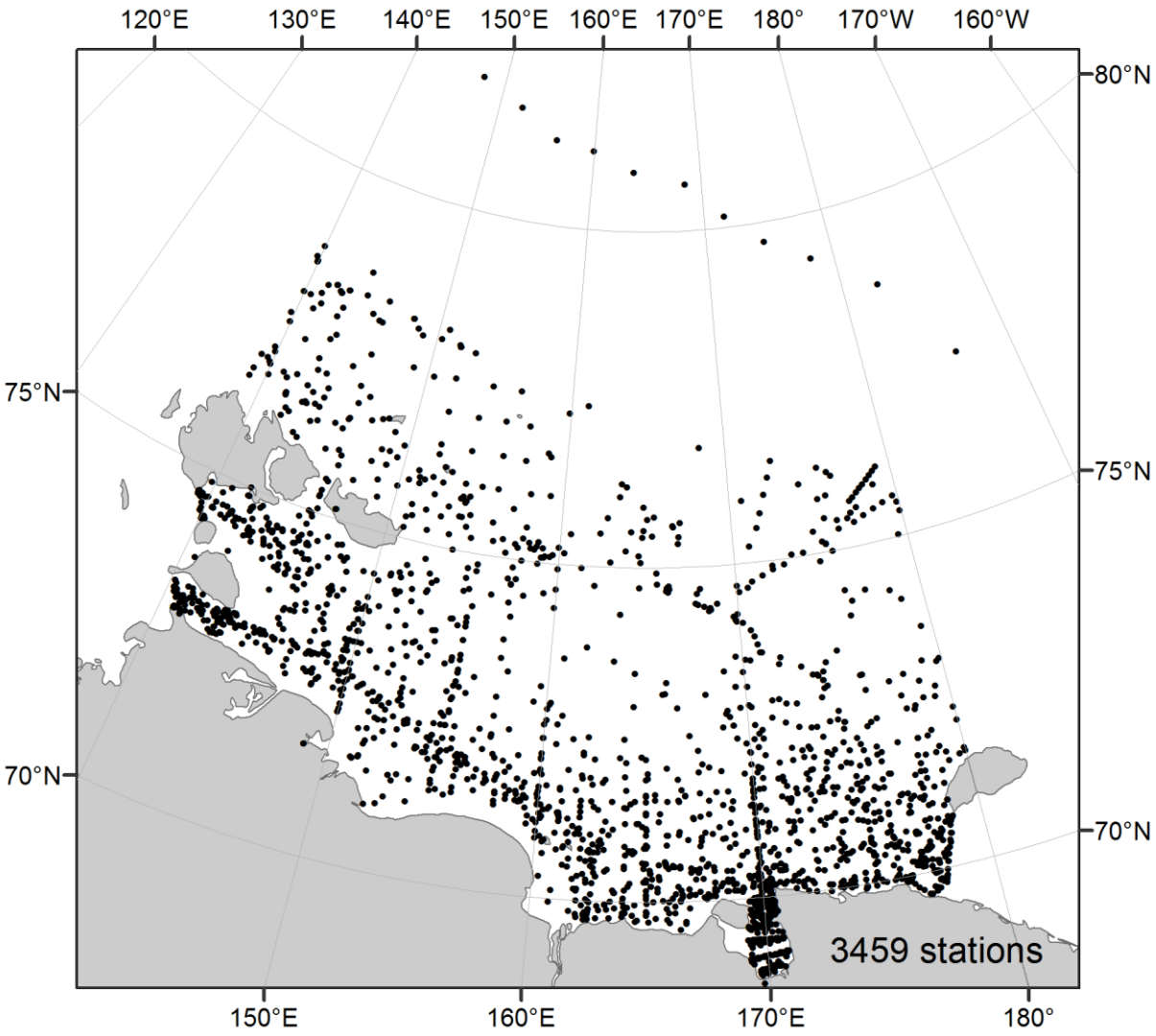

Figure 2.26. Distribution of stations over the East Siberian Sea LME (1878-2008).

The distribution of stations by years and months is provided in Figure 2.27.

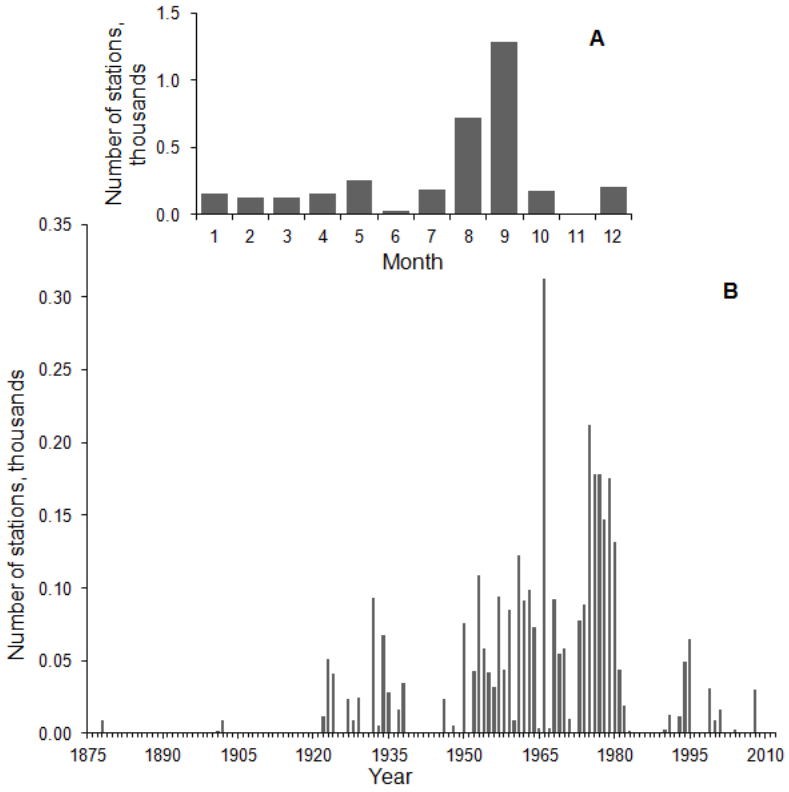

Figure 2.27. Distribution of stations by months (A) and years (B) in the East Siberian Sea LME database (1878-2008).

The East Siberian Sea database includes the following parameters (Table 2.7).

Table 2.7. List of indices included in the East Siberian Sea LME database.

Parameter		**Units of measurements**		**Number of measurements**
Name	**Sign**	**Name**	**Sign**	
Temperature	TEMP	Degree Celsius	C	30,482
Pressure	PRESS	Decibar	DBAR	2,494
Conductivity	COND	Siemens/m	SIEMENS/M	982
Salinity	SAL	Units of practical scale of salinity	PSS	26,785
Absolute content of dissolved oxygen	OXY	Ml/l	ML/L	7,444
pH	PH	-	-	2,217
Alkalinity	ALK	Milligram-equivalent/l	MEQ/L	1,048
Nitrates	NO3	Micromole/l	UMOL/L	1,108
Phosphates	PO4	Micromole/l	UMOL/L	1,434
Silicates	SIO4	Micromole/l	UMOL/L	1,321
Chlorophyll	CHL	Mkg/l	UG/L	17

2.5. The Chukchi Sea LME

Oceanographic database and inventory

The Chukchi Sea LME oceanographic database contains 50 858 stations covering the period of 1849 to 2012 (Figure 2.28).

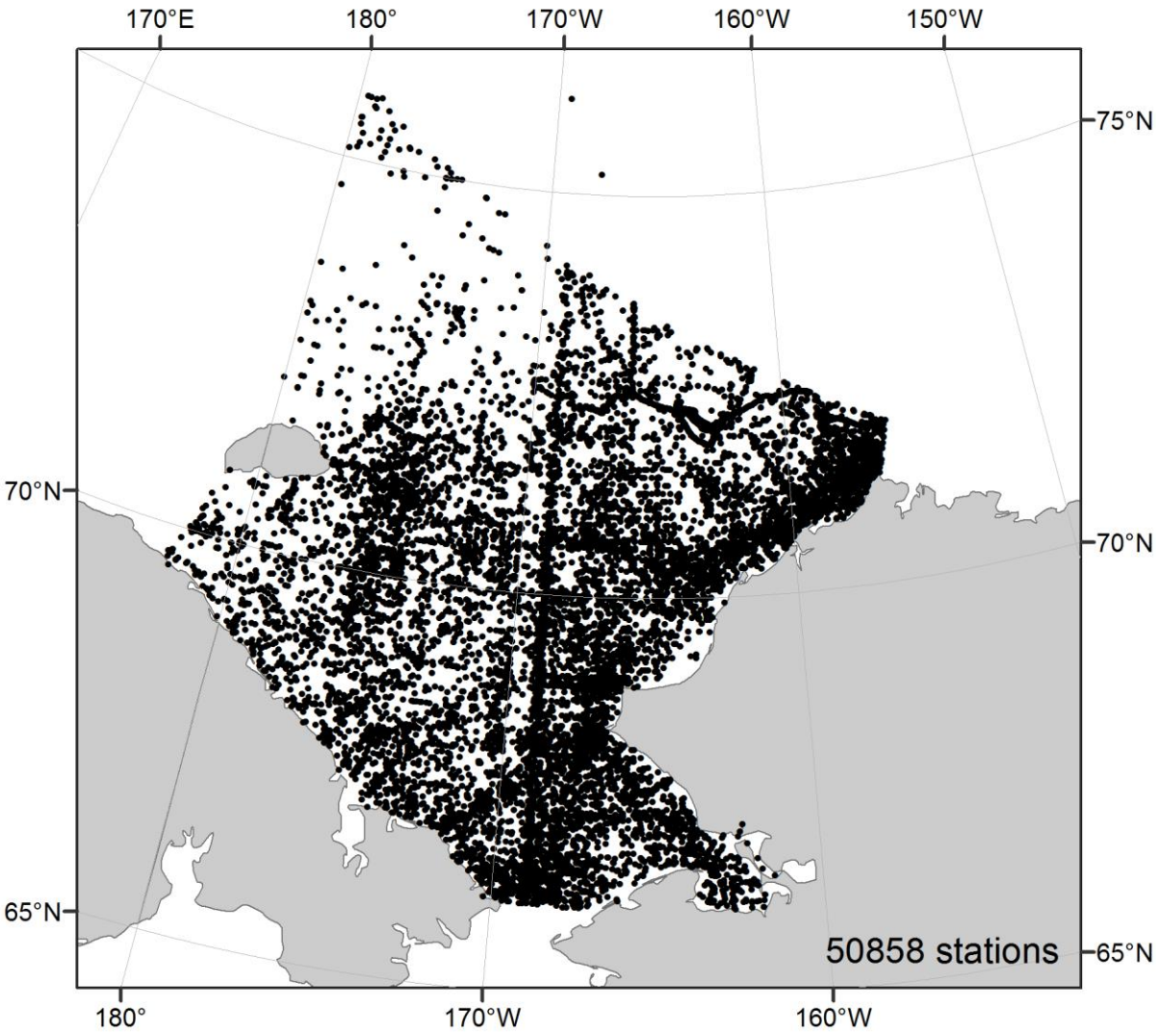

Figure 2.28. Distribution of stations over the Chukchi Sea area (1849-2012).

Distribution of stations by years and months is given at Figure 2.29.

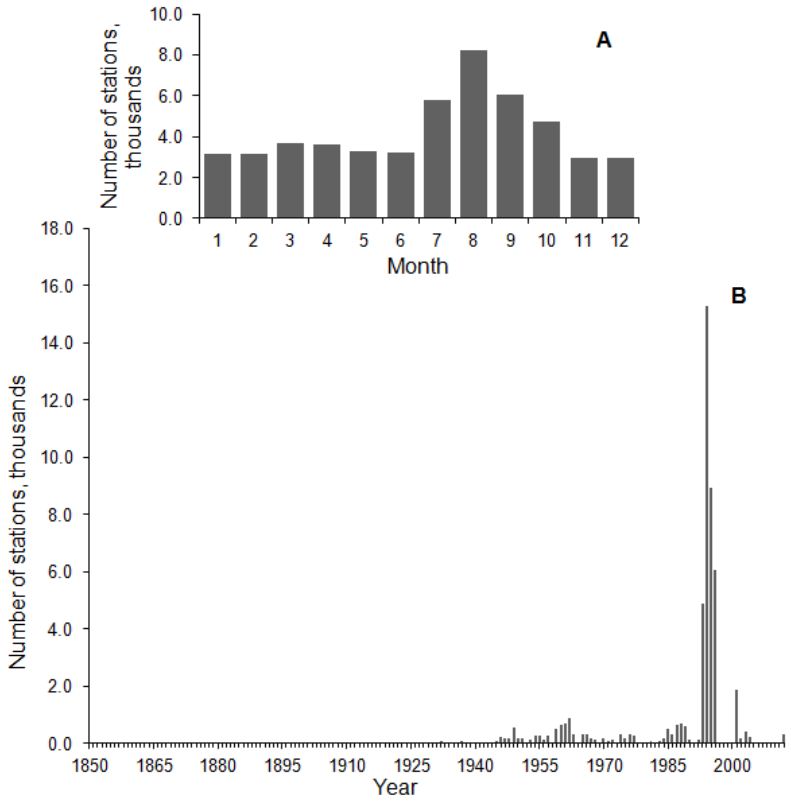

Figure 2.29. Distribution of stations by months (A) and years (B) in the Chukchi Sea LME database (1849-2012).

The Chukchi Sea database includesthe parameters listed in(Table 2.8).

Table 2.8. List of indices included in the Chukchi Sea LME database

Parameter		**Units of measurements**		**Number of measurements**
Name	**Sign**	**Name**	**Sign**	
Temperature	TEMP	Degree Celsius	C	545,946
Pressure	PRESS	Decibar	DBAR	99,426
Conductivity	COND	Siemens/m	SIEMENS/M	40,758
Salinity	SAL	Units of practical scale of salinity	PSS	484,421
Absolute content of dissolved oxygen	OXY	Ml/l	ML/L	41,106
pH	PH	-	-	855
Alkalinity	ALK	Milligram-equivalent/l	MEQ/L	314
Nitrates	NO3	Micromole/l	UMOL/L	4,762
Phosphates	PO4	Micromole/l	UMOL/L	7,080
Silicates	SIO4	Micromole/l	UMOL/L	7,970
Chlorophyll	CHL	Mkg/l	UG/L	16,901

2.6. The East and West Bering Sea LMEs

Oceanographic database and inventory

The East and West Bering Sea LMEs oceanographic database contains 81 298 stations from 1827 to 2012 (Figure 2.30a, Figure 2.30b).

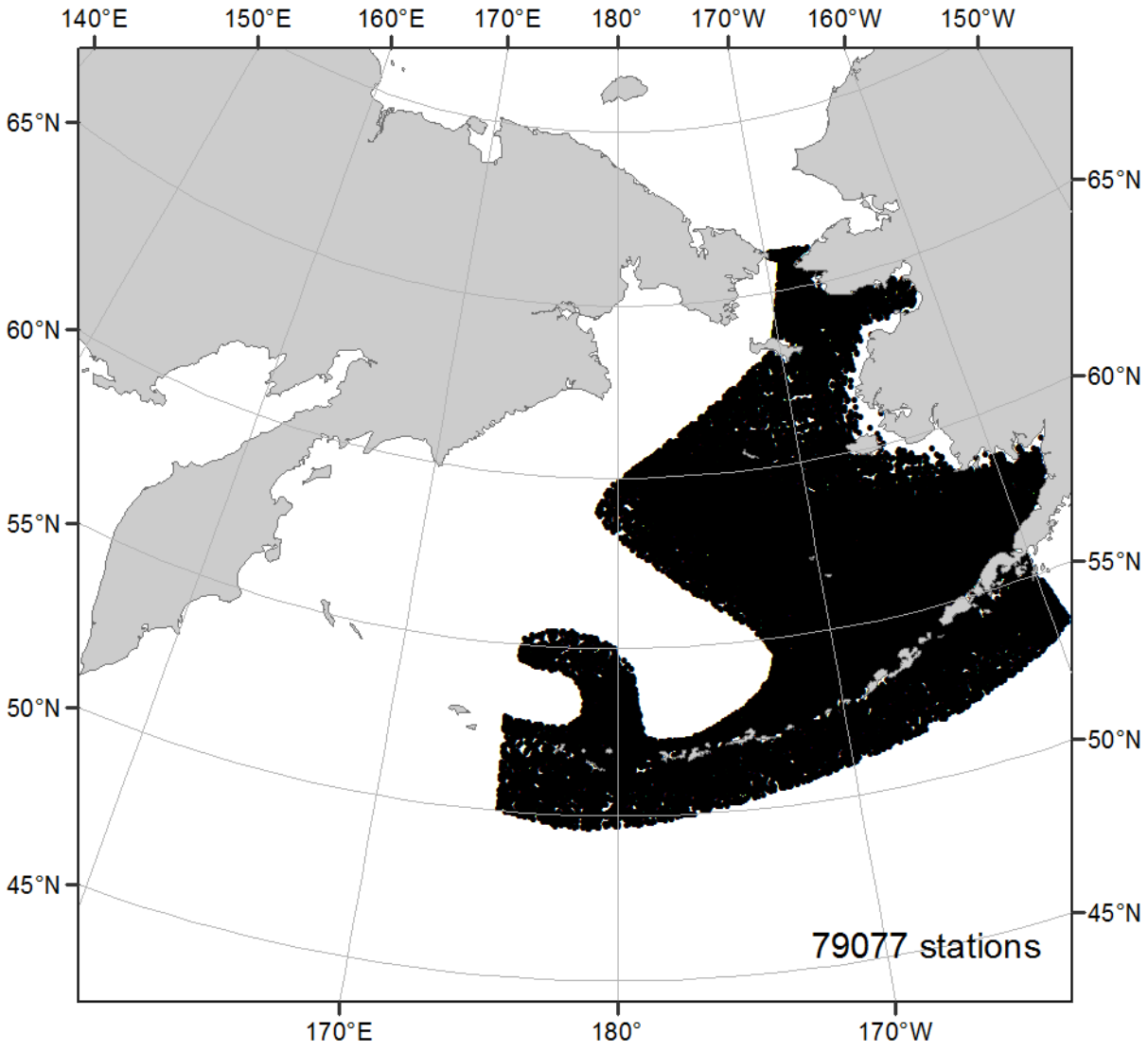

Figure 2.30a. Distribution of stations over the East Bering Sea LME (1827-2012).

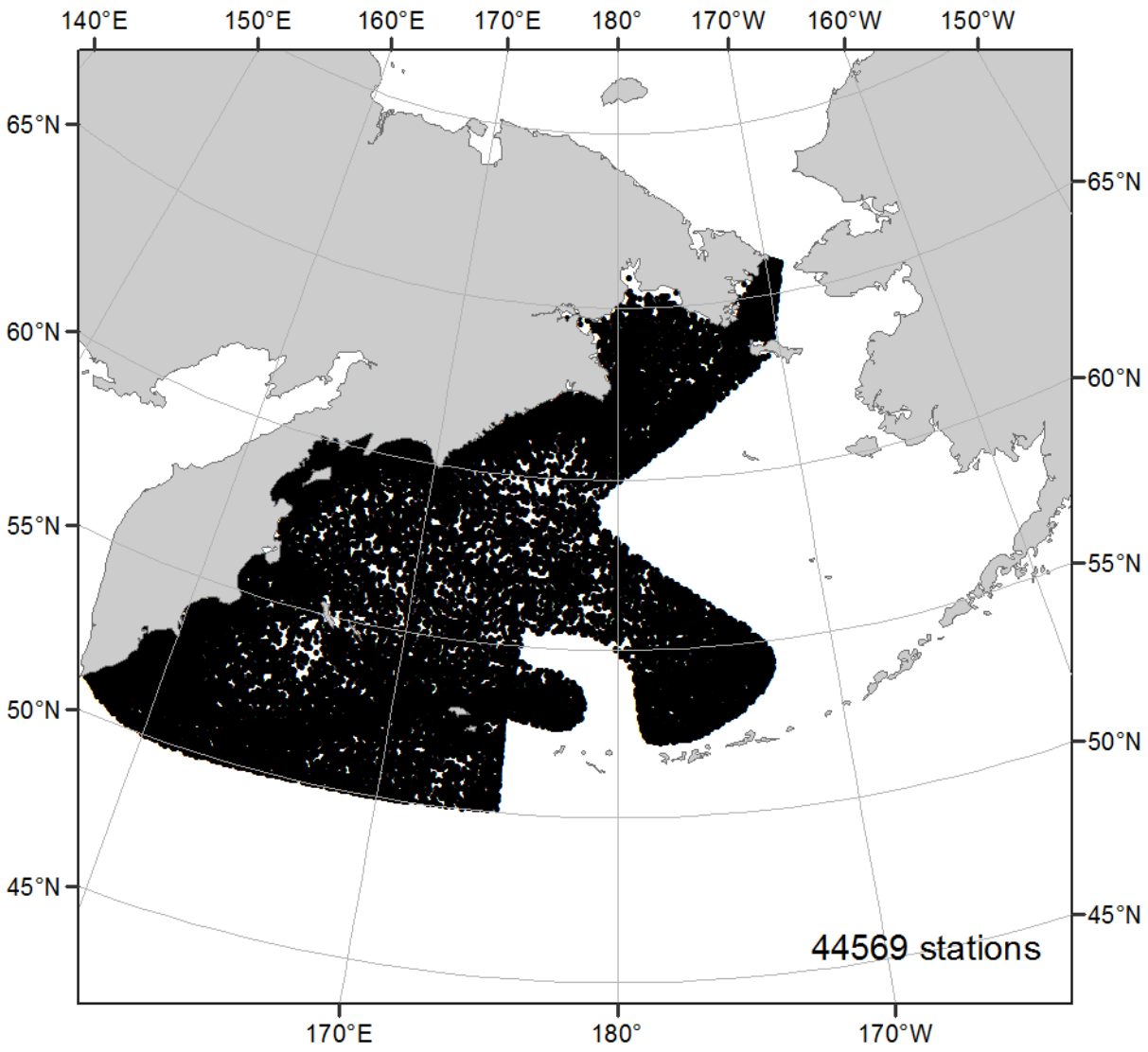

Figure 2.30b. Distribution of stations over the West Bering Sea LME (1827-2012).

The distribution of stations by years and months is provided in Figure 2.31a, 2.31b, and 2.31c.

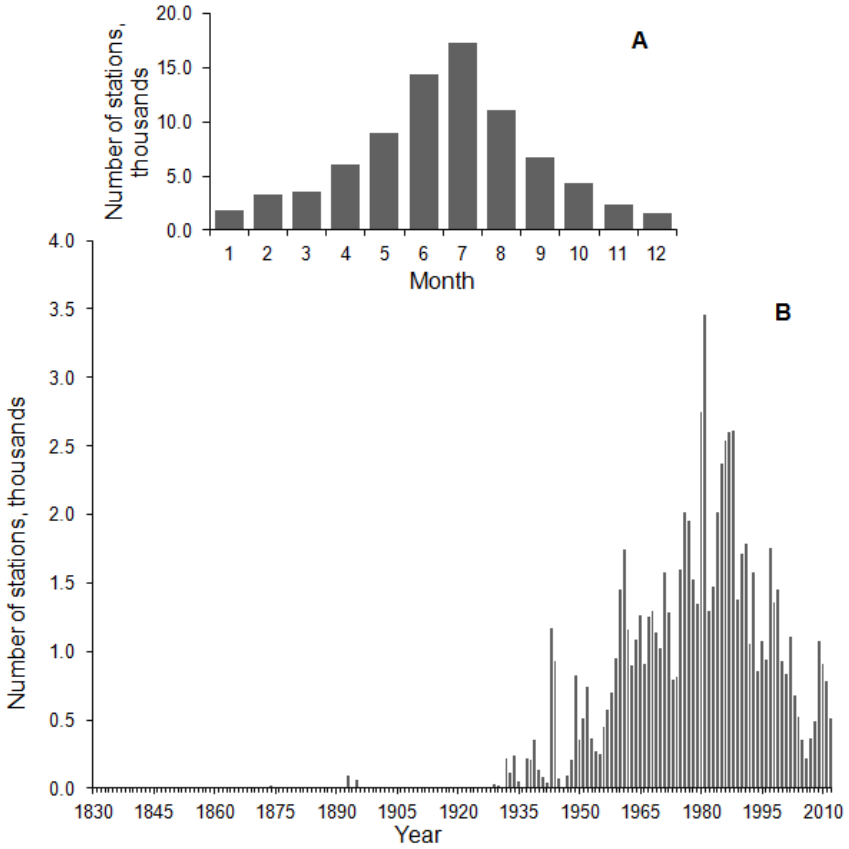

Figure 2.31a. Distribution of stations by months (A) and years (B) in the combined East and West Bering Sea LMEs database (1827-2012).

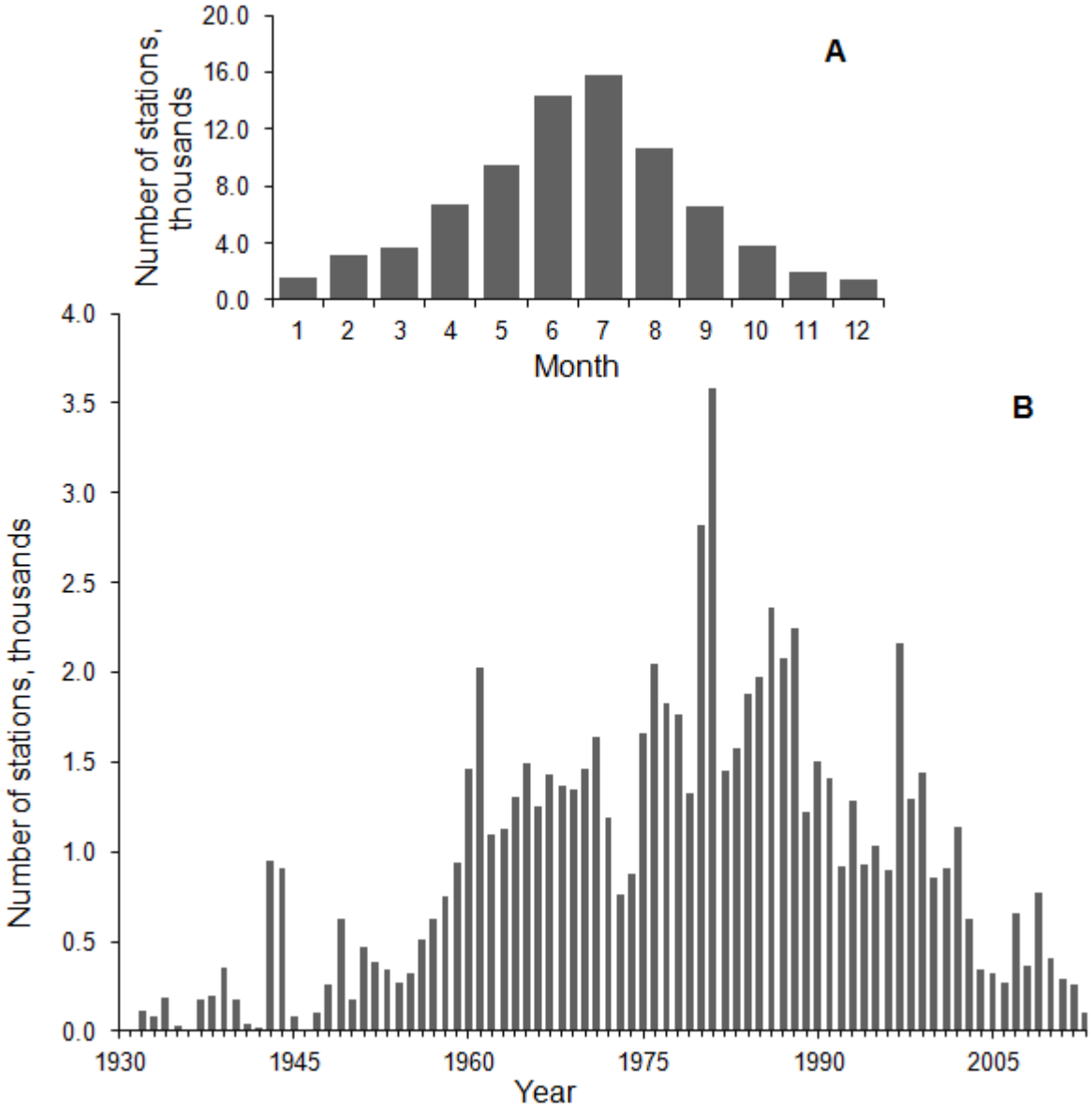

Figure 2.31b: Number of stations in the East Bering Sea LME.

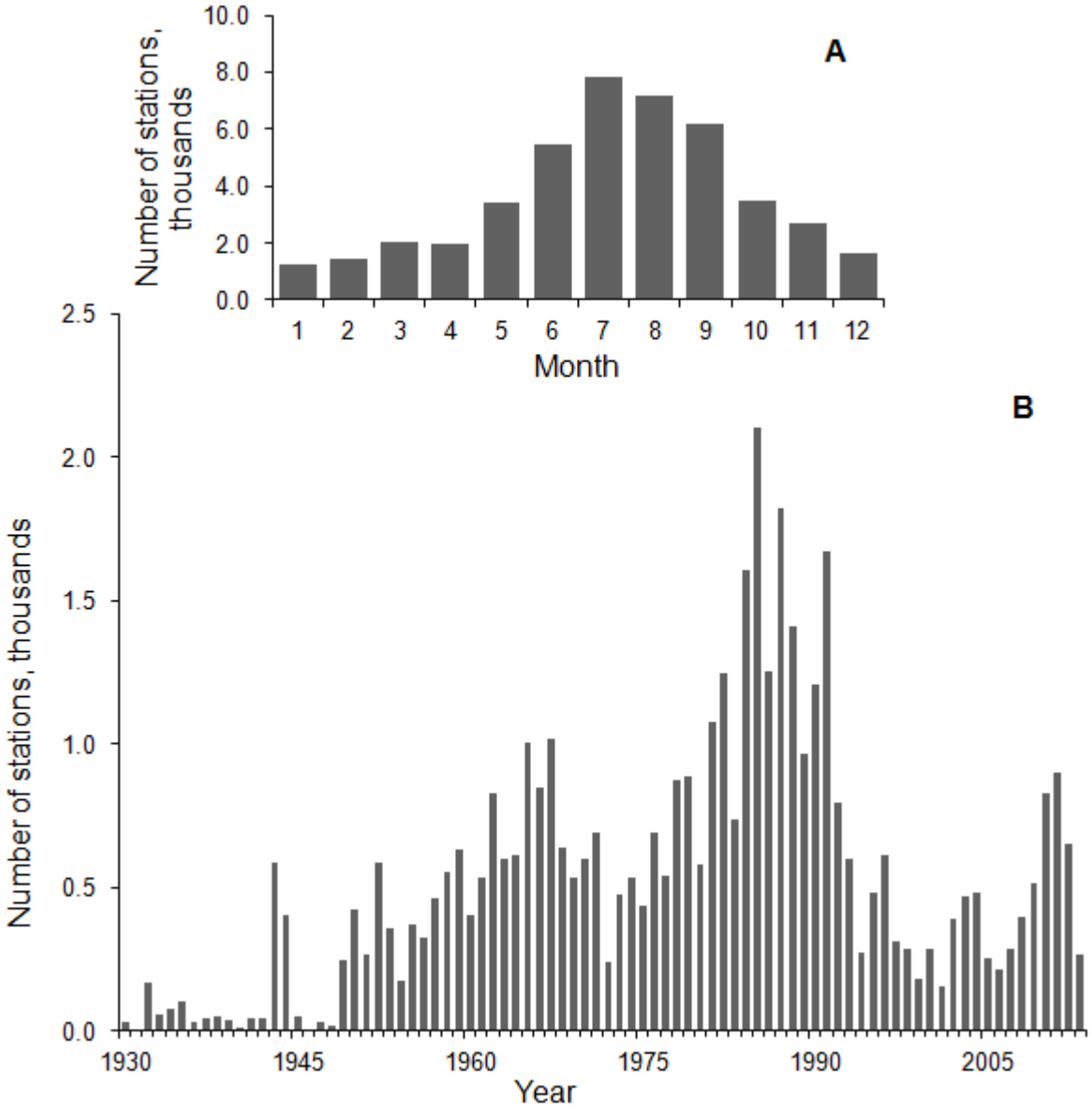

Figure 2.31c: Number of stations in the West Bering Sea LME.

The combined East and West Bering Sea LME database includes the parameters listed in (Table 2.9).

Table 2.9. List of indices included in the East and West Bering Sea LME database

Parameter		Units of measurement		Number of measurements
Name	**Sign**	**Name**	**Sign**	
Temperature	TEMP	Degree Celsius	C	5,921 723
Pressure	PRESS	Decibar	DBAR	2,384,033
Conductivity	COND	Siemens/m	SIEMENS/M	37,293
Salinity	SAL	Units of practical scale of salinity	PSS	3,695,074
Absolute content of dissolved oxygen	OXY	Ml/l	ML/L	289,632
pH	PH	-	-	7,785
Alkalinity	ALK	Milligram-equivalent/l	MEQ/L	3,119
Nitrates	NO3	Micromole/l	UMOL/L	20,269
Phosphates	PO4	Micromole/l	UMOL/L	35,877
Silicates	SIO4	Micromole/l	UMOL/L	33,073
Chlorophyll	CHL	Mkg/l	UG/L	102,740

Variability of East and West Bering Sea LMEs ice conditions in the second half of the 20th century – early 21st century

Based on available data from the combined East and West Bering Sea ice conditions from 1960 to the present, the state and progression of ice cover have been assessed. The probability of existence of a directed/focused trend in the ice processes was analyzed and a steady long-term decrease of the ice extent in the sea was noted. There appears to be quasi-periodic constituents in the ice processes for periods of 2-3 years, 12-14 years, and longer.

Initial data

The following initial data were used when developing the archives on ice conditions of the Far Eastern seas:

- Charts of ice aerial surveys (1960-1990);
- Satellite images of ice cover of the seas obtained with the help of the satellite series, such as “NOAA”, “Meteor”, ”Kosmos”, “Terra”, and “Landsat” (1972-2012);
- Hydro-meteorological monthly data on an annual basis for the Far East.

Information on ice cover was mapped and preliminarily analyzed. Data on the ice conditions of the seas before 1989 was obtained from ice aerial surveys as well as satellite observations. There are usually several charts of images of ice cover registered during a 10 day period. Data from coastal observations at the hydro-meteorological stations and sites were averaged for a particular set of 10 days for the entire sea. In other words, the minimum discreteness of ice charts covering the entire sea area and presenting almost continuous series for

the ice period was 10 days. Higher time resolution (i.e. longer than 10 days), considering the difficulty of gathering ice information (e.g. vast water areas, unfavourable weather conditions) is possible only for some local water areas. The ice extent values (the ice covered area in % of the total sea area) were determined by the mean (i.e. from the 10-day intervals) charts of ice conditions. In addition, ice edge location was registered, and values of various ice characteristics (e.g. density and closeness of ice, age, ice forms, hummocks, snow cover) were recorded. These datasets regarding the state of sea ice cover were synthesized and added to the initial data archives (Plotnikov 2002). Thus, a series of data on the sea ice conditions covered 52 years (1960-2012). Ice extent has been the research focus as an easily determined index of ice state, and in the more general case, of the climatic state. Research time interval covered the period of December to May when the ice extent variability is at its maximum. During the rest of the year, due to specific climatic features, the abundance of ice in the sea is considerably lower. Correspondingly, ice extent variability during the rest of the year is also low. A long-term series of data on the ice conditions in the Far Eastern seas allowed statistical processing of available ice information. Statistical processing was applied to analyzing the curves of the seasonal ice extent patterns and their variability (Figure 2.32), designating winter type according to ice conditions characteristics (Table 2.10) as well as assessing long-term variability of ice conditions of the sea (Figure 2.33-2.35, Table 2.11).

Results

General characteristics of ice conditions in the East and West Bering Sea LMEs

The ice period in the combined East and West Bering Sea LMEs lasts for 30 sets of 10-day periods on average, though may vary within a wide range depending on the severity of winter. Ice formation usually begins in October in the northern areas of the sea, and ice can be observed in the middle of October in some bays. Ice formation processes become stronger in December and January and move to the south covering the areas along the coasts. From February to April, the ice cover reaches its maximum (in February/March – during mild winters, in February/April – during moderate winters, and in March/April – during severe winters) and covers the entire northern half of the sea and the areas adjacent to the eastern coast of the Kamchatka Peninsula down to its southern tip. The sea begins to become ice free in the second half of April. In May and the first half of June, the ice edge rapidly shifts to the North. In June – July, the sea usually becomes free of ice. In extreme situations (winters with very thick ice conditions), the ice in the sea (the Western Bering Strait) may be registered all year round.

Characterizing winter types by ice conditions (Table 2.10)

Characterizing winter types by ice conditions allows patterns and trends to be noted. The mean ice extent for the season (December-May) was used as the parameter of classification, which was determined by the ratio: $L_j = \sum_{i=1}^{p_j} L_{ij}$ /p_j, with L_j being the mean ice extent of *j* year; L_{ij} – ice extent of *i* 10-days *of j* year; p_j, – number of 10-day periods in the ice season of j year (p_j = 15, December-May). Winters with the prevailing majority of 10-day intervals of ice extents during the ice period fitting the interval of $\overline{L} \pm 0.683\sigma_J$, where σ_j is standard deviation of ice extent in j 10-day periods, were considered as the ice extent winters.

Table 2.10. Catalogue of winter types by the mean ice extent in the combined East and West Bering Sea LMEs*.

Types of winter		
Severe	Moderate	Mild
1964-1965	1960-1963	
	1966	1967
	1968-1970	
1971-1972	1973-1974	
1975-1977		1978-1979
	1980-1985	1986
	1987-1988	1989
	1990-1996	1997
	1998	
1999	2000	2001-2005
	2006-2007	
2008-2010	2011	
2012-2013		

*Ice extent values were averaged for the period of December to May

Seasonal variability

Seasonal fluctuations of the ice cover have a clear annual period. These fluctuations are influenced by hydro-meteorological factors. Seasonal patterns of ice processes in the combined East and West Bering Sea LMEs are demonstrated in Figure 2.32. These patterns were assessed through calculations for maximum and minimum, and mean values of ice processes.

The combined East and West Bering Sea LMEs is characterized by an annual pattern of ice extent and gradual increase of variability until the end of the period of maximum development of ice cover. The variability maximum is in April and is associated with the beginning of sea ice thaw/melt.

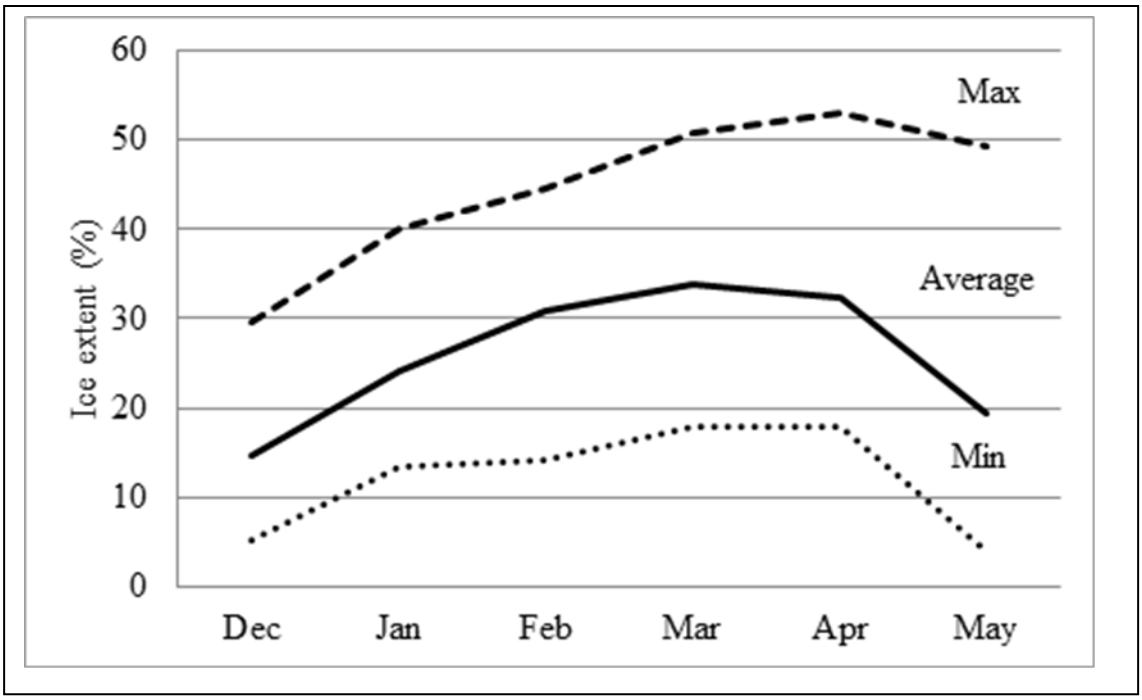

Figure 2.32. Seasonal distribution of the mean, maximum, and minimum ice extent in the combined East and West Bering Sea LMEs.

Inter-annual variability

The long-term distribution of the mean annual, maximum, and minimum ice extent in the combined East and West Bering Sea LMEs is presented in Figure 2.33.

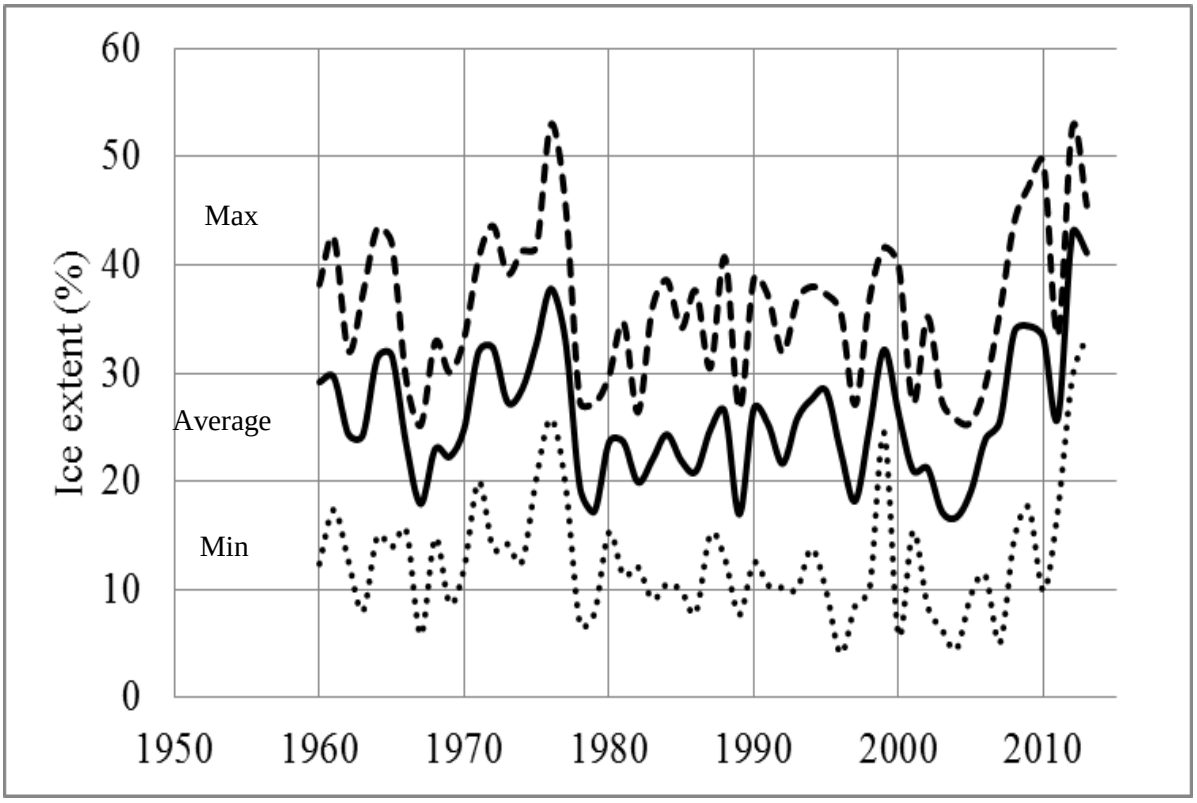

Figure 2.33. Long-term distribution of the mean annual, maximum, and minimum ice extent in the combined East and West Bering Sea LMEs.

By the distribution of the mean one, the trend component hypothesis was checked.

For that purpose, a linear filter was used, distinguishing a linear function of time φ (t) [3] in the white noise mixture. The weight function of the filter is as below:

$$h(n-1) = \frac{6}{n^2}\left(\frac{2t}{n} - 1\right), \quad t=1,2,...,n' \qquad (1)$$

and the standard error of the angle of inclination α is

$$\sigma_\alpha = \left(\frac{12\sigma_t^2}{n^3}\right)^{1/2}, \qquad (2)$$

where σ^2_t – dispersion of the analyzed time series L(t).

Calculated parameters of the long-term variability of the mean annual ice extent and distribution of its monthly components (December-May) are presented in Table 2.11.

In the table, L is the mean value of the analyzed time series L(t), α, σ_α - parameters of the linear trend (an angle of inclination and a standard error of the assessment of the angle of inclination). By the values of α/σ_α relation, the probability of existence of a linear trend in the long-term distribution of ice extent was assessed.

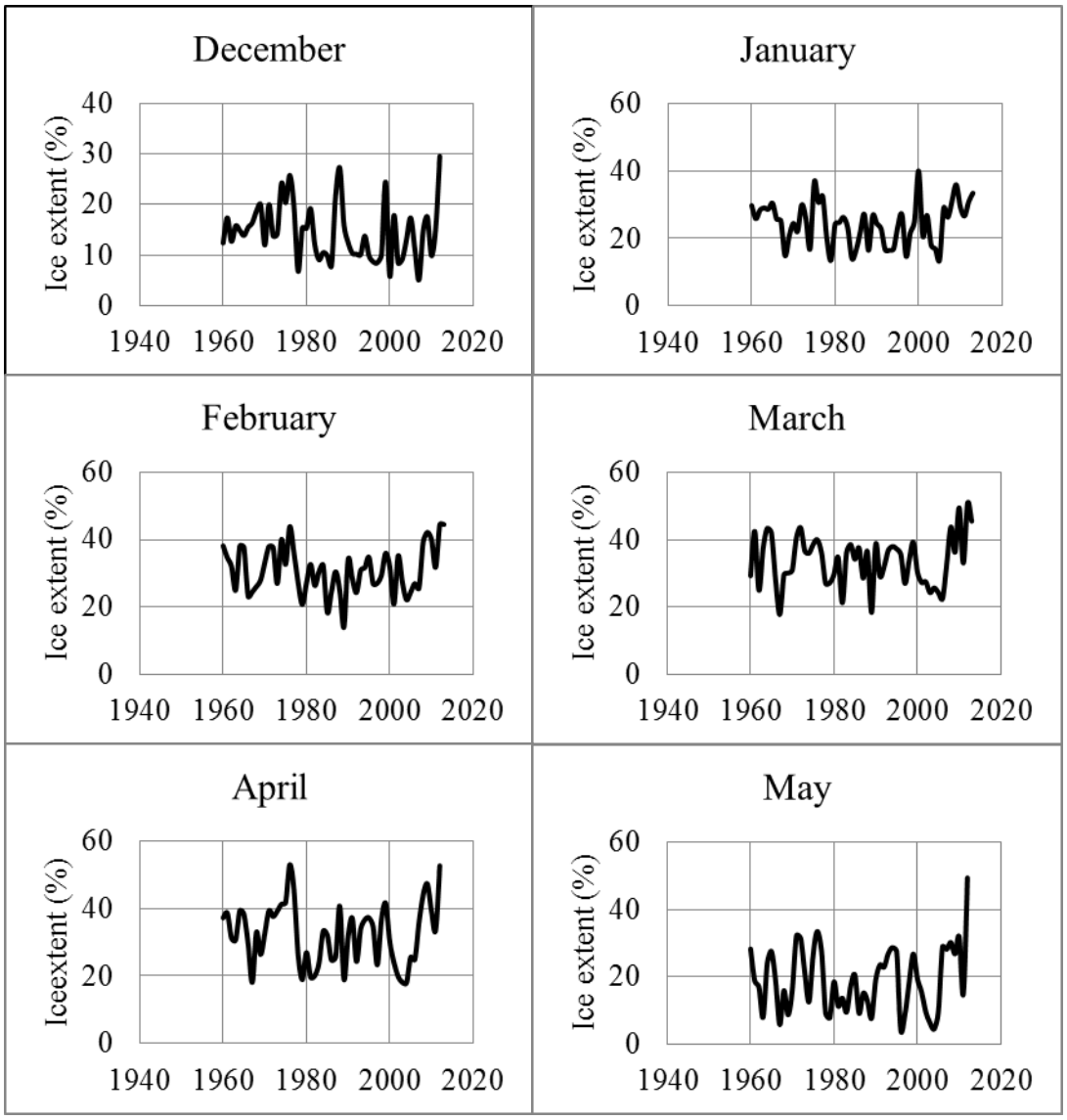

Figure 2.34. Long-term distribution of monthly values of ice extent in the combined East and West Bering Sea LMEs.

Table 2.11. Statistics calculated to profile the distributions of ice extent.

	L	α	σ_α	Probability of the linear trend (%)
Mean long-term	25.8	0.011	0.055	Less than 16%
Mean for December	14.3	-0.079	0.044	93%
Mean for January	24.2	-0.011	0.056	16%
Mean for February	30.6	-0.004	0.06	5%
Mean for March	33.4	0.007	0.065	9%
Mean for April	31.4	-0.095	0.081	75%
Mean for May	19.1	0.07	0.086	58%

Based on the assessments calculated (Figure 2.33-2.34, Table 2.11), it is possible to conclude that no directed/focused long-term trend of the ice conditions has been registered in the combined East and West Bering Sea LMEs (the probability of trend is less than 16%). This is associated with high values of ice extent in the sea for the last five years starting with 2008. This is likely associated with the geography and geology of the Aleut depression. The depression stimulates the inflow of cold air masses into and over the combined East and West Bering Sea LMEs. The only exception is the initial period of ice cover formation (December), when the negative trend (ice extent decreases in the long-term scales) is distinct (the existence probability is about 93%). This causes some slowing down of the ice formation in the initial period (December).

Different assessments of the trend probability during the analyzed periods reflect the change in seasonal processes in the combined East and West Bering Sea LMEs for the last 52 years. The following analysis of the presence of possible quasi-periodical components in the formation of long-term variability of ice conditions in the combined East and West Bering Sea LMEs was conducted using statistical assessments of frequency spectra (Figure 2.35). The analysis of spectral components of the ice extent series demonstrated that quasi-periodical components were periods of 2 years, 3-5 years, and 12-14 years (Figure 2.35). Moreover, the input of high-frequency fluctuations, covering purely accidental and quasi-periodical components within periods of up to two years is about 20-25%.

Considering the volume of available data (1960-2012), it is possible to distinguish 2-year and 3-5-year components in the ice processes. The first is usually connected with the variability in the interaction of the main action centres of the atmosphere, though specific physical causes of the phenomenon have not been fully determined (Plotnikov 2002; Maksimov 1977). Fluctuations of 3-5 years are probably the response to the disturbances in the ocean-atmosphere system. For example, periods of 3.5 years and connected with El Niño phenomenon. The peaks of spectral density within the periods of 12-14 years are likely connected to heliogeophysical factors. A pronounced impact of the powers of heliogeophysical nature, registered in many climatic systems, is the significant change in ice extent variability in the Bering Sea (Plotnikov 2003; Maksimov 1977). Spectral expression is based on the decomposition of the initial distribution

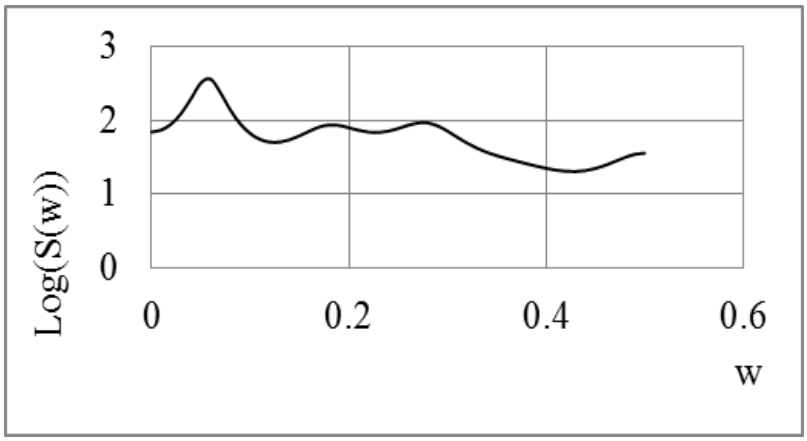

Figure 2.35. Spectral assessments *(Log(S (ω))* of the mean ice extent distribution in the combined East and West Bering Sea LMEs ($\omega = \tau^{-1}$, where τ is a period).

(ice extent in our case) into a Fourier series. The input of each harmonious component to the general variability of the process is assessed. The peaks at certain frequencies reflect the most significant inputs. Correspondingly, the periods of dominating harmonious components are determined as $T=1/\omega$. Notably, the peaks at the frequencies of 0.07-0.08, 0.18-031, and 0.5, correspond to the periods of 12-14 years, 3-5 years, and 2 years (see Figure 2.35).

Inter-annual variability of the thermal state of the East and West Bering Sea waters: 1955-2012

The East and West Bering Sea LMEs are in the subarctic, the main feature of which is the cold and warm intermediate layers (Luchin et al. 1999) (for example Arsen'ev, 1967). The elements of the subarctic are more profound in the deep-water depression of the West Bering Sea. The profiles of vertical distribution of temperature indicate that the combined East and West Bering Sea waters may be divided into several layers (Figs. 2.36, Figure 2.37).

A cold intermediate layer is an important part of the active layer. Figure 2.37 demonstrates that the center of the layer sits between the horizons of 50 and 150 m. It is formed as the result of two processes: the cooling of the active layer of water in autumn and winter, and its heating in spring and summer. Above and below the cold intermediate layer are the layers with increased vertical gradients of temperature (Figs. 2.36, Figure 2.37). The lowest temperature values in the centre of the cold intermediate layer (down to -1.2.-1.5°C) are observed in the Bering Sea shelf areas to the south and south-west of St. Lawrence Island (Figure 2.38).

The water temperature in the cold intermediate layer of the Pacific Ocean is higher than in the Bering Sea. Therefore, due to the advection of the Pacific Ocean waters, the water temperature in the center of the cold intermediate waters near the Kamchatka Peninsula reaches 1.6 °-1.8°C (see vertical distribution of temperature at 60.5°N and 177°E in Figure 2.37).

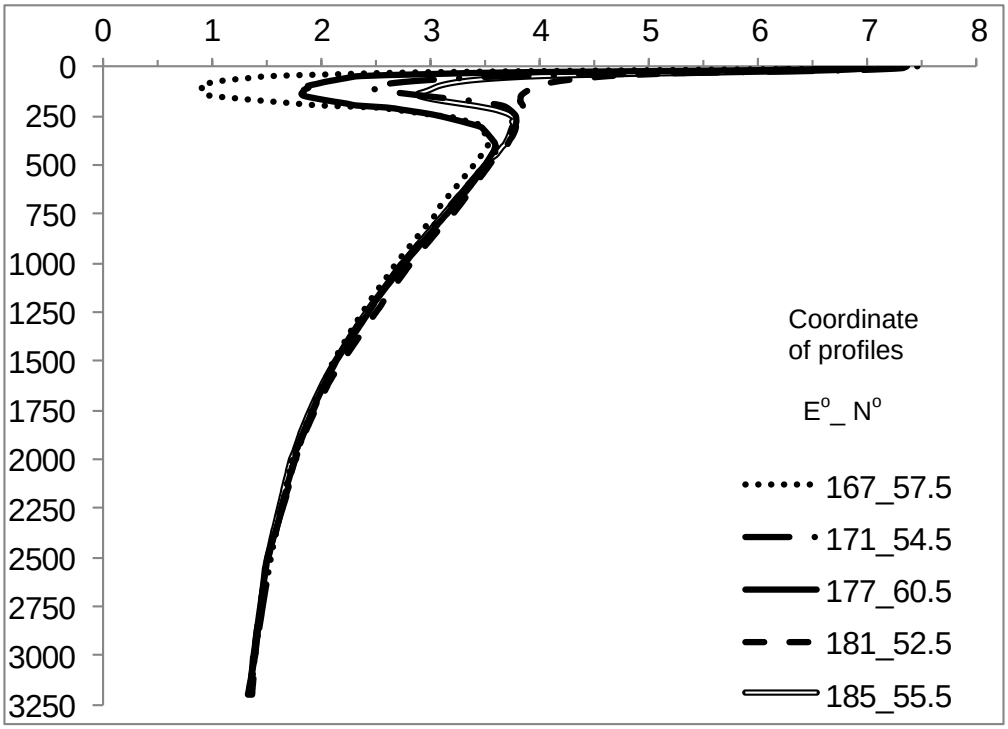

Figure 2.36. Vertical distribution of water temperature in the deep-water part of the West Bering Sea LME.

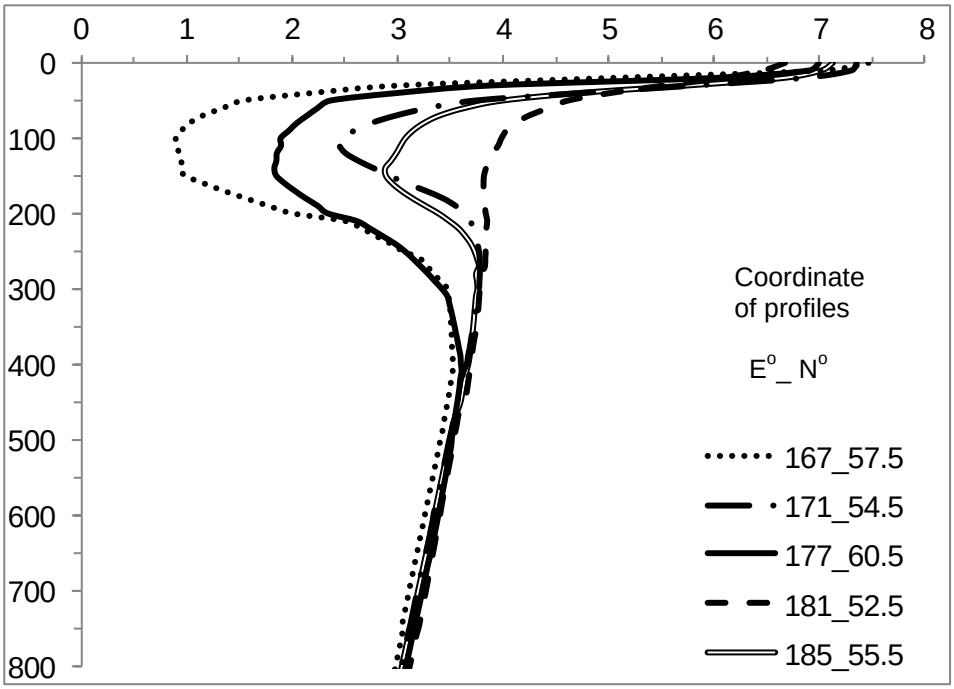

Figure 2.37. Vertical distribution of water temperature in the deep-water part of the West Bering Sea LME.

The warm intermediate layer of the combined East and West Bering Sea LMEs is the consequence of advection of the Pacific water into the sea, as well as of the change in the temperature of the Pacific water in various areas of the Bering Sea LMEs (Figure 2.37). The center of the warm intermediate layer is located between the horizons of 200 and 400 meters.

An active sea layer with seasonal fluctuations of water temperature is most sensitive to the thermal and dynamic processes taking place at the seawater-air boundary. The topography of its lower boundary depth is presented in Figure 2.39 (Luchin, 2007).

The maximum depths (400-500 m) with seasonal variability of water temperature are close to the straits of the eastern part of the Aleutian Range. The deepening (down to 200-300 m) of the lower boundary of the active layer is registered also in the near-slope areas of the Bering Sea LMEs. The minimum depths of the lower boundary location of the active layer (150-200 m) are close to east of the Blizhniy Strait and in the central part of the deep-water depression of the sea (Figure 2.39).

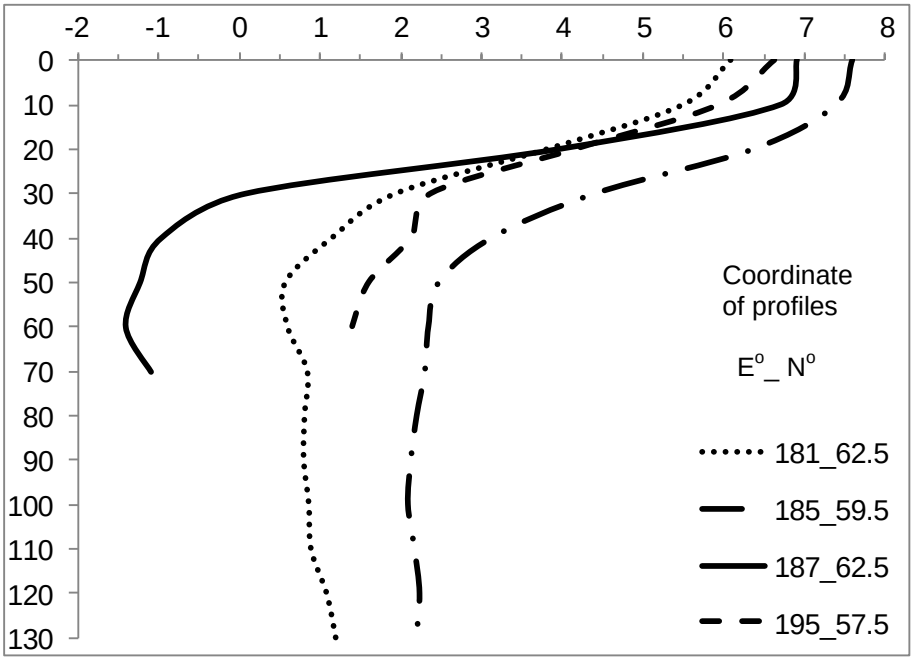

Figure 2.38. Vertical distribution of water temperature in the East and West Bering Sea LMEs shelf areas.

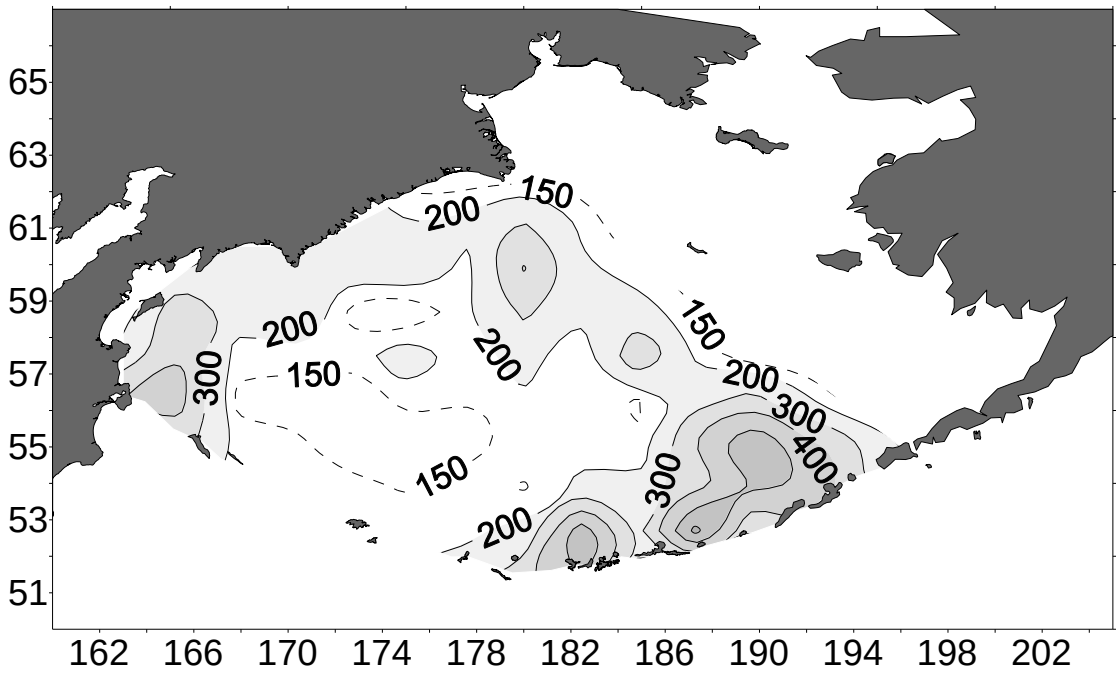

Figure 2.39. Depth (m) of the lower boundary of the active layer in the West Bering Sea LME.

Database analyses indicate that there are few oceanographic stations accessible in the East and West Bering Sea LMEs in the cold period of the year. Based on this information it is impossible to assess the inter-annual variability of the thermal state of the entire Bering Sea LMEs waters in the cold period of the year (the period of maximum cooling of the upper water layer and maximum development of the winter convection). This is particularly significant for the vast Eastern Bering Sea LME shelf, which is ice-covered in the winter period.

It is known (Koto and Maeda 1965, Maeda et al. 1968, Takenouti and Ohtani 1974, Coachman et al. 1980, Kinder 1981, Coachman 1986, Azumaya and Ohtani 1995, Luchin et al. 2002; Arsen'ev, 1967; Davydov, Kutsykh, 1968; Khen, Voronina, 1986; Luchin et al., 1999a; Luchin and Sokolov, 2007) that the specific features of water temperature distribution in the under-surface horizons, formed in the winter period, remain the same for a long period of time (until July-August). A profound layer of seasonal pycnocline blocks the inflow of heat from the sea surface to the under-surface horizons. Therefore, the thermal conditions of under-surface water depend mainly on meteorological conditions of the preceding winter, specific features of water dynamics in the sea, and advection of heat by the currents. The seasonal heating of surface water in the spring-summer period, as a rule, does not go deeper than 20-30 m. Thus, oceanographic observation data in the under-surface water layer (below the seasonal pycnocline/thermocline) may be used to study the inter-annual variability of the thermal state in the active layer of the East and West Bering Sea LMEs waters.

In a number of previous studies (Maeda et al. 1967, 1968, Takenouti and Ohtani 1974, Coachman and Charnell 1979, Azumaya and Ohtani 1995, Luchin et al. 2002) (for example, Khen and Voronina, 1986; Luchin et al., 2009; Luchin and Sokolov, 2007;), due to the limited initial data, the inter-annual variability of the East and West Bering Sea LMEs thermal conditions was considered for the coastal waters, limited sea areas, certain horizons, or near-bottom water layer of the shelf. This is mainly due to the available data of oceanographic observations, characterizing the active sea layer, which is distributed unevenly both in time and space. It should be noted that the parameters of inter-annual variability, obtained either by data of the local water areas or at certain horizons, do not fully reflect the inter-annual variability of the seawater thermal state.

The present study considers integral inter-annual fluctuations of the thermal state of two water masses of the East and West Bering Sea LMEs: cold intermediate layer (CIL) and warm intermediate layer (WIL). First, the locations of the upper and lower boundaries of these water masses were determined. Different approaches to determine the elements of vertical structure of the East and West Bering Sea LMEs waters were considered (graphs of vertical distribution of temperature and salinity, T-S curves, graphs of values of temperature and salinity vertical gradients, and vertical stability) (see Figure 2.40a and 2.40b for temperature and depth profiles for the East and West Bering Sea LMEs). In summary, the graphs of vertical distribution of values of temperature gradients can determine elements of the seawater structure.

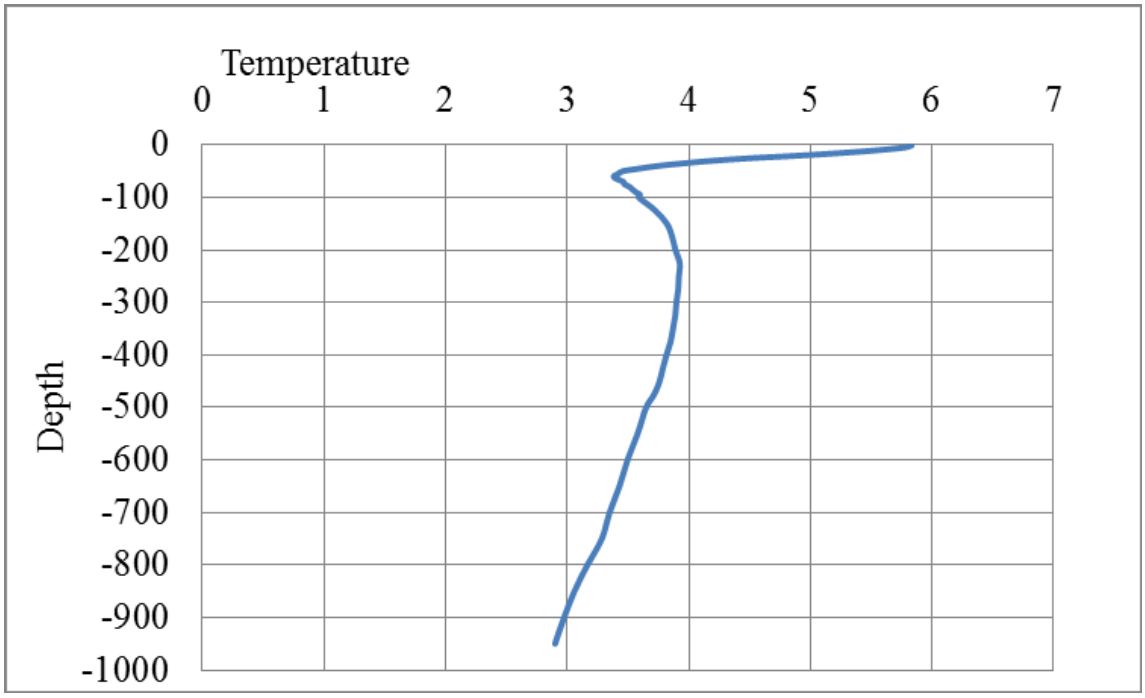

Figure 2.40a: Temperature and depth profile for the East Bering Sea LME, by months January to December.

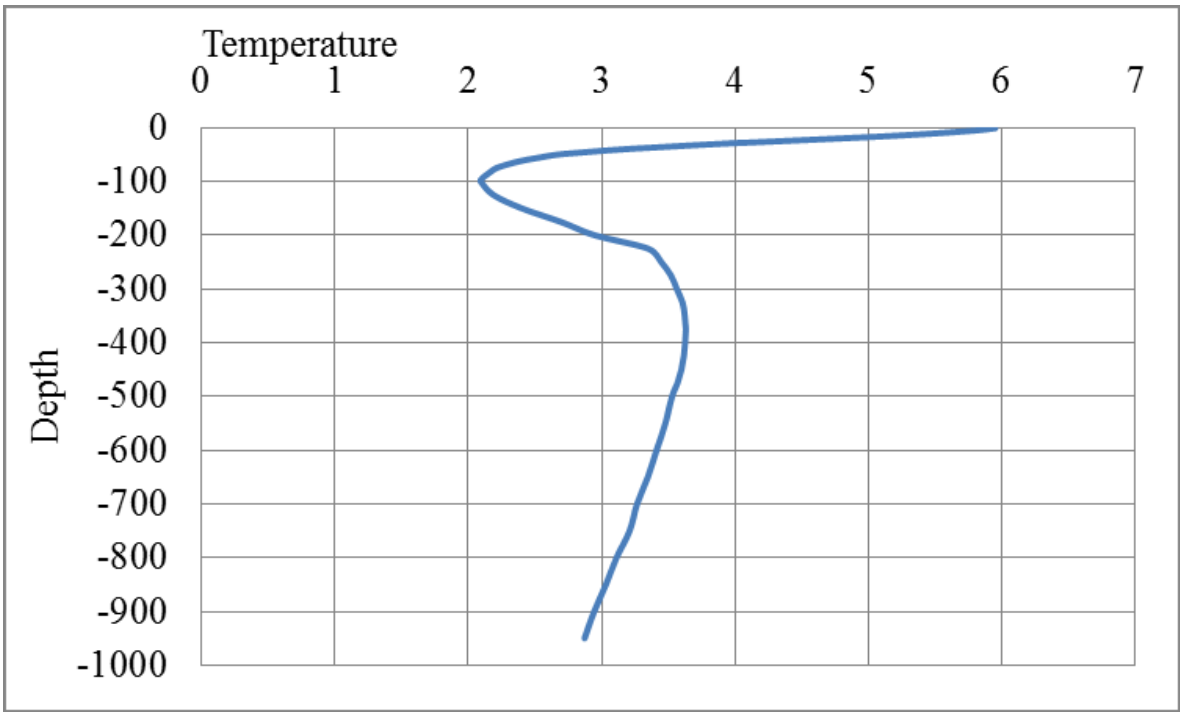

Figure 2.40b: Temperature and depth profile for the West Bering Sea LME, by months January to December.

The location of the upper boundary of the cold intermediate layer (CIL) in the East and West Bering Sea LMEs is mostly variable during the year (see Figure 2.40c and 2.41). At the same time, the period of stable vertical location of the upper boundary of the cold intermediate layer is also determined. In the deep-water part of the Bering Sea LMEs, it is observed from May-June to September, and in the shelf area – from May-June to August. Taking this regularity into account, as well as the location of the lower boundary of the active layer (Figure 2.39), the division of the Bering Sea LMEs waters into structural elements involves two blocks of oceanographic data. The first block covers data for June-August from the surface to the horizon profile of 400 m. This block of oceanographic data was used to determine the upper and lower boundaries of the cold intermediate layer. The lower boundary of the cold intermediate layer is simultaneously the upper boundary of the warm intermediate layer of the Bering Sea LMEs. The second block covers data for January-December from the horizon of 410 m to the bottom (Figure 2.42 and 2.43). This second block covers 20 998 stations from 1932 to 2012. This block of oceanographic data was used to determine the depth of the lower boundary of the warm intermediate layer of the Bering Sea LMEs.

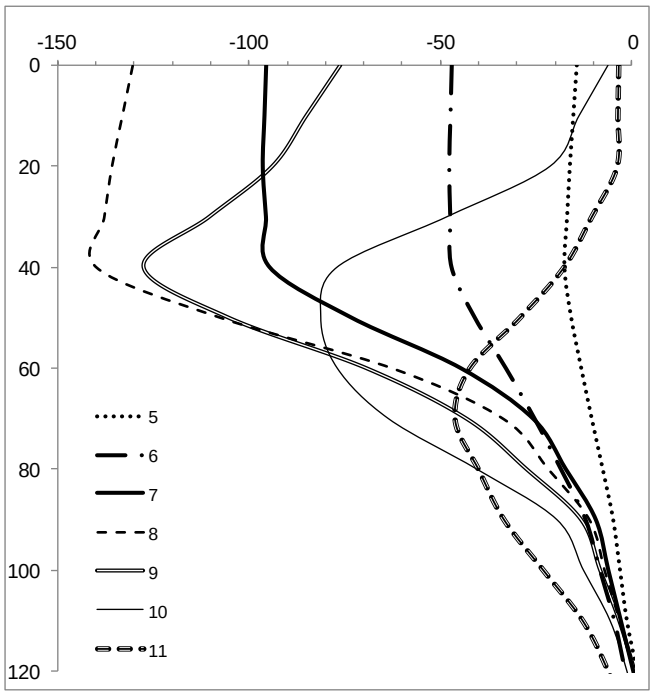

Figure 2.41a. The mean long-term vertical gradients of water temperature in the deep-water depression (56.5°N, 177°E) of the Bering Sea LMEs (numbers in the legend are months).

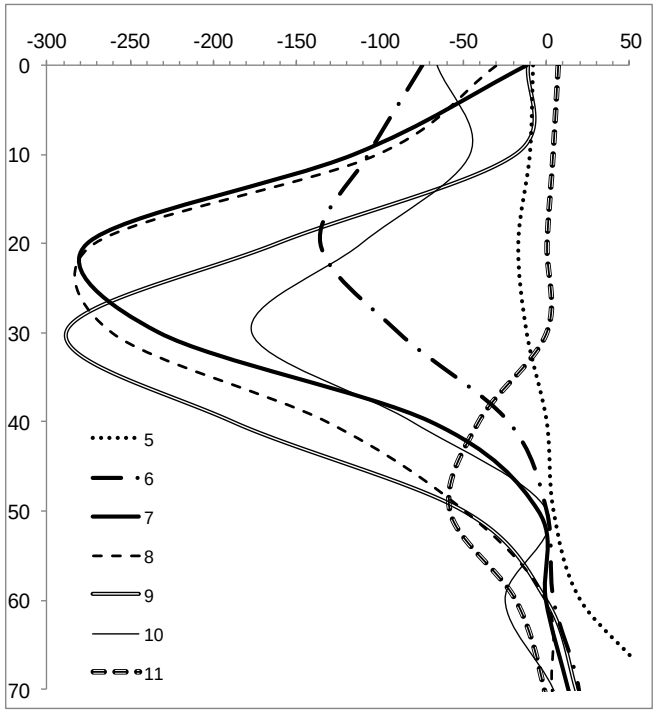

Figure 2.41b. The mean long-term vertical gradients of water temperature in the shelf areas (61.5°N, 175°W) of the Bering Sea LMEs (numbers in the legend are months).

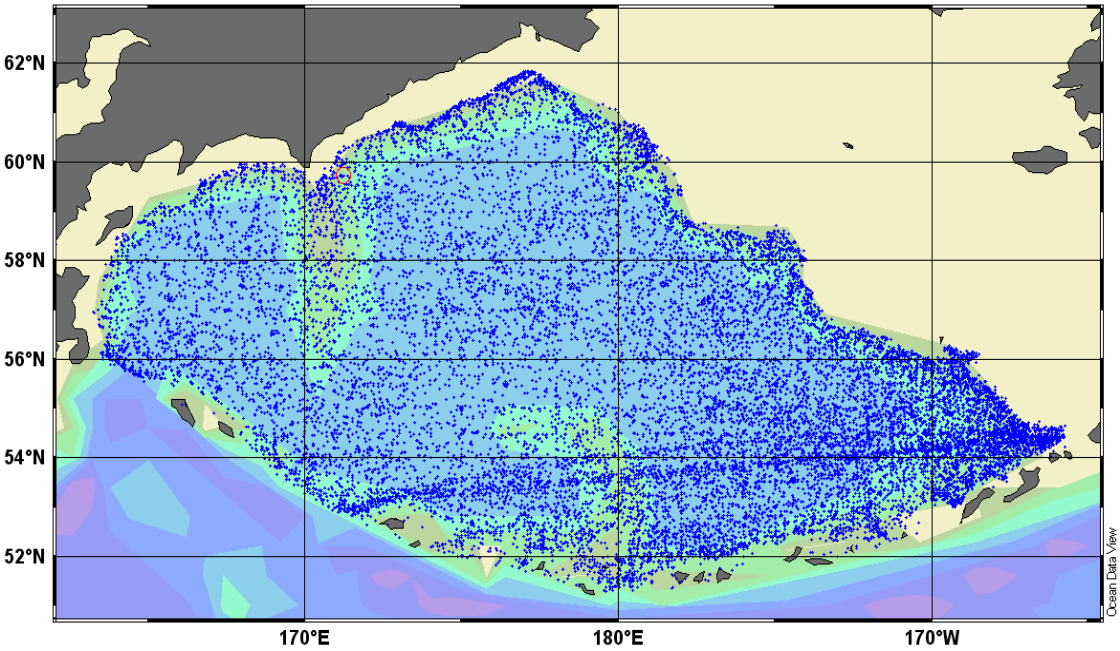

Figure 2.42. Spatial distribution of oceanographic stations in the West Bering Sea LME (with observations from 400 m to the bottom).

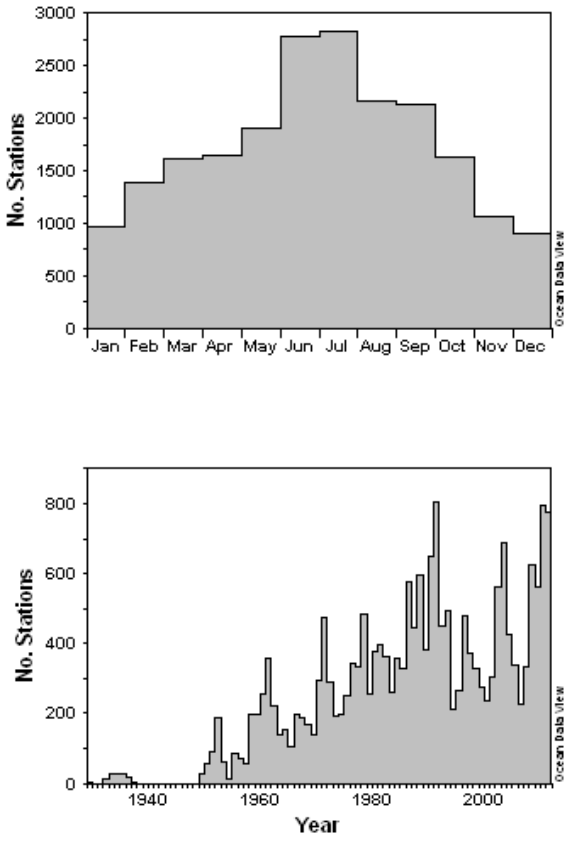

Figure 2.43. The distribution of oceanographic stations by months (upper) and by years (lower), with observations made from the horizon/profile of 400 m to the bottom.

As a start, all available data contained in the two blocks mentioned above were sorted into spherical trapeziums, also known as «grids», with a mesh size of 1° in latitude and of 2° in longitude. The mean, maximum, minimum, and standard deviation of temperature, salinity, and density of seawater (in the layer of 0-400 m – for June-August, and in the layer of 410 m to the bottom – from January to December) were calculated in every grid at all the horizons of 10 m. The indicated parameters were for the centers of corresponding grids. Based on these data, the graphs of vertical distribution of potential temperature and salinity, and T-S curves were developed for every grid. Also, graphs of values of vertical gradients of potential temperature, salinity, density, and vertical stability were drafted. The boundaries of water masses (Ivanov-Frantskevich 1953, Moroshkin 1966) are the horizons (or layers) with the maximum (or relatively high) values of vertical stability and vertical gradients of temperature and salinity.

The upper boundary of the cold intermediate layer may be determined by all indicated parameters. Figure 2.44 and Figure 2.45 demonstrate the vertical gradients of potential temperature, with profound negative extremes being observed in the upper water layer (to the horizon of 50 m). These graphs show that the upper boundary of the cold intermediate layer in the Bering Sea LMEs is within the depths of 10 to 40 m. This may be either a specific horizon with profound extremes of vertical temperature gradients or the lower boundary of the layer with the maximum values of vertical temperature gradients.

The lower boundary of the cold intermediate layer in the Bering Sea LMEs shelf, as seen at Figure 2.38, is at the near-bottom horizons. The lower boundary of the cold intermediate layer in the deep-water depression of the Bering Sea LMEs is unambiguously determined by the positive maximums of gradients of potential temperature. Figure 2.45 demonstrates that the lower boundary of the cold intermediate layer is found at depths of 150 to 250 m. The lower boundary of the cold intermediate layer is simultaneously the upper boundary of the warm intermediate layer. The lower boundary of the warm intermediate layer in the Bering Sea LMEs may be determined by the negative maximum of vertical gradients of potential temperature. Figure 13 demonstrates that the lower boundary of the warm intermediate layer in the Bering Sea LMEs is within depths of 400 to 900 m.

This method was used to determine the values of upper and lower boundaries of two studied layers (cold intermediate layer and warm intermediate layer) in every spherical trapezium grid. The integral (total) heat content in a specific (individual) layer at every station was calculated according to the formula:

$$Q = \sum_{h_2}^{h_1} \Delta h_i * \bar{t}_i \ ,$$

where Q – heat content in the layer, $\bar{t}_i$ – mean value of potential temperature of *i* layer, Δh_i – the thickness of *i* layer, h_1, h_2 - upper and lower boundaries of the layer, for which the heat content was calculated.

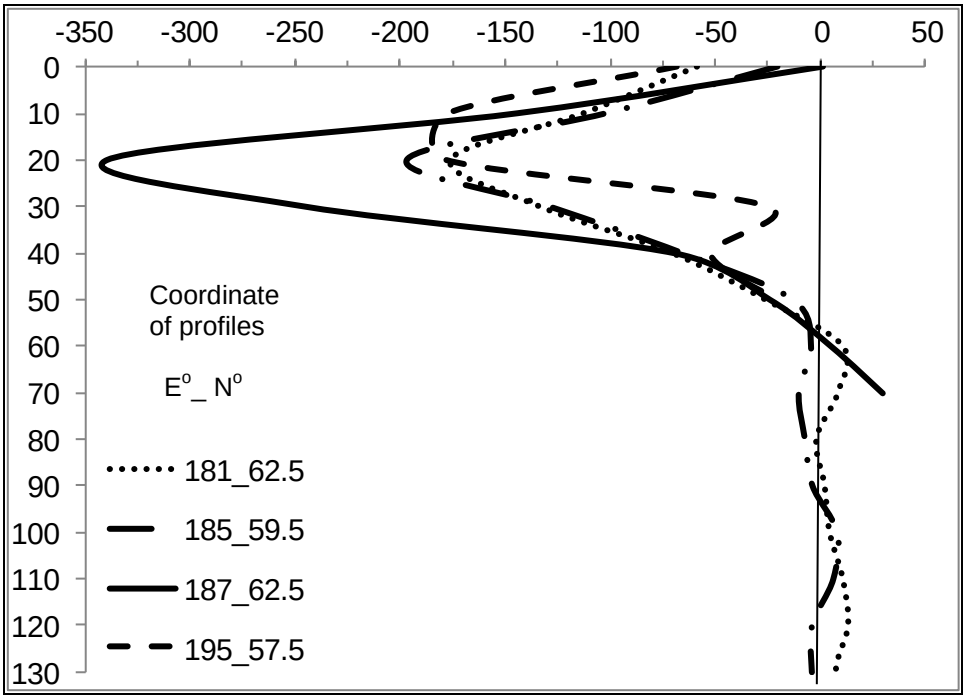

Figure 2.44. The mean long-term (for June-August) gradients of potential water temperature (10^3 * °C/m) in the East and West Bering Sea LMEs shelf areas.

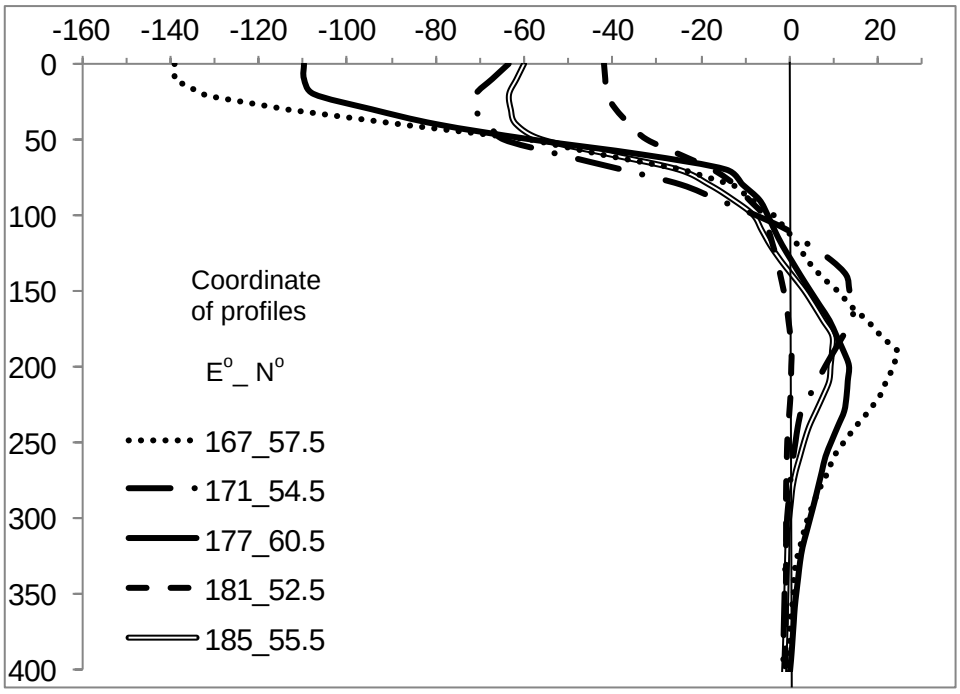

Figure 2.45. The mean long-term (for June-August) gradients of potential water temperature (10^3 * °C/m) in the deep-water depression of the West Bering Sea LME.

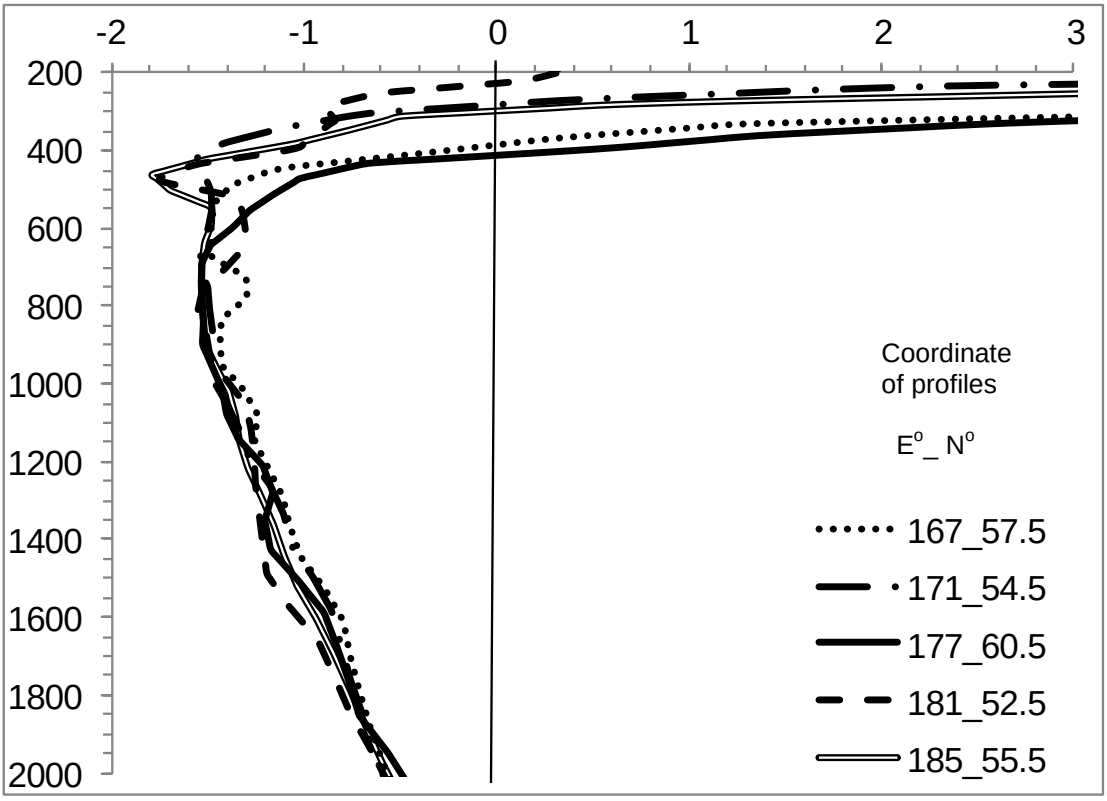

Figure 2.46. The mean long-term gradients of potential water temperature (10^3 * °C/m) in the deep-water depression of the West Bering Sea LME.

The calculation of parameters of inter-annual variability of the thermal states of two layers in the East and West Bering Sea LMEs was according to the following algorithm (Luchin et al. 1999). First, the calculated values of Q, obtained at every station, were sorted into a trapezium with a mesh size of 1.5° in latitude and of 3° in longitude. Then, the mean long-term monthly values of integral (total) content of heat were calculated in every trapezium, as well as the mean monthly values of integral (total) content of heat for a specific year. Based on these data, the monthly anomalies were calculated for every year (for the cold intermediate layer for the period of May to August, and for the warm intermediate layer – from January to December). At the final stage, the mean anomaly of the integral (total) content of heat for a specific year was calculated in every trapezium (for the cold intermediate layer – for the period of May to August, and for the warm intermediate layer – from January to December).

At the present moment, there are no areas in the East and West Bering Sea LMEs with a continuous dataset for the last 40-50 years. Therefore, filling-in the gaps in the three-dimensional blocks (latitude, longitude, year) of anomalies of the integral (total) content of heat is conducted using regression correlations (Luchin, Zhigalov, 2006). Single data gaps (after the correlation procedure is carried out to obtain the missing values) are filled-in by the kriging-method of the SURFER software.

The correction coefficient for the mean anomalies of the integral (total) content of heat in a trapezium with a mesh size of 1.5° in latitude and of 3° in longitude was calculated according to the following formula:

$$K = 1.5 * (3*\cos\gamma) * \mathbf{C},$$

where γ – the latitude of site, 1.5 – the height of trapezium, 3 – the width of trapezium, C – a decreasing parameter, considering the cuts of the coastline trapezium within the cold intermediate layer and the cuts of trapezium by the isobath of 500 m within the warm intermediate layer. For the offshore open water areas (outside the coastline and the isobath of 500 m), the parameter of **C** was considered as equal to 1. Then, Q*K was calculated in every trapezium for every year, as well as the mean anomaly of the integral (total) content of heat for the entire layer (the cold and the warm intermediate layers). The obtained values were standardized within the range (max-min) of the mean anomalies of the integral (total) content of heat for the layer. As a result, dimensionless series were obtained, characterizing the inter-annual variability of the thermal state of the considered layers (e.g. the cold the warm intermediate layers).

A two-stage analysis of the long-term variability of the obtained time series was made. The presence of the trend component was assessed at the first stage. A filter was applied for the purpose, distinguishing the linear function of time from the white noise mixture (Plotnikov 2002). The second stage was a spectral analysis of the considered series. Preliminary filtration of the trend components was made to correct the spectral assessments. The analysis of frequency spectra of the considered series was by the maximum entropy method (Privalsky 1985). All calculations were for the 95% level of significance.

The upper boundary of the cold intermediate layer in the Bering Sea is within the range of the upper 10-40 m (Figure 2.47). It is most close to the surface (the horizons of 5-10 to 20 m) in the peripheral areas of the sea shelf due in part to a thin heated and freshened layer formed in the sea surface in spring and the first half of summer (resulting from the ice melt, river runoff, and the heating of surface waters). A thick layer of seasonal pycnocline, located close to the sea surface and blocking the transport of heat to the below lying horizons, is formed between them and the cold near-bottom waters. Additional factors are the recurrence of weak winds and calm situations, as well as low velocity of tidal and non-periodic currents in the Bering Sea LMEs shelf.

The upper boundary of the cold intermediate layer in the active areas of the Bering Sea (close to the continental slope, in the straits of the Aleutian-Commander Range, and neighboring areas), as well as in the deep-water depression, is at its maximum depth (to 30-40 m). This is due to the increase in velocity of the tidal and non-periodic currents, as well as the generation of whirlwinds, finally resulting in the intensification of horizontal and vertical exchange of seawater properties.

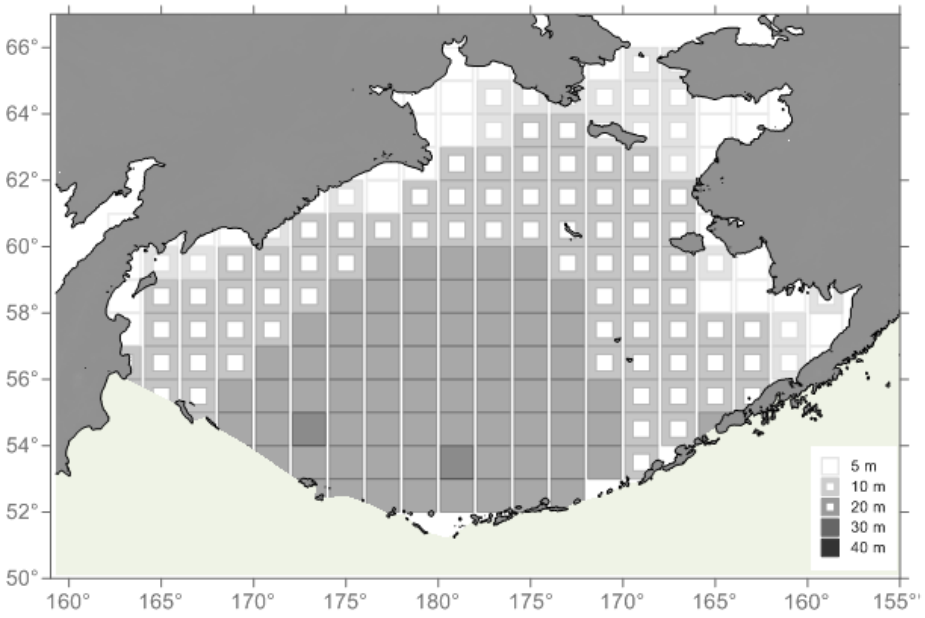

Figure 2.47. The upper boundary of the cold intermediate layer in the combined East and West Bering Sea LMEs (in metres).

The lower boundary of the cold intermediate layer, which is simultaneously the upper boundary of the warm intermediate layer in the deep-water depression of the sea in the Bering Sea LMEs is within a wide range of depths (from 20 to 240 m). Figure 2.48 demonstrates that maximum depth (from 160 to 220-240 m) is in the area of the continental slope and close to the straits of the Eastern Aleutian Range. This area is characterized by high velocity values of tidal and non-periodic currents, as well as by the generation of anti-cyclone whirlwinds. The overcooled shelf waters contact the transformed Pacific waters close to the continental slope. As a result, the intensification of vertical exchange of seawater properties takes place and the lower boundary of the cold intermediate layer goes deeper.

In the Blizhniy Strait, as well as to the north and the northeast, a vast area is observed with the lower boundary of the cold intermediate layer being a bit closer to the sea surface (the horizons of 160-180 m). This is because the Blizhniy Strait is rather wide and deep, especially when compared to the shallow straits of the Aleutian Range. As a result, a weak transformation of the Pacific waters' vertical structure takes place. Also, the Pacific waters that enter the East and West Bering Sea LMEs are characterized by high heat content in the active layer. Generally, intensive autumn-winter convection does not go deeper than the upper 100 m.

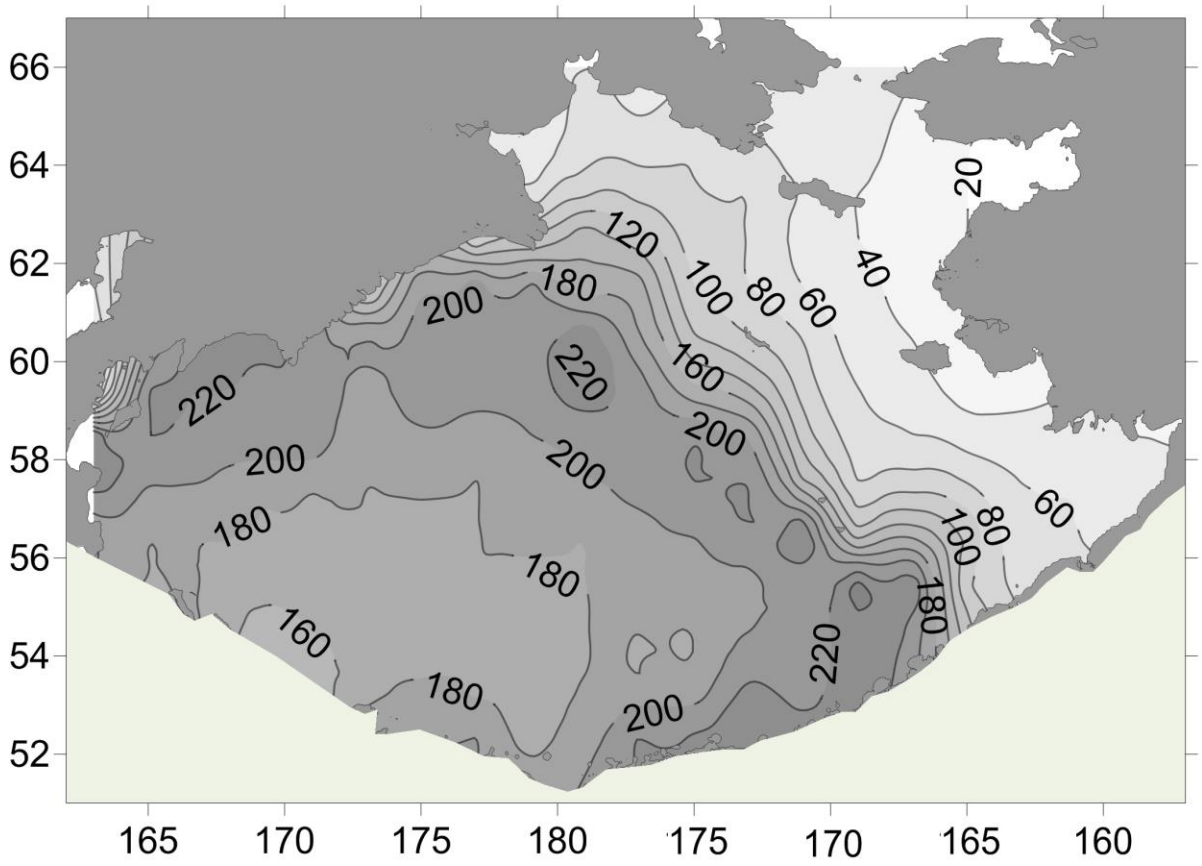

Figure 2.48. The lower boundary of the cold intermediate layer in the combined East and West Bering Sea LMEs (in metres).

The lower boundary of the cold intermediate layer over the vast eastern Bering Sea shelf is in the near-bottom horizons (Figure 2.48). Therefore, a line of the lower boundary of the cold intermediate layer (from 100-120 m near the slope to 20-40 m in the Northern Bering Sea) toward the surface is observed.

The lower boundary of the warm intermediate layer over the major part of the deep-water depression of the Bering Sea ranges within the depths of 700 to 800 m (Figure 2.49). Two areas with the maximum depth of the lower boundary of the warm intermediate layer are also visible in Figure 2.49. The first area is to the north of the Kamchatka Strait. Its formation is connected with the maximum penetration depth of the autumn-winter convection and the interaction of overcooled shelf waters and near-slope waters of the deep-water depression. The second area of the maximum depth of the lower boundary of the warm intermediate layer is to the north of the central straits of the Aleutian Range. Its formation is connected with the increased horizontal and vertical exchange of seawater properties in narrow and depth-limited straits, in which high velocity of tidal and non-periodic currents is observed.

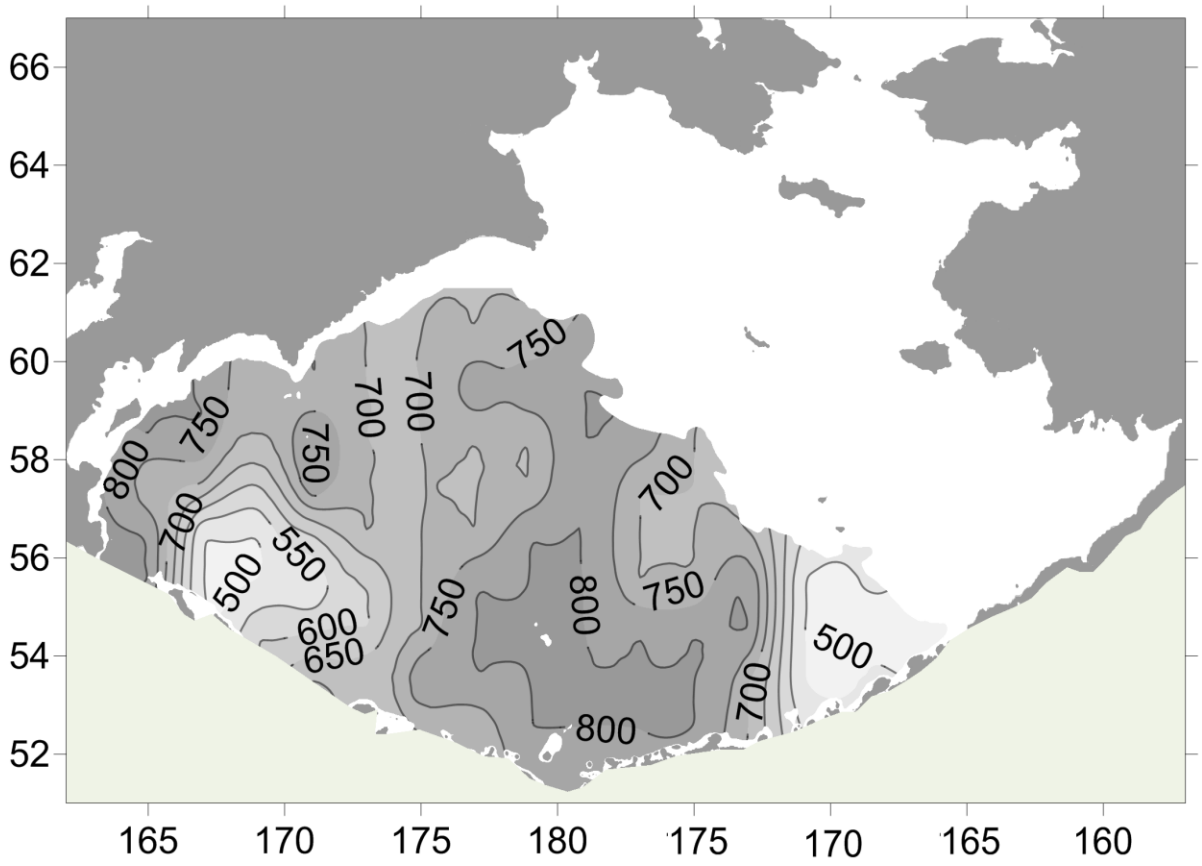

Figure 2.49. The lower boundary of the warm intermediate layer in the West Bering Sea LME (in metres).

The lower boundary of the warm intermediate layer in two areas of the East Bering Sea is at its minimum depth (500-600 m) (Figure 2.49). The first area covers the Blizhniy Strait and water area to the northeast of it. This area contains the slightly transformed Pacific waters. The lower boundary of the warm intermediate layer in the Northern Pacific Ocean is closer to the surface than in the East Bering Sea. The second area with the minimum depths of the lower boundary of the warm intermediate layer is in the utmost south-eastern part of the deep-water depression of the Bering Sea LMEs (Figure 2.49). This specific feature of distribution is likely associated with high temperature of the Pacific intermediate waters entering the sea. It is also likely associated with the input of shallow straits.

Figure 2.50 presents inter-annual variability of the standardized anomalies of the integral (total) content of heat in the cold intermediate layer. Figure 2.50 demonstrates that a series of quasi-periodic cycles is noted in the inter-annual variability of the thermal state of waters of the cold intermediate layer. Based on the results of the spectral analysis, the following fluctuations have been registered: 12-14 years and 5-6 years. The calculations indicate that the statistically significant linear trend in the cold intermediate layer of the East Bering Sea is not observed.

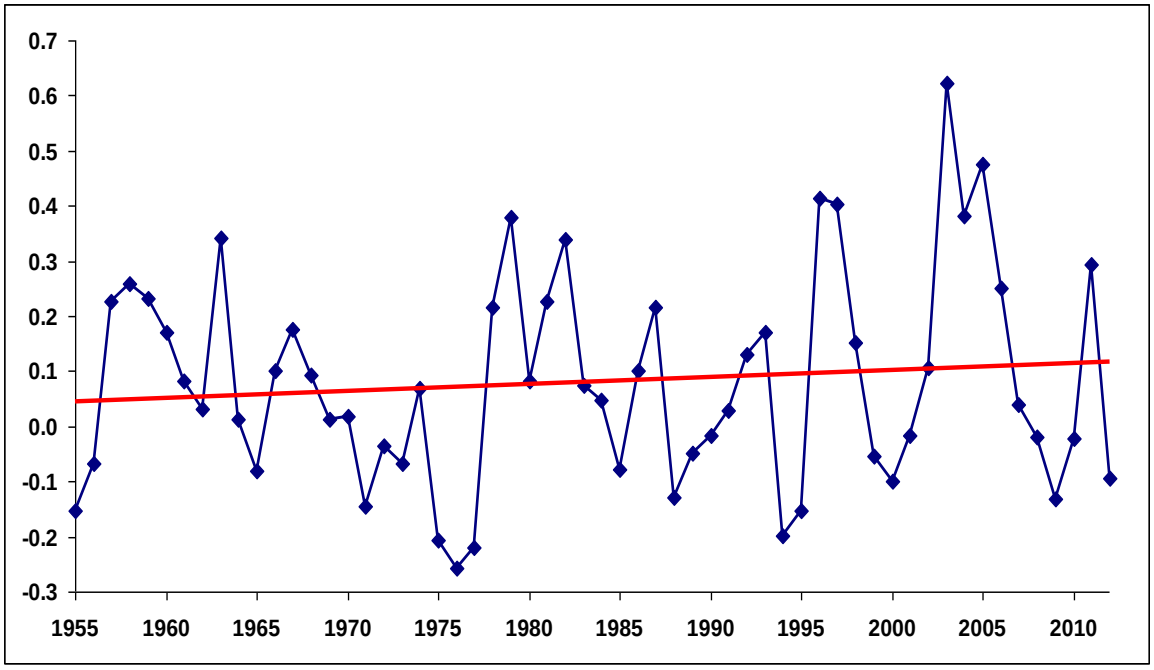

Figure 2.50. Inter-annual variability of the standardized anomalies of the integral (total) content of heat in the cold intermediate layer of the East and West Bering Sea LMEs.

The inter-annual fluctuations of the standardized anomalies of the integral (total) content of heat in the warm intermediate layer are presented in Figure 2.51. As it may be concluded from the figure, a series of quasi-periodic cycles may be traced in the inter-annual variability of the thermal state of the warm intermediate layer. Also, a significant linear increase of the thermal state of the waters of the warm intermediate layer was noted. Based on the results of the spectral analysis, the following fluctuations have been determined: 6 years, 3-4 years, and quasi-two-year ones.

It should be noted that a series of inter-annual variability of the standardized anomalies of the integral (total) content of heat in the warm intermediate layer is presented in Figure 2.51. Three periods are noted. The first period (1955-1964) is characterized by significant inter-annual fluctuations of anomalies of the integral (total) content of heat and the lack of a significant linear trend. The second period (1965-1981) is characterized by a significant linear trend, which proves a statistically significant decrease of the content of heat in the warm intermediate layer (Figure 2.52). The third period (1982-2012) is characterized by a significant linear trend, which proves a statistically significant increase of the content of heat in the warm intermediate layer (Figure 2.52).

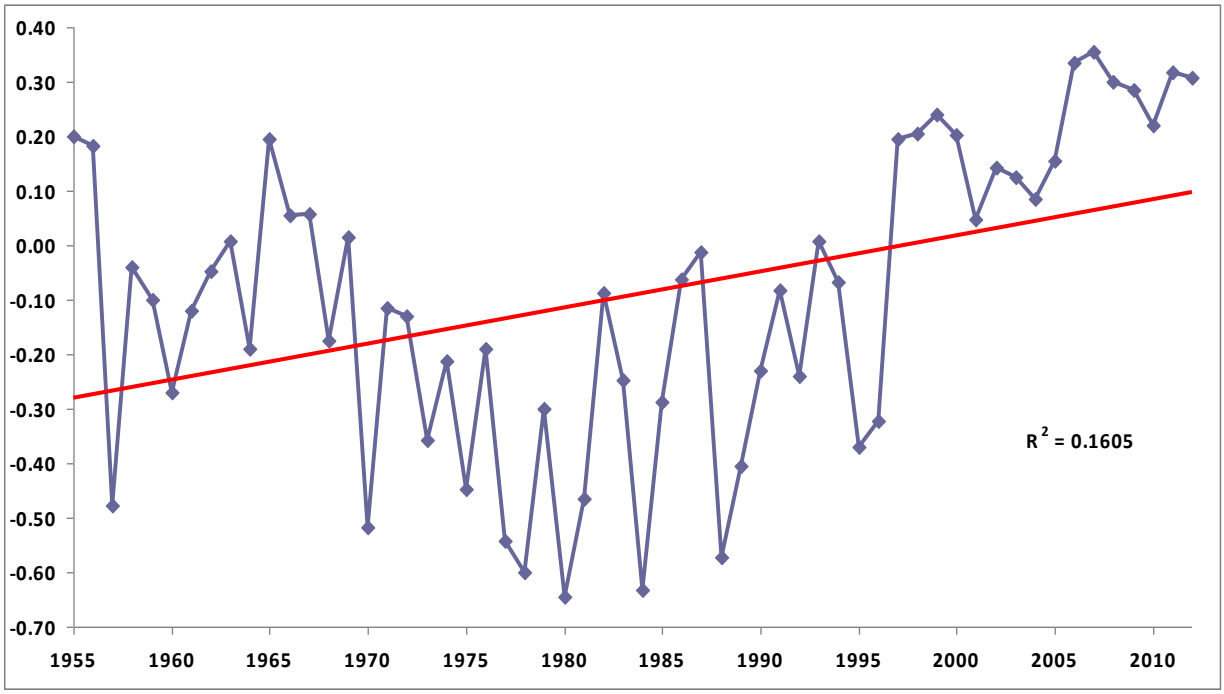

Figure 2.51. Inter-annual variability of the standardized anomalies of the integral (total) content of heat in the warm intermediate layer of the East and West Bering Sea LMEs.

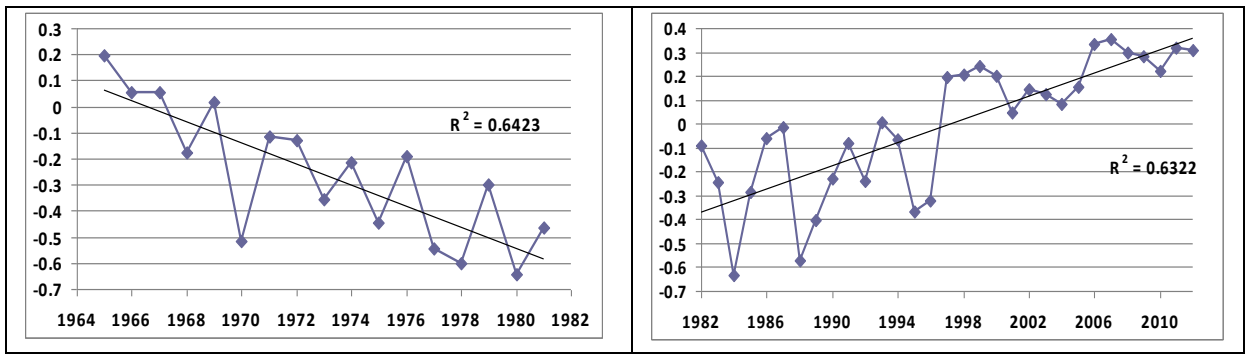

Figure 2.52. Inter-annual variability of the standardized anomalies of the integral (total) content of heat in the warm intermediate layer of the East and West Bering Sea LMEs by year.

Application of fuzzy sets for data quality control

Fuzzy sets were applied to formalize data quality control criteria (Zadeh 1975).

One of the criteria of data quality control is information regarding maximum allowable variability of marine environment parameters for various spatial-temporal intervals (Boyer et al. 2009). If the value of a parameter is outside the allowable range then the value is considered to be an outlier (e.g. uncertain). Such values are flagged and are not used in analyses (Boyer et al. 2009). The diversity of measurements with the application of the set and range criteria is divided into two categories: a) measurements with uncertainties; and b) measurements without uncertainties.

Data contained in the World Ocean Database characterizes the state of the marine environment of coastal areas. Hydrological variability of these areas is under heavy influence of the river runoff and the tides/tidal currents. The Arctic seas, the Caspian Sea, and the Sea of Azov are typical examples of such an impact. The situation in these seas is even more aggravated by the influence of intensive ice thaw/melting. Also, there are areas in the Caspian Sea and the Sea of Azov with anomalous characteristics.

In the Caspian Sea LME, the Kara-Bogaz-Gol Bay has a salinity of > 40 per mille. In the Sea of Azov, Sivash has a salinity exceeding 38 per mille. The measurements in the Arctic seas (from the Kara Sea to the Chukchi Sea) were mainly made during the ice-free period of the summer. The impact of the river runoff on the coastal areas during this period is at its maximum. A relatively small area of the coastal zone has its own specific features of variability of marine environment characteristics, which may be used for data quality control. These regularities describe the allowable variability of marine environment characteristics in qualitative terms. For example,

The water temperature in the Bering Strait ranges (3)
from approximately +2 to +8 ^{o}C in the surface layer in summer.

Based on the statement above, it becomes clear that both the space (the Bering Strait) and time (summer) are in imprecise terms. For example, if the temperature in the centre of the Bering Strait in the middle of the summer is 8.1 ^{o}C then this value is not necessarily uncertain, though it is outside the allowable ranges of the parameter. To formalize the criteria it is necessary to describe the qualitative concepts, such as «the Bering Strait», «summer», and «approximately +2 – +8 ^{o}C», in quantitative terms. Fuzzy sets were applied to solve this problem.

Applying the continuous scale [0, 1] the concept of «approximately +2 – +8 ^{o}C» was examined (Figure 2.53). For example, the gradient of temperature value of 8.3 ^{o}C in relation to the notion «approximately +2 – +8 ^{o}C» is equal to 0.9. The notion «summer» for the Bering Strait is demonstrated by a graph at Figure 2.54.

The chart at Figure 2.55 demonstrates the notion «the Bering Strait». The number in each square determines the relationship to the notion of «the Bering Strait».

The algorithm for quality control to check against statement (3) afore-mentioned is as follows:

- Imprecise notions «summer», «the Bering Strait», and «approximately +2 – +8 ^{o}C» are presented in tables;
- Stations with values over zero are selected with respect to (K_1) in relation to the notion of «summer», (K_2) in relation to the notion of «the Bering Strait», and (K_3) in relation to the notion of «approximately +2 – +8 ^{o}C»;
- For each station selected, L, the values of K_1, K_2, K_3 are calculated based on the decision tables;
- K(q) of station q in relation to the notion determined by statement (3). $K=(K_1 +K_2+K_3)/3$ is calculated.

The value K, when the temperature of water meets the quality criterion (1), is determined by the specificity of the task being solved. The approach to formalizing data quality control criteria allows the use of a priori information regarding the regularities of the spatial-temporal variability of the marine environment. This eliminates the need for additional analysis of the results of data quality control. The disadvantage of this method is the time required to design and develop the software for data comparisons with the original allowable ranges.

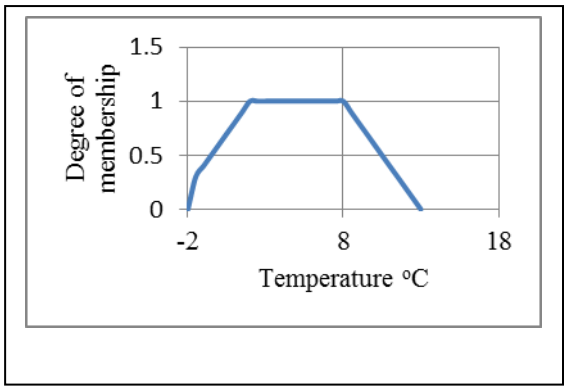

Figure 2.53. Formalization of the notion of *Temperature ranges are approximately +2-+8 ^{o}C.*

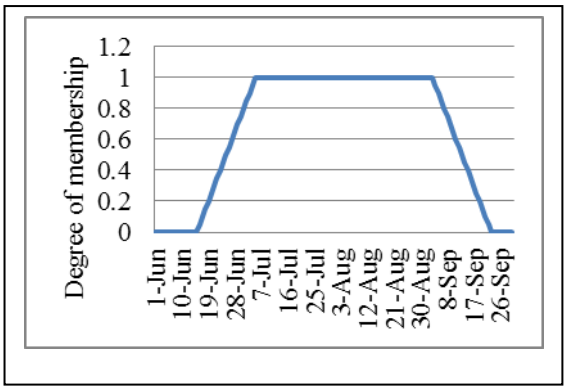

Figure 2.54. Formalization of the notion of *Summer* for the Bering Strait.

Figure 2.55. An example of formalization of the notion of *The Bering Strait*.

Comparison of historical and contemporary navigation charts

The search for new trading routes from Europe to Asia fuelled the studies of shipping conditions in the Eastern Arctic seas. Books, travel logs, reports, and charts provide an overview of the changes in the Polar Regions during the 16th – 18th centuries (Wiese, 1948). These written accounts characterize the climate of the Arctic. Specifically, the changes in shorelines are the most significant aspects of ensuring shipping safety.

Instrumental observations of the Arctic seas began at the turn of the 18th century. These observations resulted in navigation charts of different areas of the shoreline from the Barents Sea LME to the Bering Sea LMEs, and surface and profile water temperature values (Badigin, 1956). The database of the Arctic seas contains information regarding the variability of temperature, salinity, and density of seawater for a period longer than 100 years. The database also contains digital archives of navigation charts of the Arctic seas. Thus these data are the baseline for impact assessment of temperature, salinity, and seawater density fluctuations. As trends are followed, they will be useful for understanding changes in Large Marine Ecosystem function, as well as ensuring shipping safety in the Polar Regions. Comparison of navigation charts is an important element when evaluating trends of shoreline changes.

The algorithm to compare navigation charts is described below. Current information is gathered from Google Earth, and historical information is gathered from the charts of the eastern and western coasts of the Bering Strait of 1849 (Figure 2.56). Comparison of these charts necessitated a few steps. First, the historical charts were converted from the raster format to the vector format in Map Viewer. At times, the tracing method was applied using Corel Paint X6. Next, the vector format was converted into shape files with Map Viewer, which were then imported to Google Earth. Third, the shape files of the historical charts (Figure 2.56) were assessed in Google Earth and compared with current information. Comparisons were made specific to the shorelines, but were not included in this Atlas as they were beyond the scope of this report. The coast/shoreline is not within the scope of the present publication. However, the continuation of the studies within such a direction may, presumably, answer the question raised.

Figure 2.56. Comparison of charts: 1849 in relation to the early 21st century.

3. Region 2. Black Sea LME (including the Sea of Azov subarea) and Caspian Sea LME

The problems of changes in thermal conditions and ice cover of the seas at global and regional scales have been discussed and considered in the scientific literature (Levermann et al. 2012, Matishov et al. 2012). Climatologist A.I. Voeikov analyzed the linkages between wind and pressure at the end of the 19th century and concluded that a «large axis of European-Asian Continent» was present (Voeikov 1884).

The Siberian Anticyclone with a spur stretching toward Europe was named the Voeikov Axis. This climatic axis arises as a «wind ridge» and separates winds with the southern component (to the north of the axis) from the winds with the northern component (to the south of the axis). This results in abnormal advection of cold from the Siberian Anticyclone towards the Pyrenees and of heat of the Gulfstream to the Arctic in the direction of the Franz Josef Land during the winter months. Reduction of the ice cover during summer and autumn months in the Arctic Basin causes changes of a large-scale atmospheric circulation (Overland and Wang 2010). These chances lead to an increase of blocking and precipitation in Europe during the winter months (Liu et al. 2012).

At the same time, abnormally cold weather of the second half of winter over the territory of Central and Southern Europe and the water areas of the neighbouring seas (the Sea of Azov, Northeastern Black Sea, Northern Caspian Sea) has become a common event since the early 21st century (Matishov et al. 2012, Moore and Renfrew 2012, Tourpali and Zanis 2013). Anomalies in January-February 2006 and 2012 were pronounced. Air temperature over the south of European Russia decreased to -32/-33°C in January 2006. Mean monthly values were around -15° (12-15° lower than the standard). Similar conditions were registered in January-February 2012. During that period, the impact of the Siberian Anticyclone spread to the English Channel and Portugal.

Ice in the Sea of Azov subarea and Caspian Sea LME became a factor that challenged shipping activities. Approximately 100 vessels were trapped in the ice in the areas and ports of the Sea of Azov subarea and Kerch Strait in February-March 2012 (Matishov et al. 2012). Drift ice in the Caspian Sea spread along the western coast to the Apsheron Peninsula.

The third part of Atlas focuses on Large Marine Ecosystems of the southern European Russian seas – the Black Sea LME, Sea of Azov subarea, and the Caspian Sea LME (Figure 3.1).

The total number of stations, included in this part of the Atlas database is 196,778. Their distribution by seas is presented in Table 3.1 and Figure 3.2.

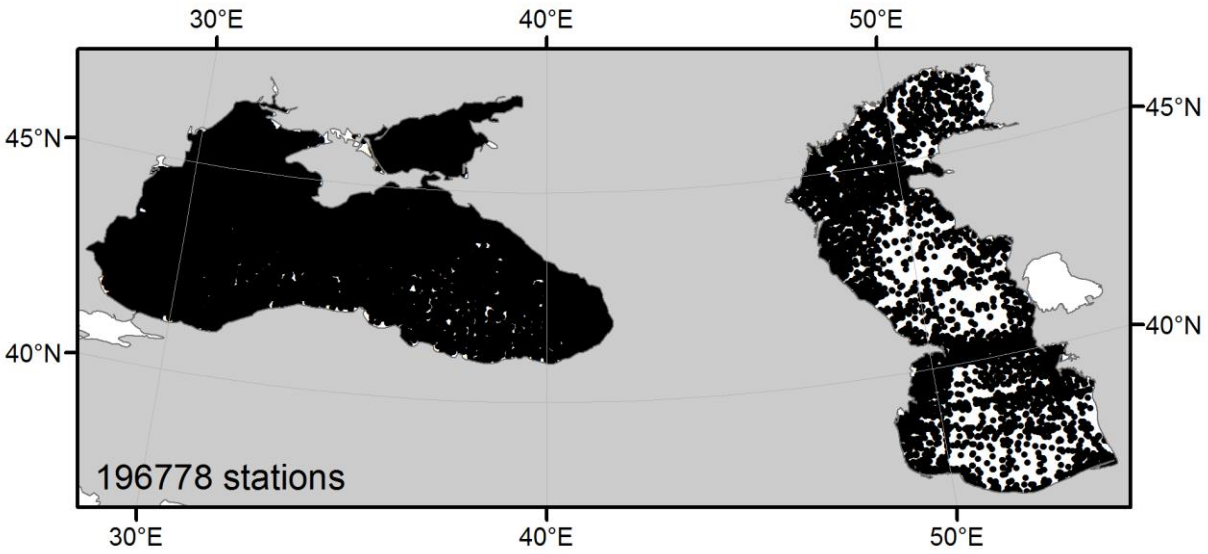

Figure 3.1. Distribution of stations over the Black Sea LME, Sea of Azov subarea, and the Caspian Sea LME in 1884-2012.

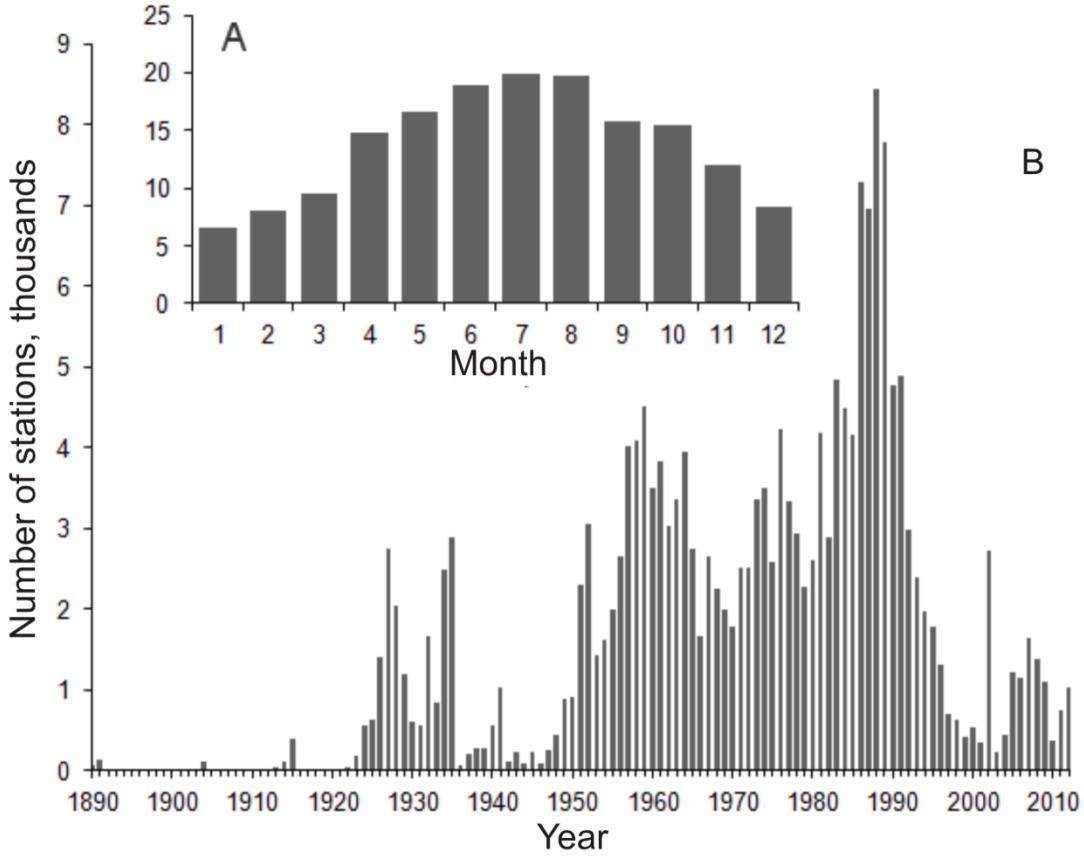

Figure 3.2. Distribution of stations by months (A) and years (B) in the Black Sea LME, Sea of Azov subarea, and the Caspian Sea LME database (1884-2012).

Table 3.1. Distribution of stations by Large Marine Ecosystems of the southern seas.

Large Marine Ecosystems	Number of stations	Period
Black Sea	86,836	1884-2012
Sea of Azov	66,609	1891-2012
Caspian Sea	43,333	1897-2011
Total by seas	196,778	

Murmansk Marine Biological Institute has been carrying out its expeditionary studies in the Sea of Azov since 1997. The Azov Branch of the Institute and a research station were established in 1999. The Southern Scientific Centre of the Russian Academy of Sciences was established in 2002 in Rostov-on-Don. With the establishment of the Centre, observations over the state of the Sea of Azov subarea were made regularly, and were extended to cover the Black Sea LME and the Caspian Sea LME.

A total of 281 sea cruises to the Sea of Azov subarea, Black Sea LME, and the Caspian Sea LME were performed for the period of 1997 – 2012; the primary data for 8 302 stations are presented in Figure 3.3.

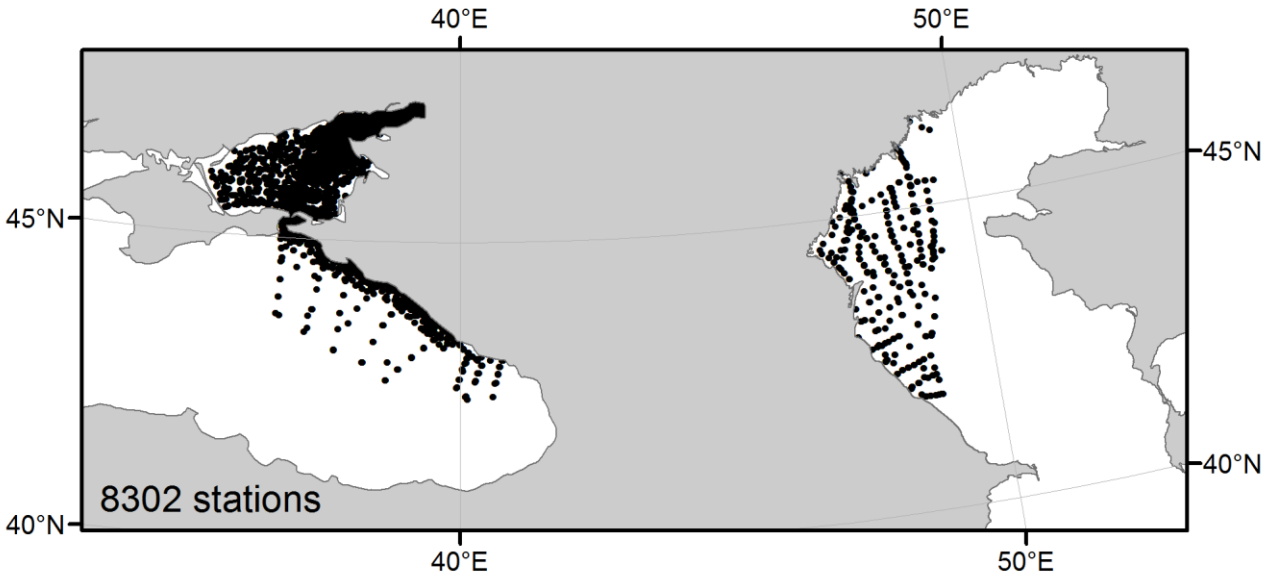

Figure 3.3. SSC RAS marine expeditions and cruises in the Sea of Azov subarea, Black Sea LME, and the Caspian Sea LME in 1997-2012.

3.1. The Black Sea LME

Oceanographic database and inventory

The oceanographic database of the Black Sea LME covers 86,836 stations, from 1884 to 2013 (Figure 3.4).

The distribution of stations by years and months is presented in Figure 3.5.

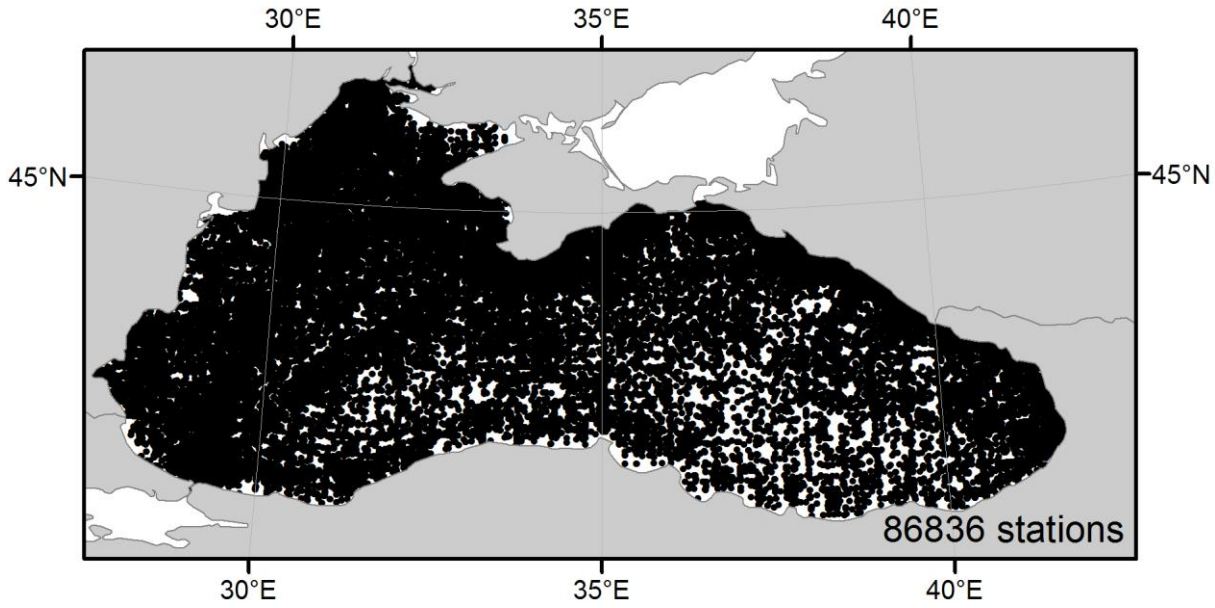

Figure 3.4. Distribution of stations over the Black Sea LME area (1884-2012)

To analyze long-term variability of hydrological characteristics of the Eastern Black Sea, two transects are considered in the Atlas:

- « Samsun – The Kerch Strait» (Figure 3.6);
- «Yalta – Batumi» (Figure 3.7).

A number of stations located in a belt of 20 km wide from each side and used for the construction of climatic standards and anomalies is correlated with each transect. The total number of stations for Samsun– the Kerch Strait Transect is around 1,555 and the Yalta – Batumi Transect includes 9,134 stations.

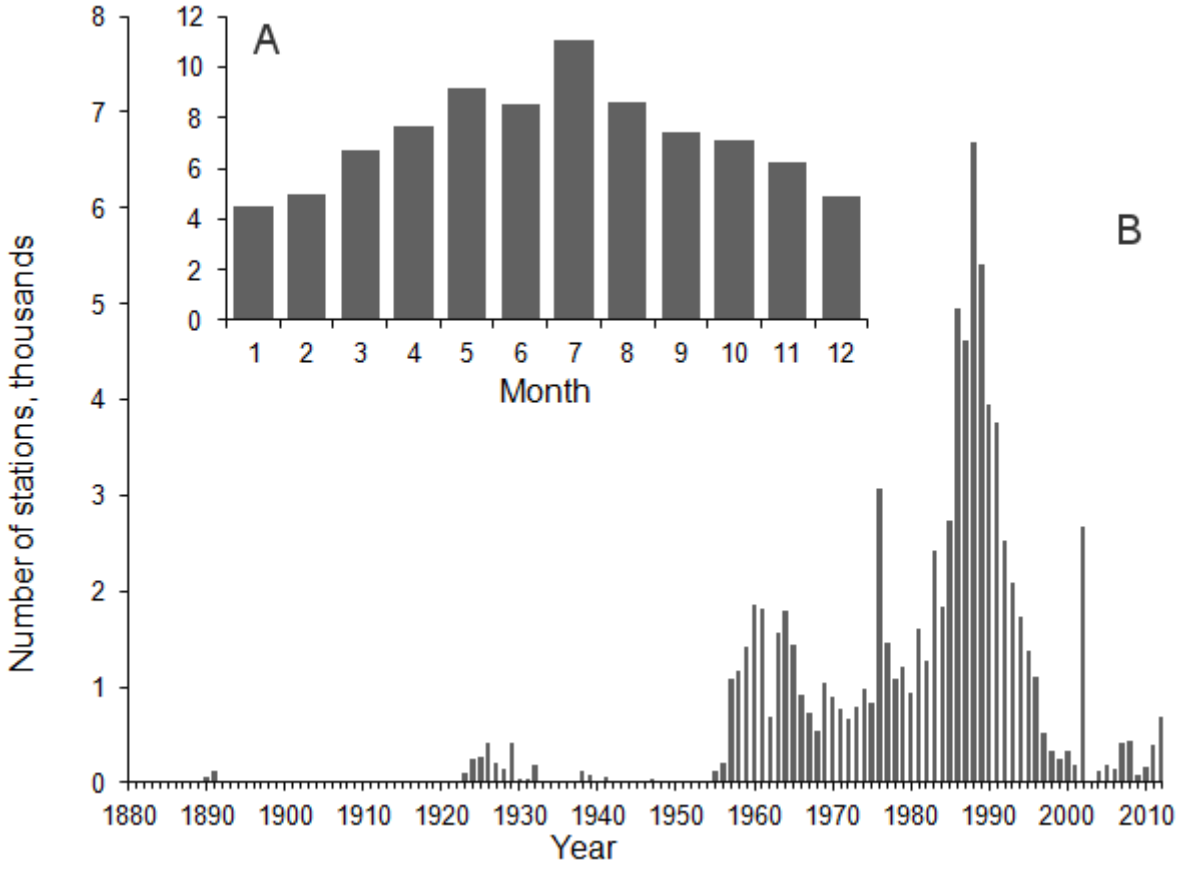

Figure 3.5. Distribution of stations by months (A) and years (B) in the Black Sea LME database (1884-2012)

The Black Sea database includes the following parameters (Table 3.2).

Table 3.2. List of indices included in the Black Sea LME database.

Parameters		**Units of measurement**		**Number of measurements**
Name	**Sign**	**Name**	**Sign**	
Temperature	TEMP	Degree Celsius	C	3,870,608
Pressure	PRESS	Decibar	DBAR	3,492,296
Conductivity	COND	Siemens/m	SIEMENS/M	242,807
Salinity	SAL	Units of practical scale of salinity	PSS	3,689,684
Chlorinity	CL	Per mille	PPT	28
Absolute content of dissolved oxygen	OXY	Ml/l, mg/l	ML/L, MG/L	142,921
Relative content of dissolved oxygen	OXY SATUR	%	PERCENT	421
pH	PH	-	-	42,876
Alkalinity	ALK	Milligram-equivalent/l	MEQ/L	18,829
Nitrites	NO2	Mg/l, mkg/l	MG/L, UG/L	412
Nitrates	NO3	Micromole/l, mg/l, mkg/l	UMOL/L, MG/L,	25,962

Parameters		Units of measurement		Number of measurements
Name	**Sign**	**Name**	**Sign**	
			UG/L	
Ammonium	NH4	Mg/l	MG/L	51
Total content of nitrogen	TOTN	Mg/l	MG/L	70
Phosphates	PO4	Micromole/l, mg/l, mkg/l	UMOL/L, MG/L, UG/L	95,965
Content of dissolved organic carbon	DOC	Mg/l	MG/L	45
Content of suspended organic carbon	POC	Mg/l, mkg/l	MG/L, UG/L	53
Silicates	SIO4	Micromole/l	UMOL/L	79,902
Chlorophyll	CHL	Mkg/l	UG/L	10,041
Total suspended suspension	TSS	Mg/l	MG/L	20

Time series of water temperature and salinity

Vertical distributions of temperature and salinity are averaged for the period of 1884-2012 (climatic standards) for the transects of the Eastern Black Sea LME. Their location by the vertical corresponds to standard horizons of 0, 5, 10, 15, 20, 25, 30, 50, 75, 100, 150, 200, 250, 300, 350, 400, 450, 500, and further in (every) 100 m to 2500 m. They are located 40 km of each other along the transect.

To construct time series of water temperature and salinity anomalies, (root-) mean square deviations (σ) of mean values were calculated and set in ratio of σ.

To calculate the anomalies, data from the period of 1891 to 2008 was considered. Based on the data of inter-annual variability of temperature and salinity of sea water, number of cases with «whirling» negative anomalies of water salinity per year, air temperature, sediments, and river runoff (Tuzhilkin 2008), three time periods were distinguished: 1891-1959, 1960-1979, and 1980-2008. Thus, anomalies of temperature and salinity for the Black Sea LME were calculated for these time intervals.

Charts with vertical distribution of climatic standard of water temperature and temperature anomalies in September for the period of 1980-2008 for the Yalta – Batumi transect are presented in Figures 3.8 and 3.9.

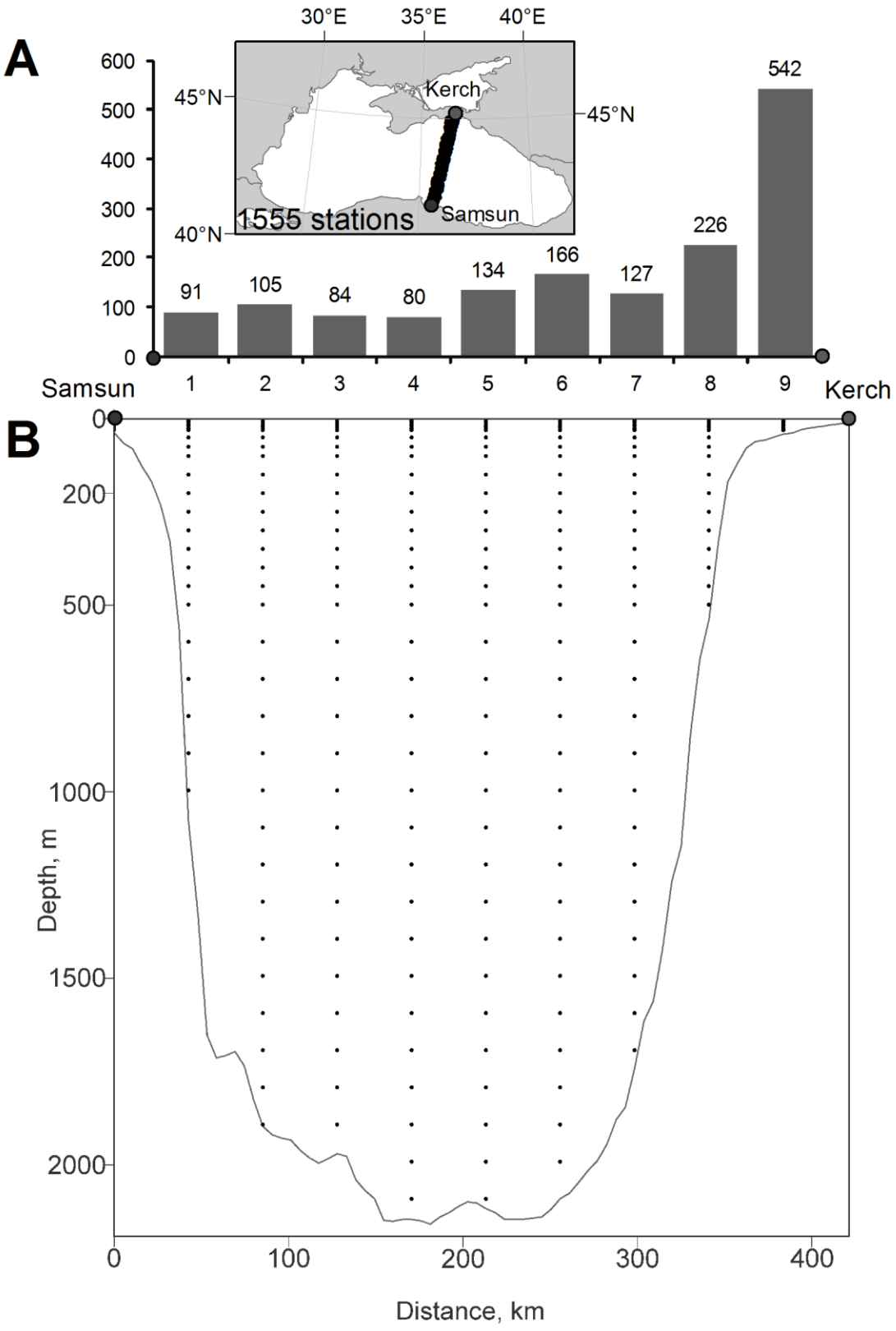

Figure 3.6. Distribution of stations in the 40-km buffer zone (A) and bottom relief (B) along the Samsun – Kerch Strait Transect.

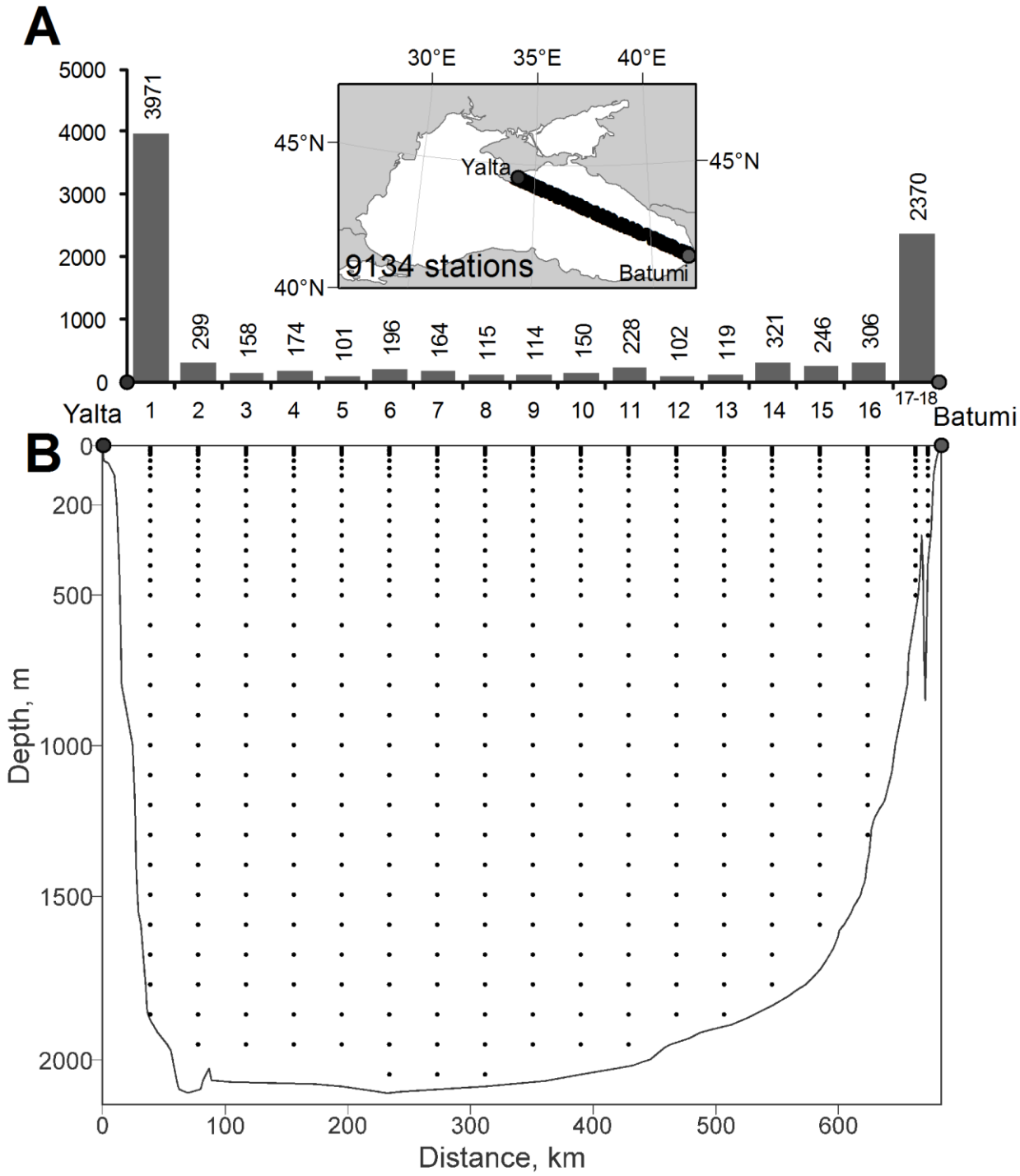

Figure 3.7. Distribution of stations in the 40-km buffer zone (A) and bottom relief (B) along the Yalta – Batumi Transect.

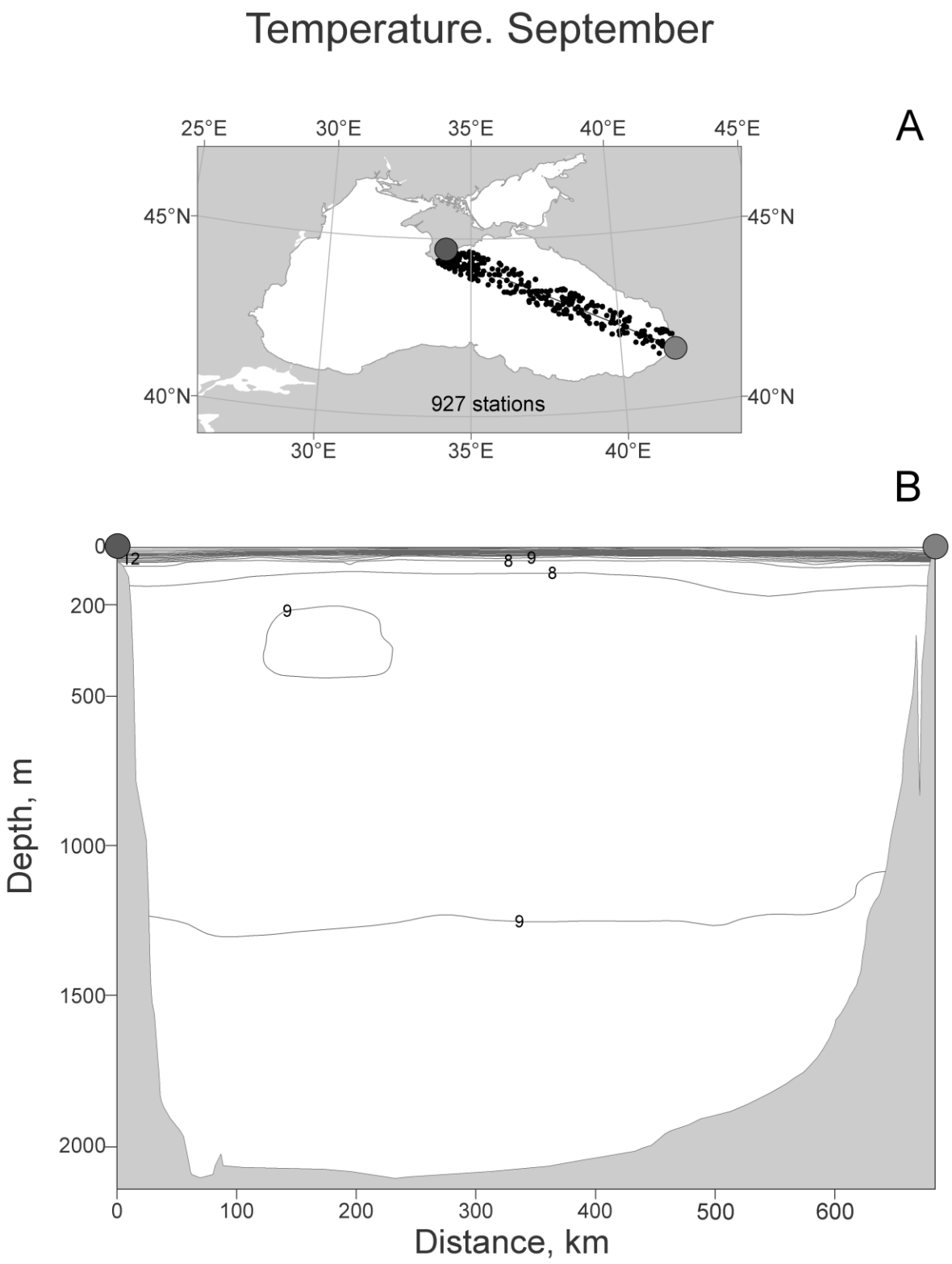

Figure 3.8. A sample of construction of the mean long-term vertical distribution of water temperature for the Yalta – Batumi Transect (A) in September (B), 1890-2008.

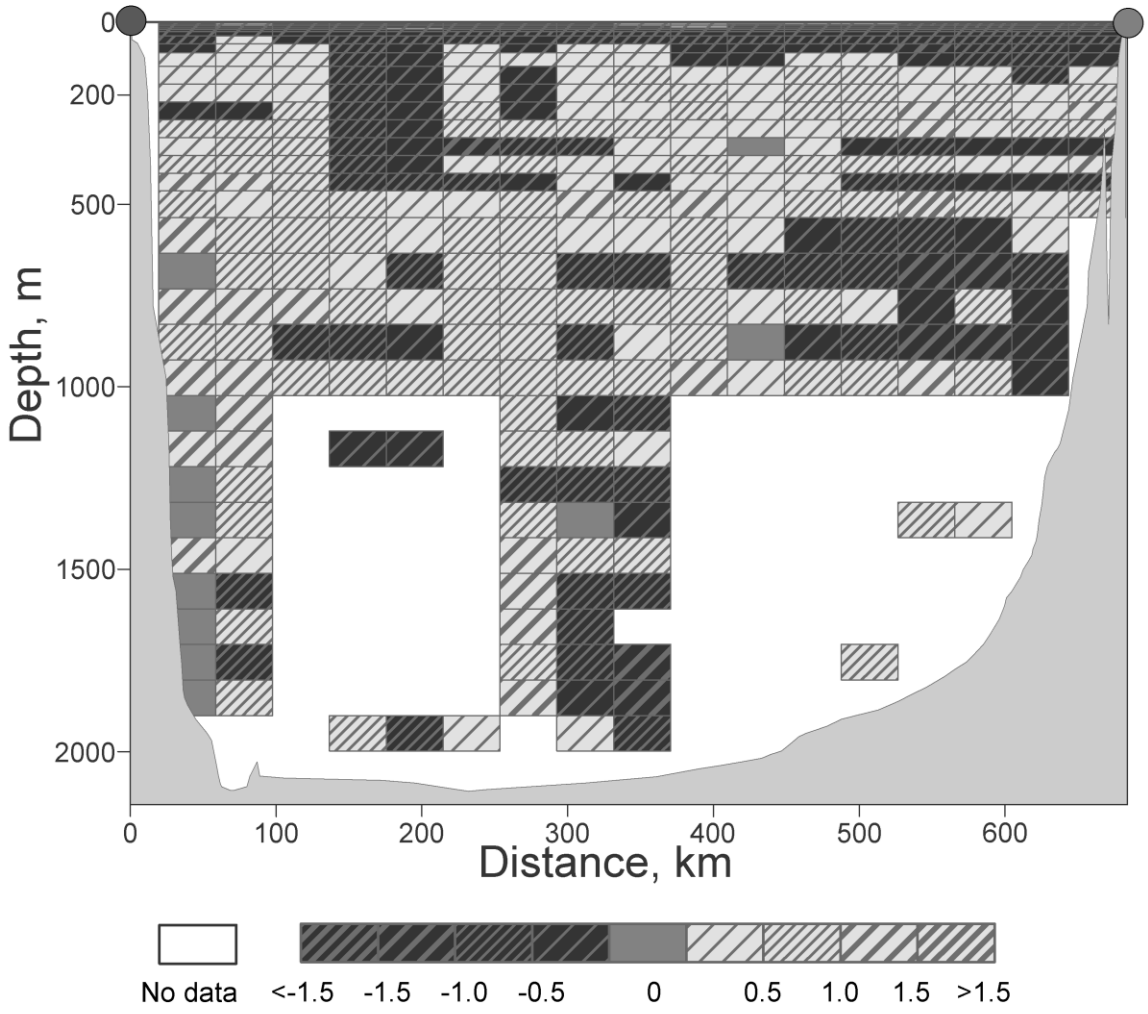

Figure 3.9. An example of calculated water temperature anomaly along the Yalta – Batumi Transect in September for the period of 1890-2008.

3.2. The Black Sea LME and Sea of Azov subarea

Oceanographic database and inventory

The oceanographic database of the Sea of Azov subarea of the Black Sea LME contains 66,609 stations for the period of 1891 to 2012 (Figure 3.10).

The distribution of stations by years and months is presented in Figure 3.11.

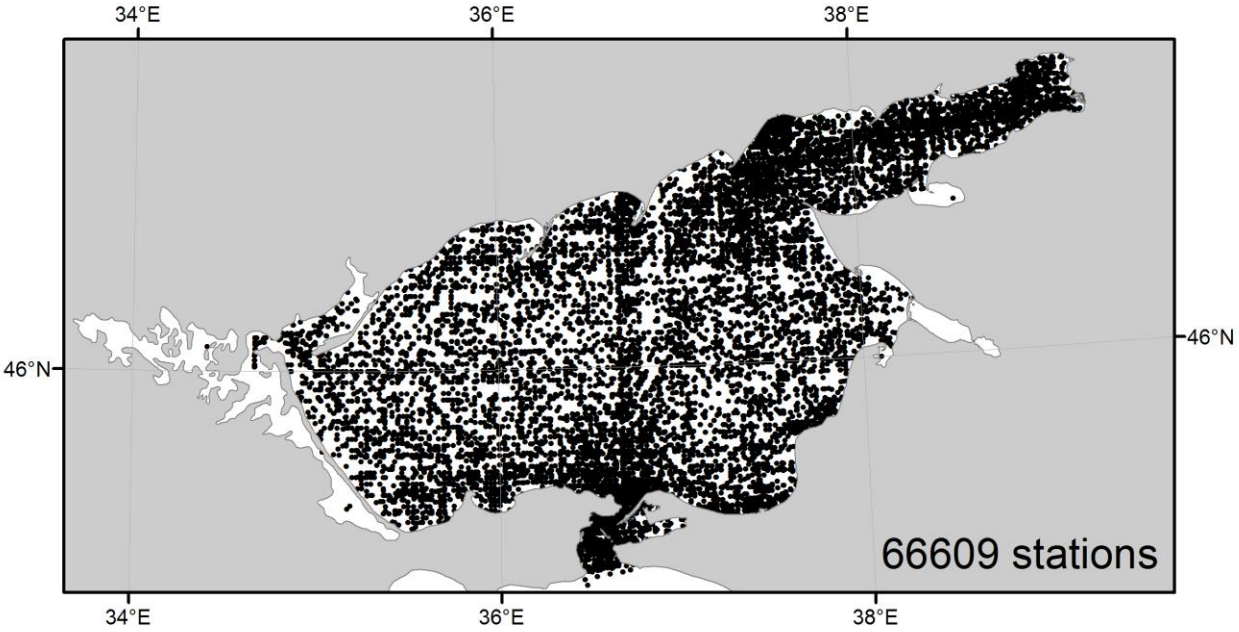

Figure 3.10. Distribution of stations over the Sea of Azov subarea (1891-2012).

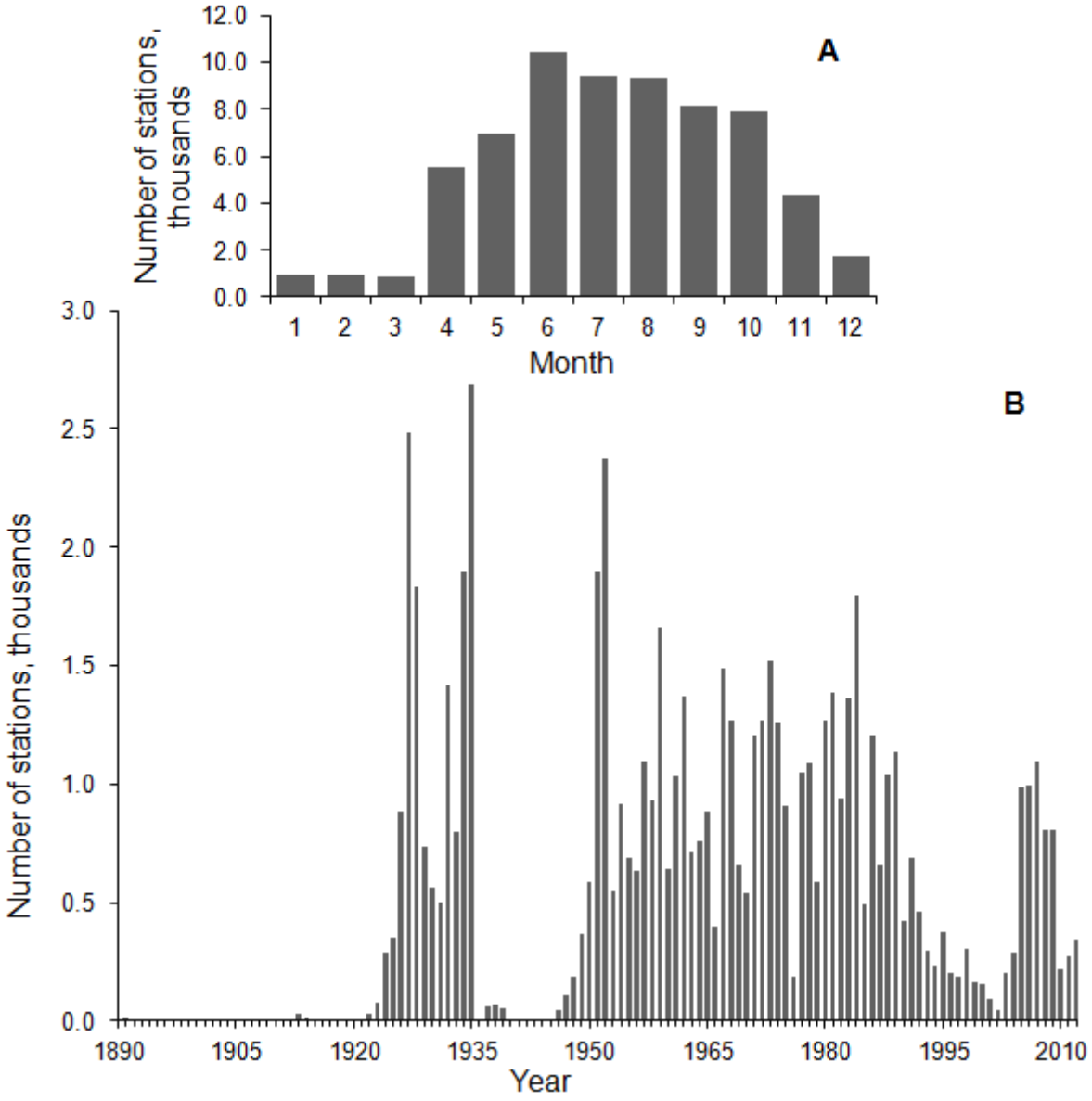

Figure 3.11. Distribution of stations by months (A) and years (B) in the Sea of Azov subarea database (1891-2012).

Compared to the Climatic Atlas of the Sea of Azov 2008 (Matishov et al. 2008), the database covers an additional 31 192 stations (Figure 3.12), which fills in the existing data gaps for the periods of 1960-1970, and 1980-1990.

To analyze the long-term variability of hydrological characteristics of the Sea of Azov, two transects are considered:

- The Kerch Strait–Don Delta (Figure 3.13), which is a continuation of Samsun – the Kerch Strait Transect;
- The Igorevka–Kuban Delta (Figure 3.14).

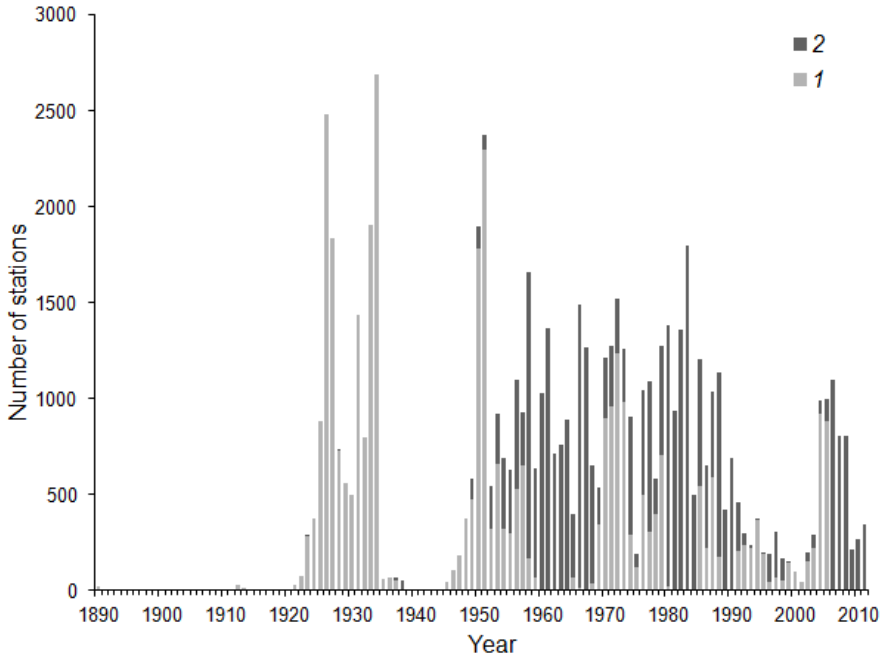

Figure 3.12. Distribution of stations by years in the database of the Climatic Atlas of the Sea of Azov 2008 (Matishov et al. 2008) (1), and the increase in the number of stations in the present Atlas (2*)*.

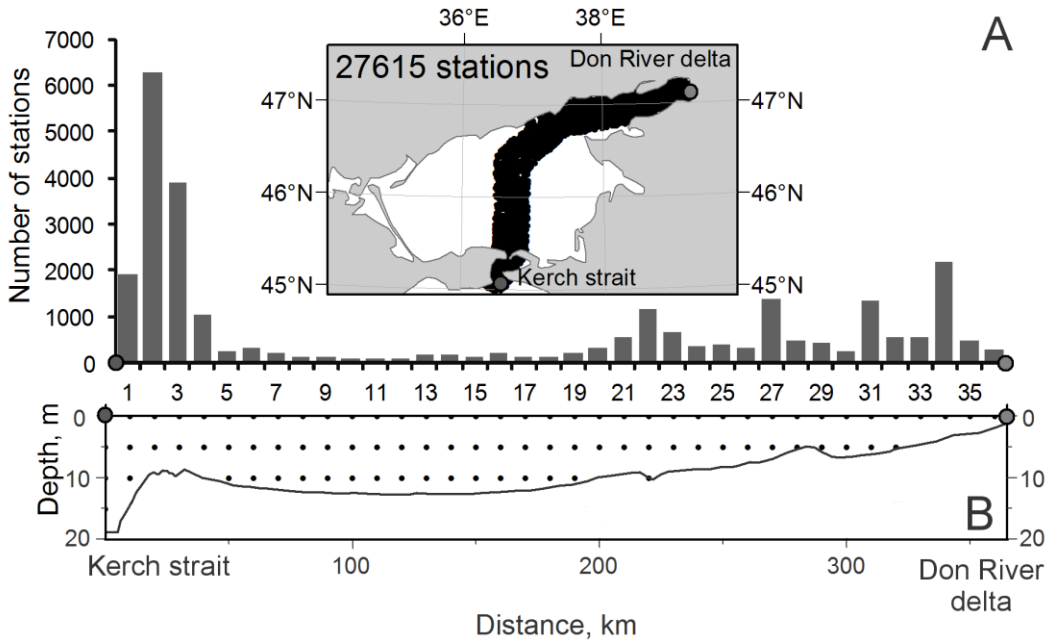

Figure 3.13. Distribution of stations in the 40-km buffer zone (A) and bottom relief (B) along the Kerch Strait – Don Delta Transect.

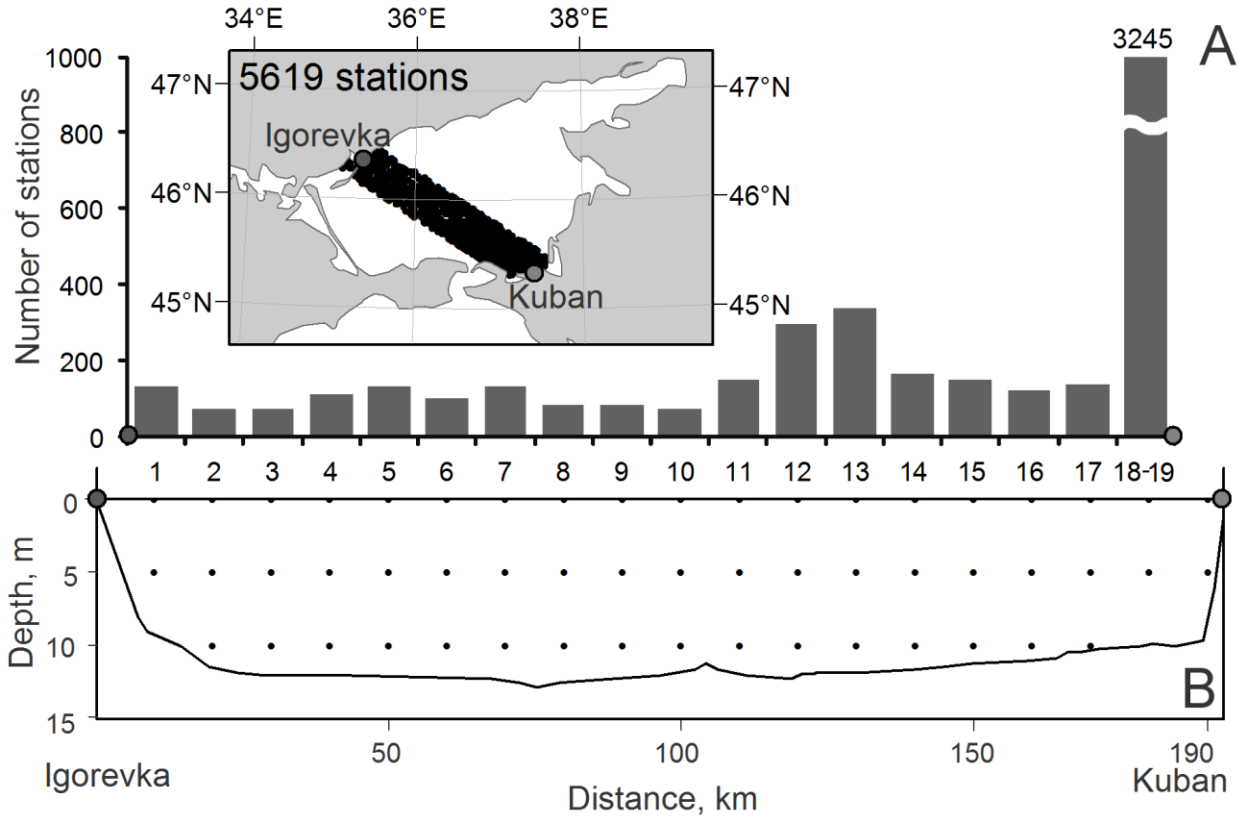

Figure 3.14. Distribution of stations in the 40-km buffer zone (A) and bottom relief (B) along the Settlement of Igorevka – Kuban Delta Transect.

A number of stations located in the belt of 20 km on both sides and used for the construction of climatic standards and anomalies is correlated with every transect. The total number of stations for the Kerch Strait–Don Delta is 27,615, and the Igorevka – Kuban Delta covers 5 619 stations. The Sea of Azov subarea database includes the following parameters (Table 3.3).

Table 3.3. List of indices included in the Sea of Azov database.

Parameter		**Units of measurement**		**Number of measurements**
Name	**Code**	**Name**	**Sign**	
Temperature	TEMP	Degree Celsius	C	231,174
Pressure	PRESS	Decibar	DBAR	53,965
Conductivity	COND	Siemens/m	SIEMENS/M	52,604
Salinity	SAL	Units of practical scale of salinity	PSS	187,296
Chlorine levels	CL	Per mille	PPT	11,393
Absolute content of dissolved oxygen	OXY	Ml/l, mg/l	ML/L, MG/L	29,593
Relative content of dissolved oxygen	OXY SATUR	%	PERCENT	3,213

Parameter		Units of measurement		Number of measurements
Name	**Code**	**Name**	**Sign**	
pH	PH	-	-	12,458
Alkalinity	ALK	Milligram-equivalent/l	MEQ/L	11,687
Nitrites	NO2	Mg/l, mkg/l	MG/L, UG/L	691
Nitrates	NO3	Micromole/l, mg/l, mkg/l	UMOL/L, MG/L, UG/L	1,866
Ammonium	NH4	Mg/l	MG/L	54
Total content of nitrogen	TOTN	Mg/l, mkg/l	MG/L, UG/L	127
Phosphates	PO4	Micromole/l, mg/l, mkg/l	UMOL/L, MG/L, UG/L	10,004
Total content of dissolved phosphorus	PTOTP	Mg/l, mkg/l	MG/L, UG/L	75
Total content of suspended phosphorus	DTOTP	Mg/l, mkg/l	MG/L, UG/L	76
Total content of phosphorus	TOTP	Mg/l, mkg/l	MG/L, UG/L	85
Content of dissolved organic carbon	DOC	Mg/l	MG/L	115
Content of suspended organic carbon	POC	Mg/l, mkg/l	MG/L, UG/L	154
Silicates	SIO4	Micromole/l	UMOL/L	4,639
Chlorophyll-a	CHL A	Mg/l, mkg/l	MG/L, UG/L	307
Total suspension	TSS	Mg/l	MG/L	219

Time series of water temperature and salinity

Vertical distributions of temperature and salinity, averaged for the period of 1891-2010 (climatic standards), are constructed for transects of the Sea of Azov subarea. Their location by the vertical corresponds to standard horizons of 0, 5, and 10 m. They are located within 10 km of each other along the transect. Tables of vertical distribution of water salinity in August for the Don Delta – the Kerch Strait Transect are presented in Figure 3.15.

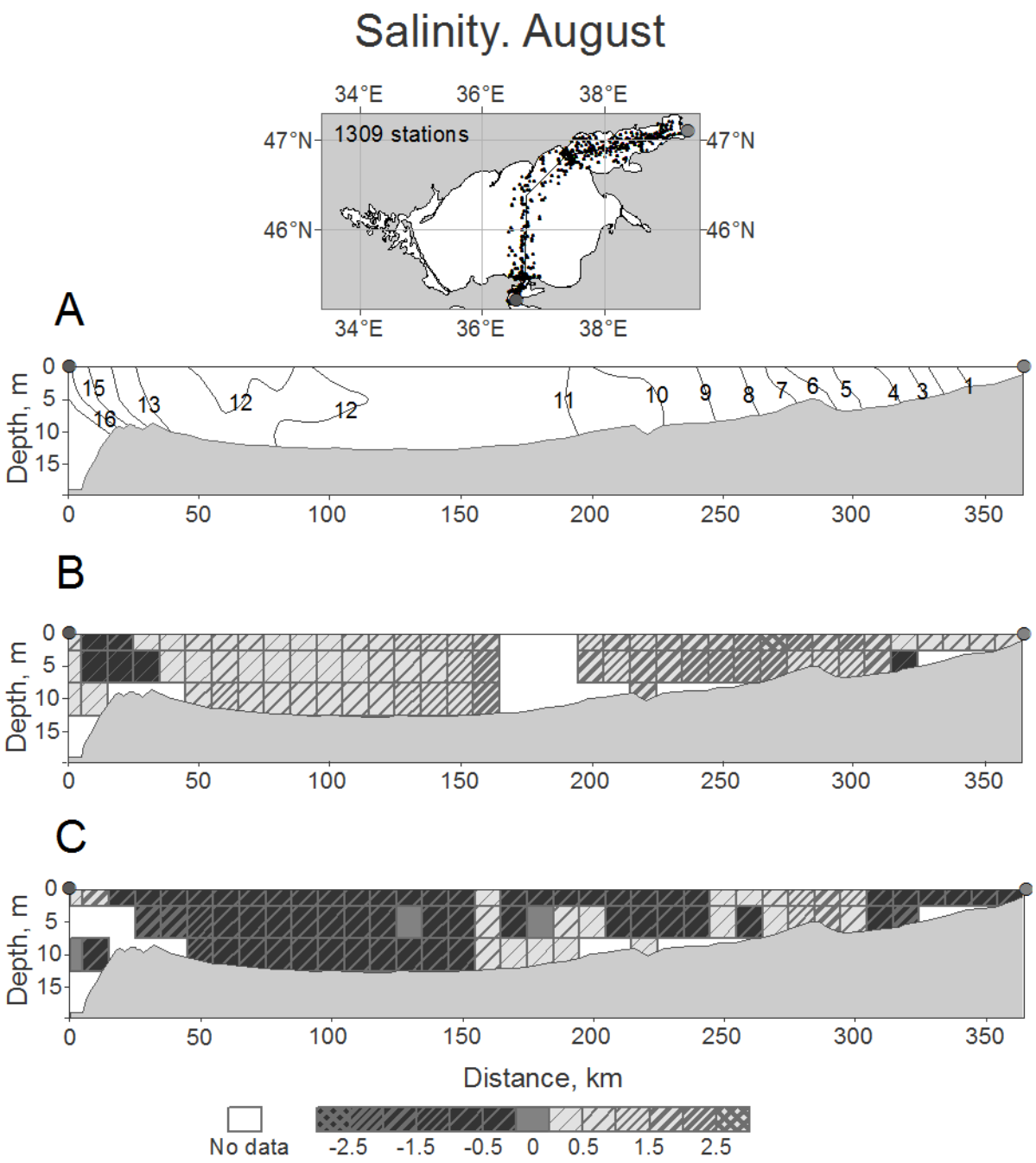

Figure 3.15. A sample of construction of the mean long-term vertical distribution of water salinity in August for the transect (A), anomalies of vertical distribution of salinity in August for the period of 1971-1981 (B) and the period of 1982-2000 (C). At top is the distribution of stations, which were considered when averaging within the belt of 40 km wide.

To calculate the anomalies, inter-annual variability of average salinity data from the period of 1922-2010 was considered (Figure 3.16). Calculations following the mathematical model of (Matishov et al. 2006) were made. The period of 1922-2010 was subdivided into 8 time intervals (1922-34, 1935-41, 1946-49, 1950-57, 1958-1970, 1971-81, 1982-2000, and 2001-2010), and

temperature and salinity anomalies for the Sea of Azov subarea were calculated within the ranges of these intervals.

An example of the distribution of salinity is presented in Figure 3.15.

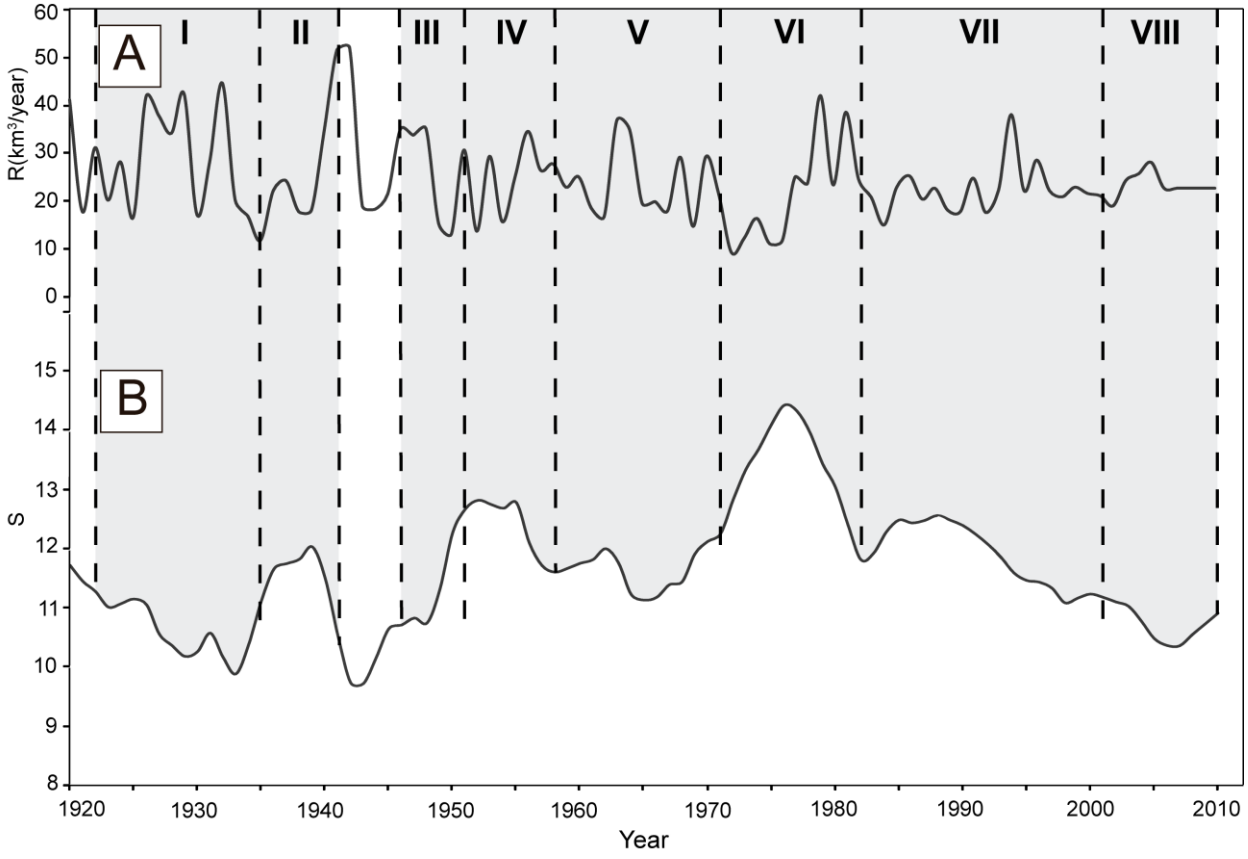

Figure 3.16. Inter-annual variability of mean salinity (S) and river runoff (R, km^3/year) of the Sea of Azov subarea, from 1922-2010.

Time series of ice conditions

The Sea of Azov subarea is a sea with ice cover formed each year. Shipping activities are not possible in winter without the assistance of icebreakers. To characterize the ice conditions of the Sea of Azov, the data from coastal hydro-meteorological sites (Figure 3.17) have been collected and presented in this Atlas. Data is organized by the date of the first registration of ice in the coastal zone and the date when the entire water area becomes ice free.

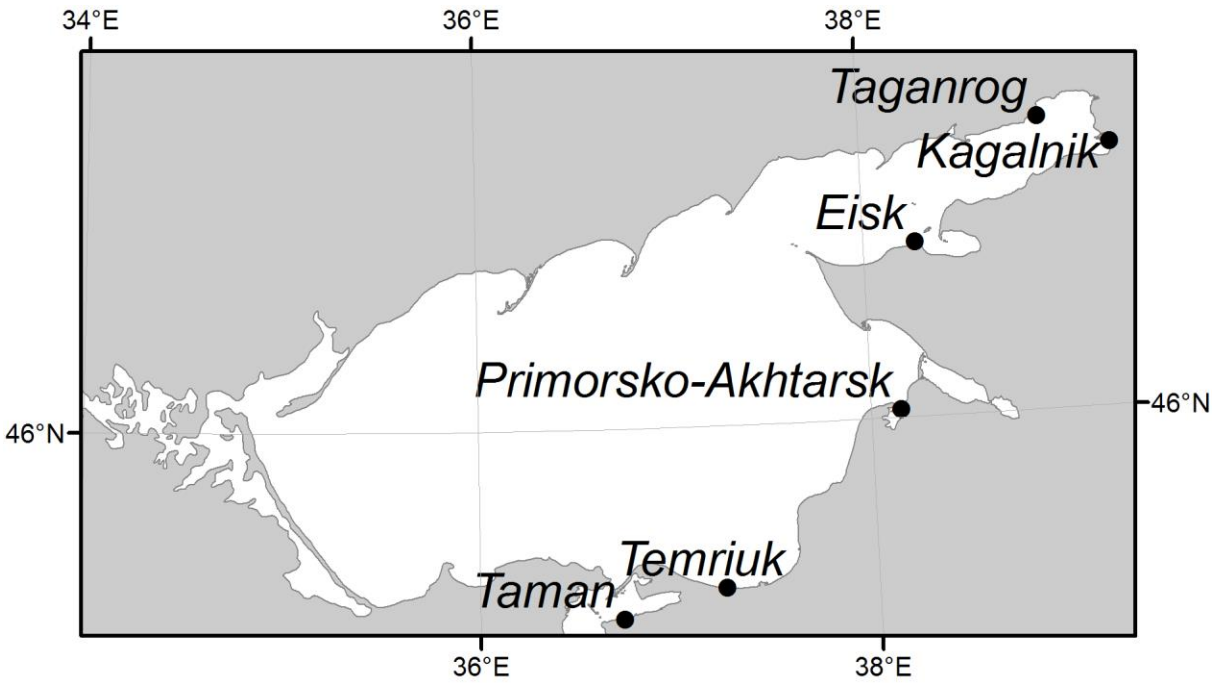

Figure 3.17. Coastal hydro-meteorological stations with observation data on the Sea of Azov subarea ice conditions.

These data have been generalized and presented in the way of graphs, illustrating the climatic dynamics of the ice conditions in the Sea of Azov subarea. Figure 3.18 gives an example for Taganrog.

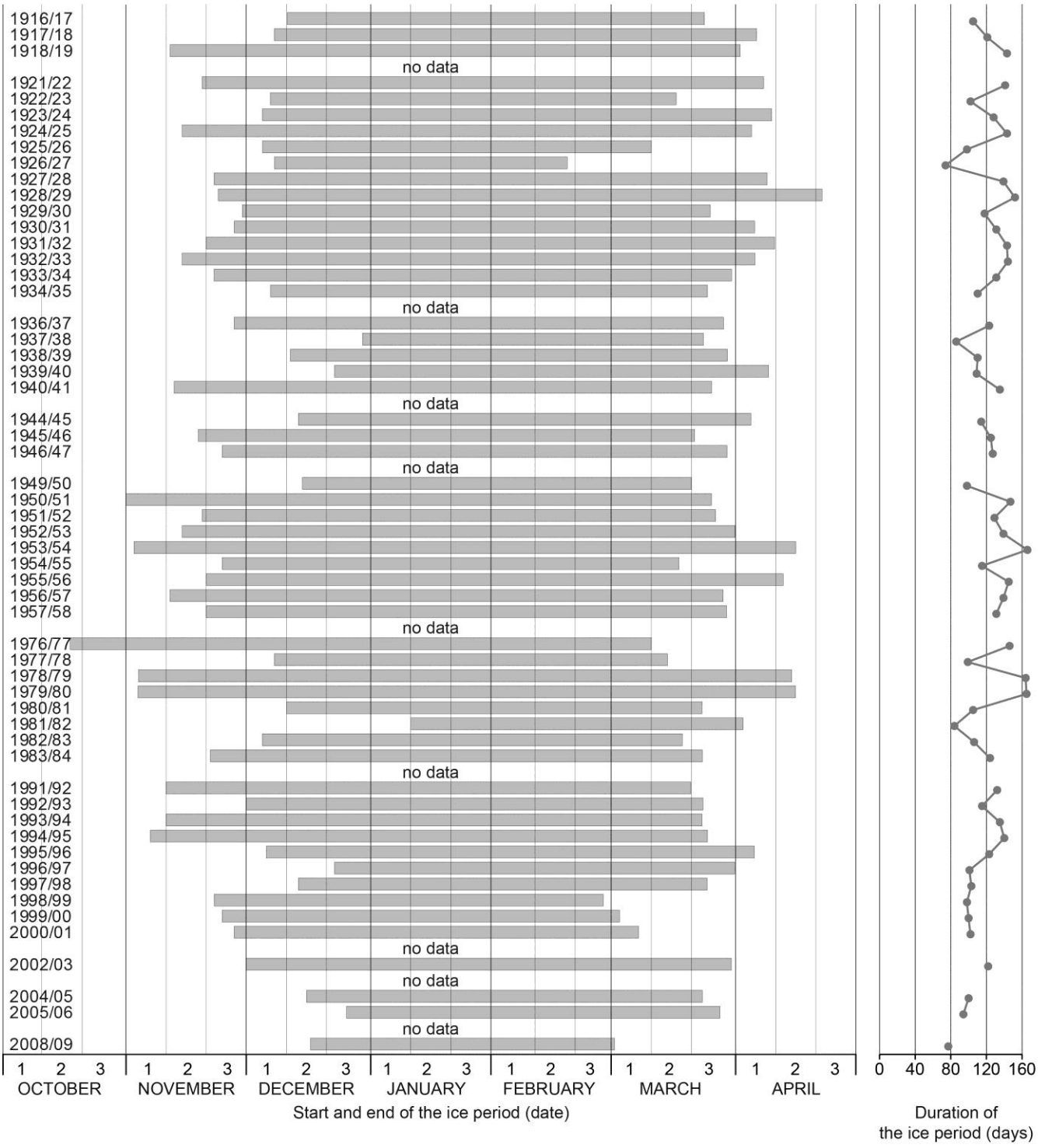

Figure 3.18. Long-term dynamics of the duration of ice period in Taganrog.

3.3. The Caspian Sea LME

Oceanographic database and inventory

The Caspian Sea LME database contains 43,333 stations for the period of 1897 to 2011 (Figure 3.19).

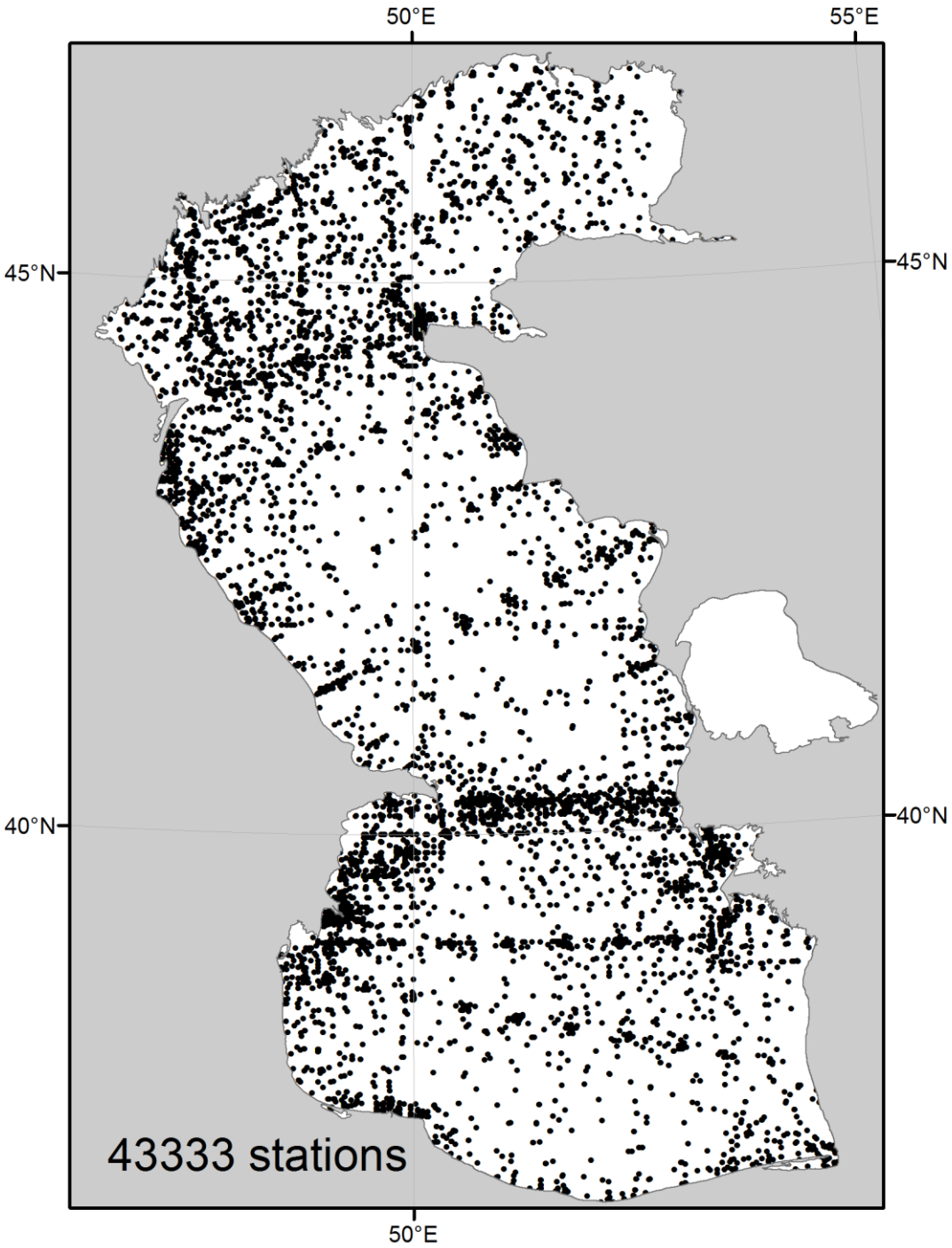

Figure 3.19. Distribution of stations over the Caspian Sea LME area (1897-2011).

Distribution of stations by years and months is presented in Figure 3.20.

Measurements were performed along 8 transects in the Caspian Sea LME (Figure 3.21, Table 3.4).

A number of stations located within the belt of 20 km on each side and used for the construction of climatic standards and anomalies is correlated with every transect.

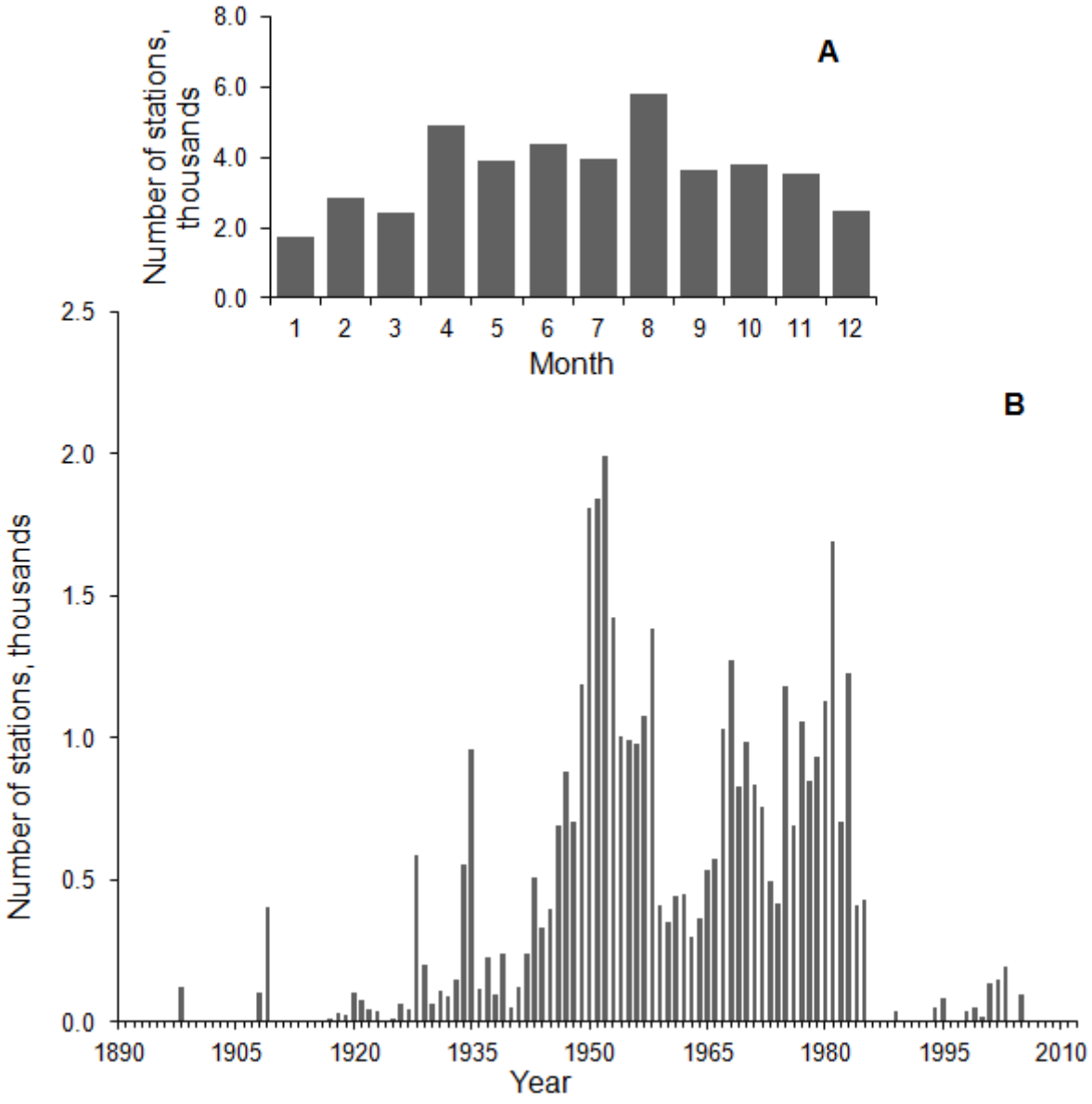

Figure 3.20. Distribution of stations by months (A) and years (B) in the Caspian Sea LME database (1897-2011).

Table 3.4. Characteristics of the transects of the Caspian Sea LME.

Area of the sea			Number of stations
No. of transect	**Name of the transect**	**Description of the transect**	
1	«Zuidwest Shalyga Island – Kulaly Island»	Eastern part of the Northern Caspian Sea LME	771
2	«Novinsky Island – Kulaly Island»	Boundary between the Eastern and Western parts of the Northern Caspian Sea LME	1,092
3	«Belinsky Canal – to the South to the Chechen' Island – Mangyshlak Peninsula Transect»	Western part of the Northern Caspian Sea LME	925
3a	«Volga-Caspian Canal to the Chechen' Island – Mangyshlak Peninsula Transect»	Western part of the Northern Caspian Sea LME	2,832
4	«Chechen' Island – Mangyshlak Peninsula»	Boundary between Northern and Central Caspian Sea LME	1,562
5	«Divichi – Kenderly»	Central Caspian Sea LME	962
6	«Zhiloi Island – Kuuli Cape»	Boundary between the Central and Southern Caspian Sea LME	2,380
7	«Kurinsky Kamen' Island – Ogurchinsky Island»	Southern Caspian Sea LME	1,159

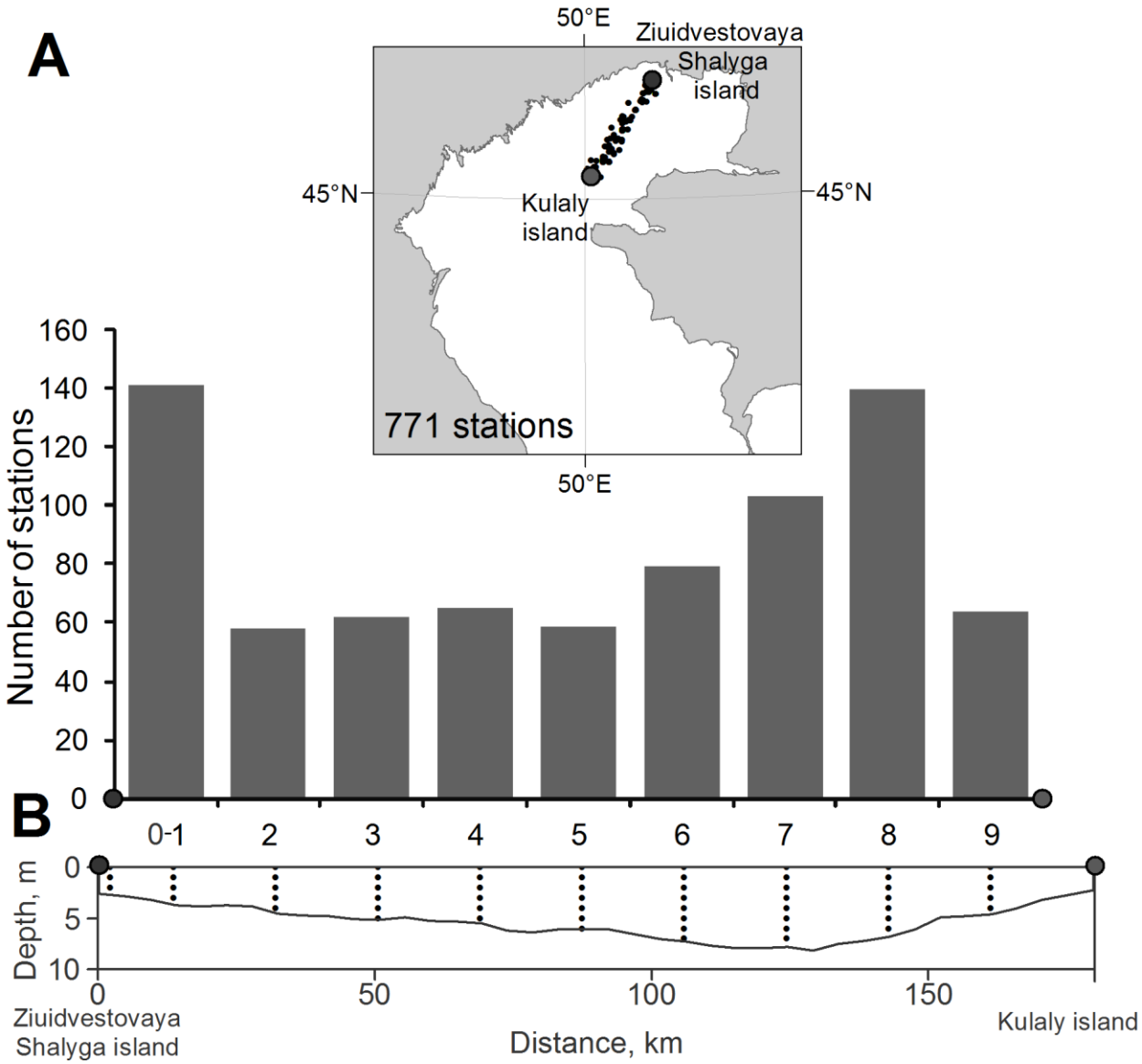

Figure 3.21. Distribution of stations in the 40-km buffer zone (A) and bottom relief (B) along Transect No. 1.

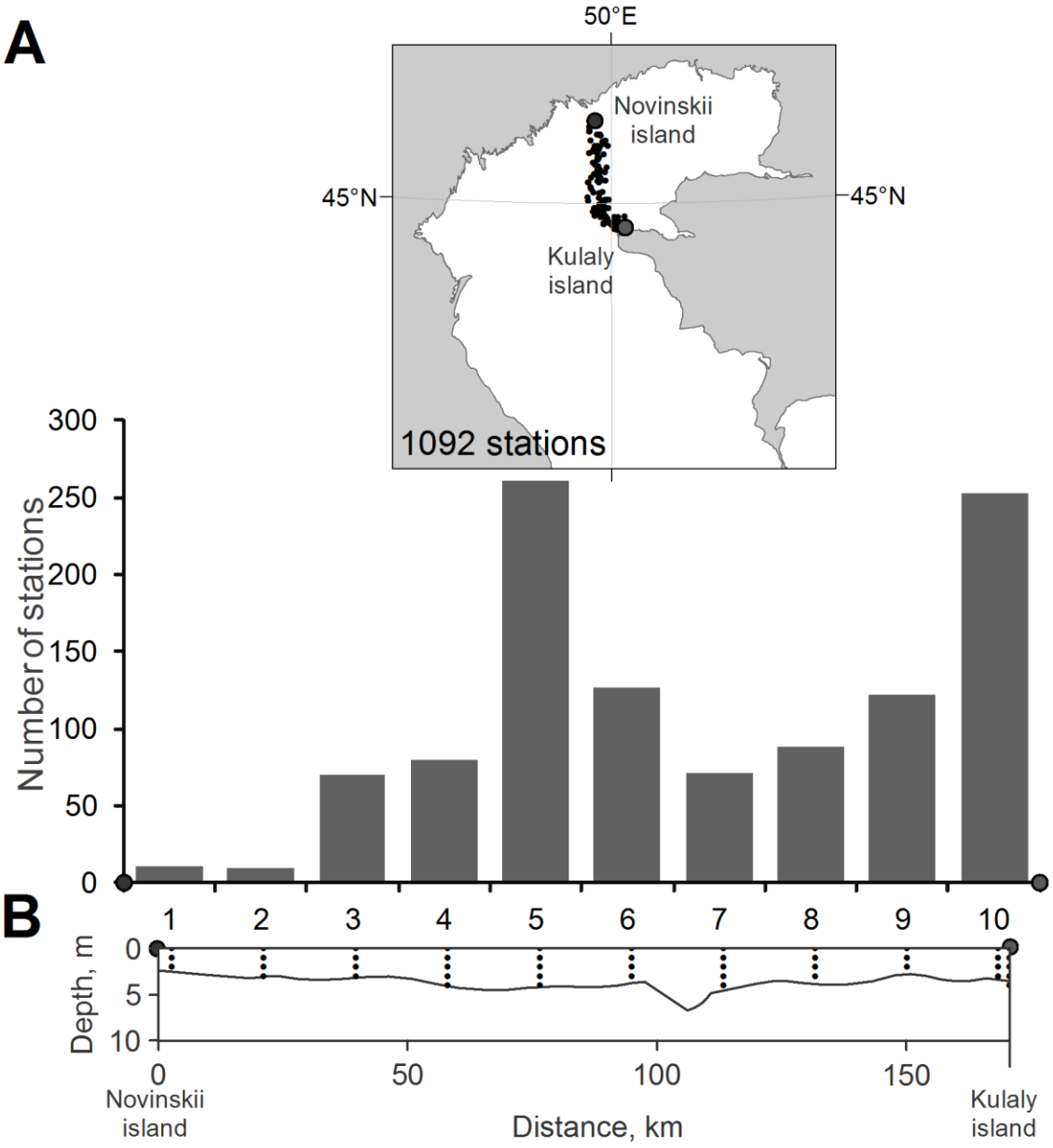

Continuation of Figure 3.21. Distribution of stations in the 40-km buffer zone (A) and bottom relief (B) along Transect No. 2.

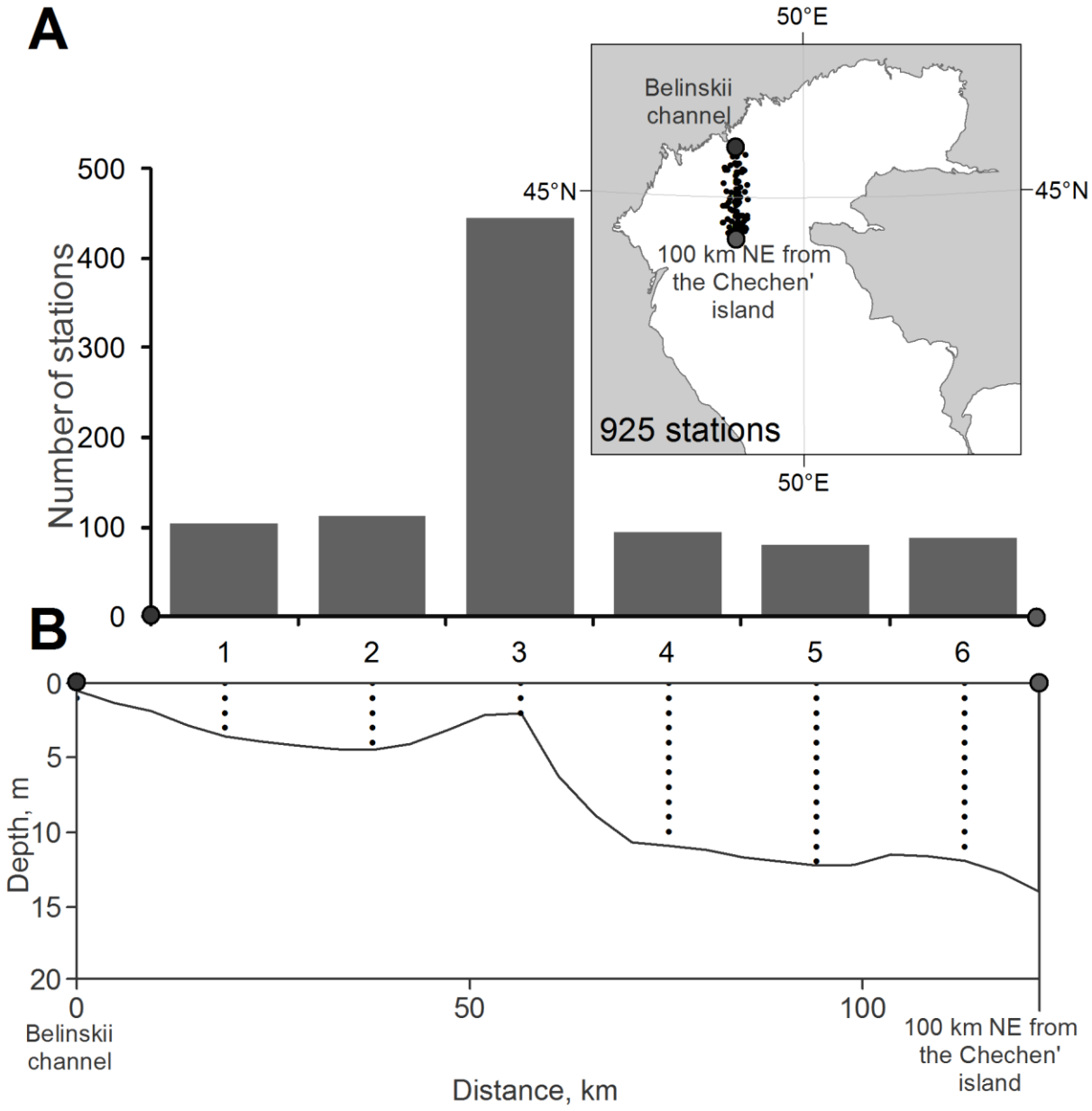

Continuation of Figure 3.21. Distribution of stations in the 40-km buffer zone (A) and bottom relief (B) along Transect No. 3.

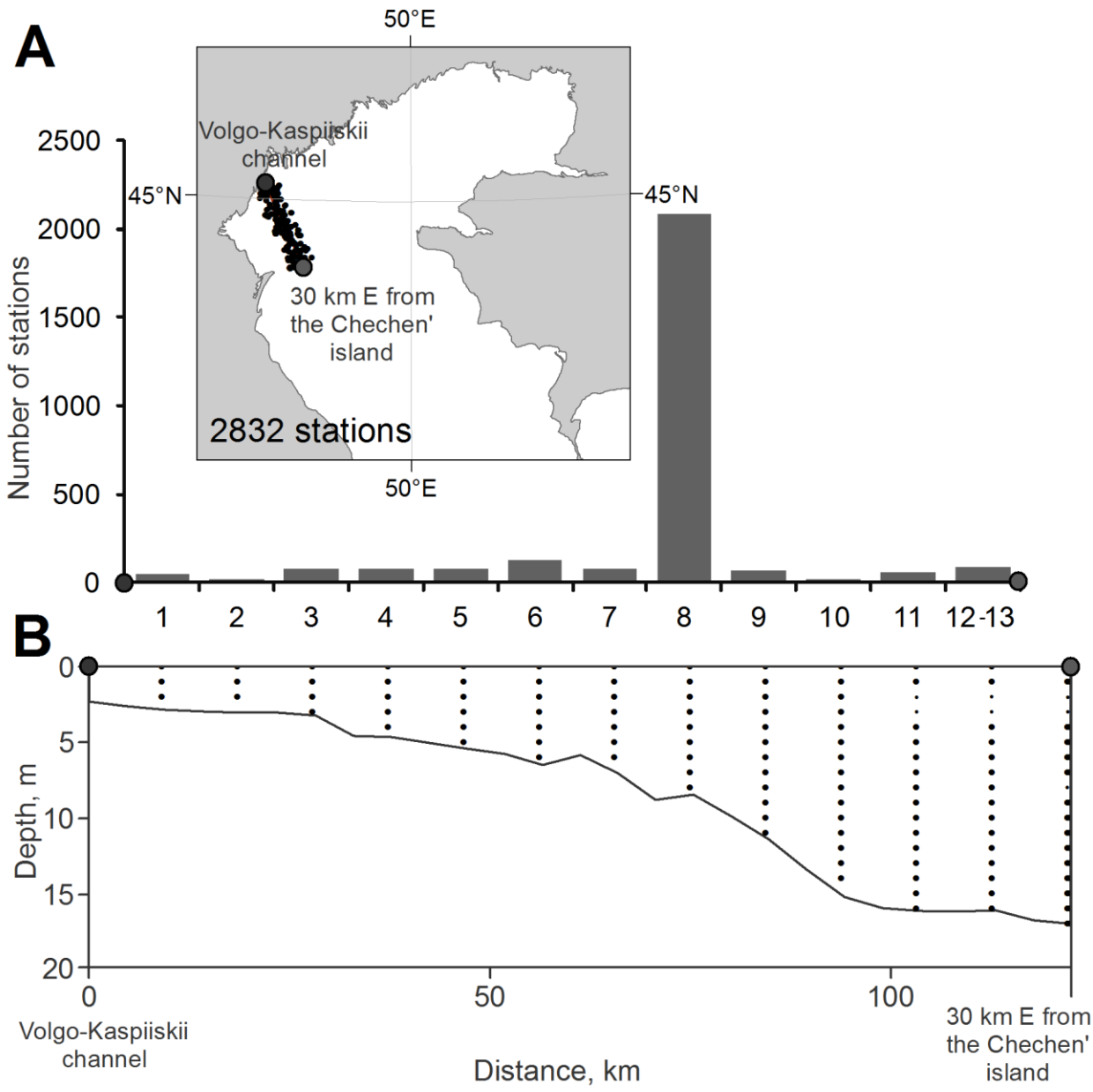

Continuation of Figure 3.21. Distribution of stations in the 40-km buffer zone (A) and bottom relief (B) along Transect No. 3a.

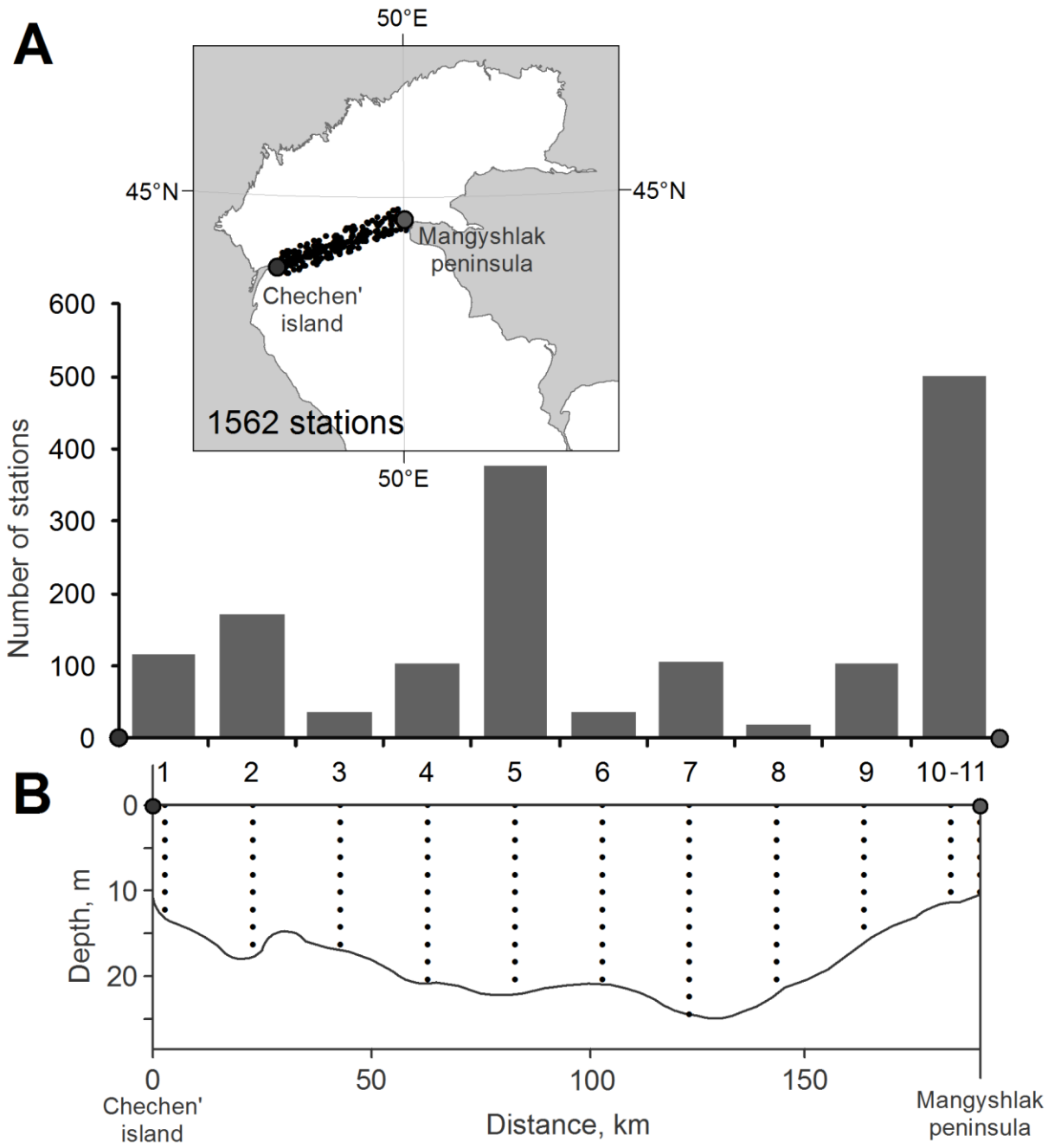

Continuation of Figure 3.21. Distribution of stations in the 40-km buffer zone (A) and bottom relief (B) along Transect No. 4.

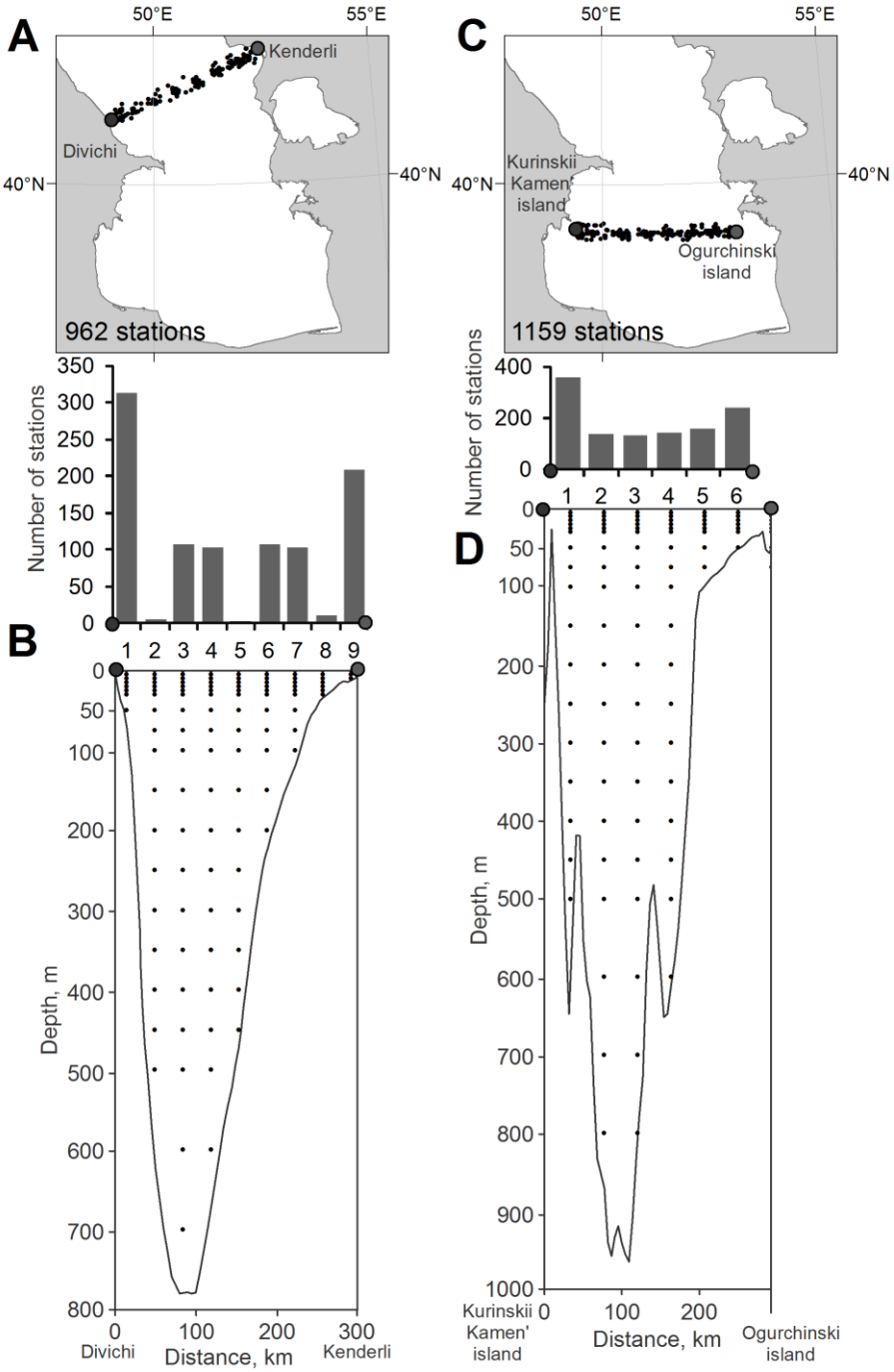

Continuation of Figure 3.21. Distribution of stations in the 40-km buffer zone (A) and bottom relief (B) along Transect No. 5 (Left). Distribution of stations in the 40-km buffer zone (A) and bottom relief (B) along Transect No. 7 (Right).

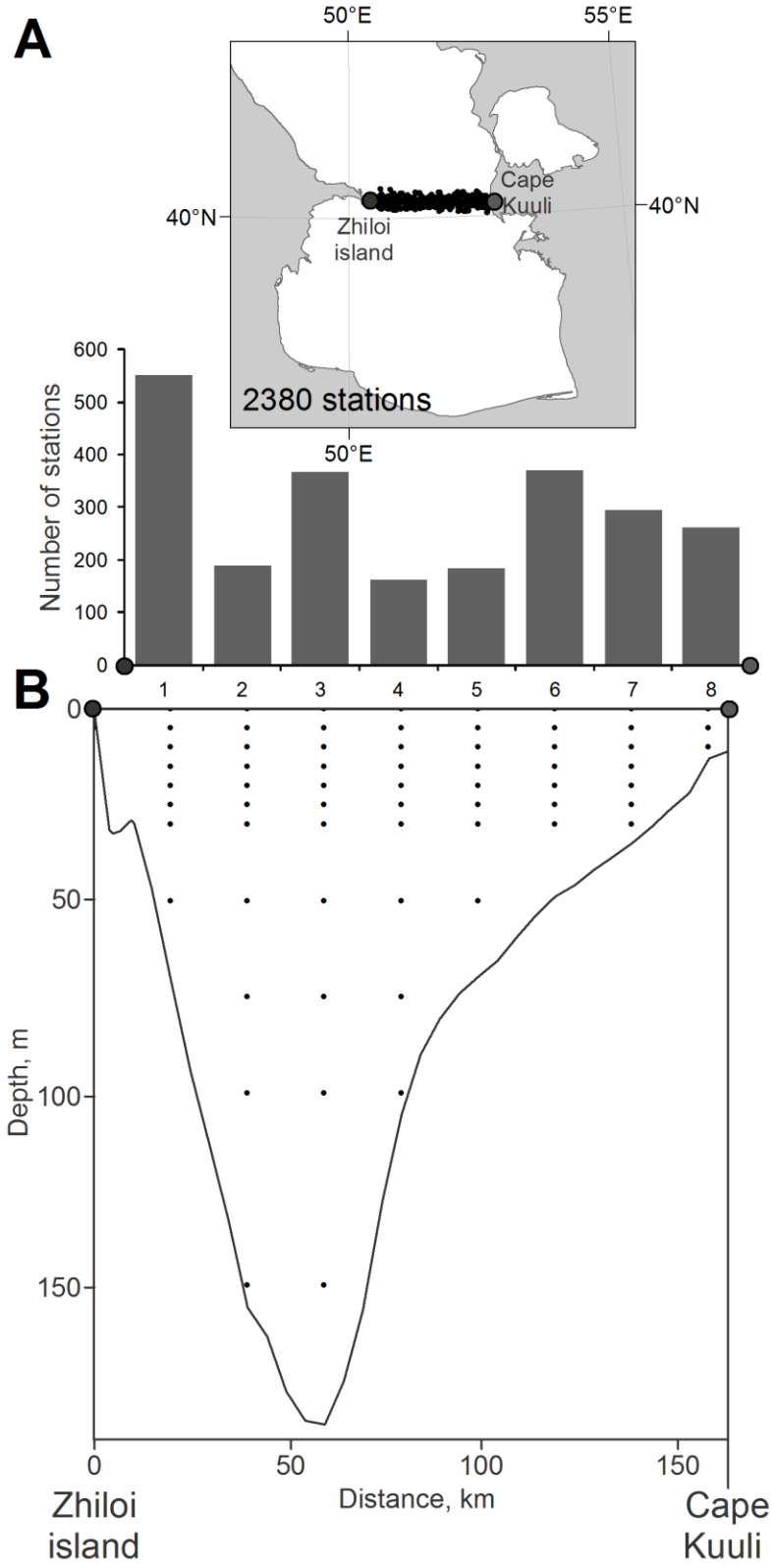

Continuation of Figure 3.21. Distribution of stations in the 40-km buffer zone (A) and bottom relief (B) along Transect No. 6.

The Caspian Sea LME database includes the following parameters (Table 3.5).

Table 3.5. List of indices included in the Caspian Sea database.

Parameter		Units of measurement		Number of measurements
Name	**SCode**	**Name**	**Sign**	
Temperature	TEMP	Degree Celsius	C	216,040
Pressure	PRESS	Decibar	DBAR	41,371
Conductivity	COND	Siemens/m	SIEMENS/M	42,814
Salinity	SAL	Units of practical scale of salinity	PSS	191,620
Chlorinity	CL	Per mille	PPT	14,647
Absolute content of dissolved oxygen	OXY	Ml/l, mg/l	ML/L, MG/L	59,335
Relative content of dissolved oxygen	OXY SATUR	%	PERCENT	3,633
pH	PH	-	-	49,455
Alkalinity	ALK	Milligram-equivalent/l	MEQ/L	19,705
Hydrogen sulphide	H2S	Ml/l	ML/L	27
Nitrites	NO2	Mg/l, mkg/l	MG/L, UG/L	4,668
Nitrates	NO3	Micromole/l, mg/l, mkg/l	UMOL/L, MG/L, UG/L	6,185
Ammonium	NH4	Mg/l, mkg/l	MG/L, UG/L	407
Total content of nitrogen	TOTN	Mg/l	MG/L	46
Phosphates	PO4	Micromole/l, mg/l, mkg/l	UMOL/L, MG/L, UG/L	30,718
Total content of phosphorus	TOTP	Mg/l, mkg/l	MG/L, UG/L	30
Content of dissolved organic carbon	DOC	Mg/l	MG/L	19
Content of suspended organic carbon	POC	Mg/l	MG/L	15
Silicates	SIO4	Micromole/l, mkg/l	UMOL/L, UG/L	12,645
Chlorophyll-a	CHL A	Mkg/l	UG/L	28
Total suspension	TSS	Mg/l	MG/L	20

Time series of water temperature and salinity

Vertical distributions of temperature and salinity averaged for the period of 1897-2011 have been constructed for transects of the Caspian Sea LME (Table 3.6 and Figure 3.21). For the Northern Caspian Sea Transects, a vertical grid of 1m x 1m was used. For the deep-water transects of the Central and Southern Caspian Sea LME, standard horizons/profiles were used.

Table 3.6. Construction parameters of vertical fields of hydrological characteristics' distribution for the transects of the Caspian Sea.

No. of Transect	Mesh step along the transect line (km)	Mesh step by depth (m) / Standard horizons/profiles (m)
Transect 1	20	1
Transect 2	20	1
Transect 3	20	1
Transect 3a	10	1
Transect 4	20	2
Transect 5	40	0, 5, 10, 20, 25, 30, 50, 75, 100, 150, 200, 250, 300, 350, 400, 450, 500, 600, 700, 800, 900, 1000
Transect 6	20	0, 5, 10, 20, 25, 30, 50, 75, 100, 150, 200
Transect 7	40	0, 5, 10, 20, 25, 30, 50, 75, 100, 150, 200, 250, 300, 350, 400, 450, 500, 600, 700, 800, 900, 1000

To construct time series of water temperature and salinity anomalies, the absolute difference of values in the knots of the mesh were calculated for each transect by periods: 1914-1934, 1961-1967, 1972-1979, 1984-1991, and 2004-2010 (Berdnikov et al. 2010; Matishov et al. 2012).

These periods were distinguished based on the graphs of long-term dynamics of the Caspian Sea level and the river runoff (Figure 3.22).

Examples of water temperature for February and temperature anomalies in February of 1961-1967 for Transect 6 are presented in Figure 3.23 and Figure 3.24.

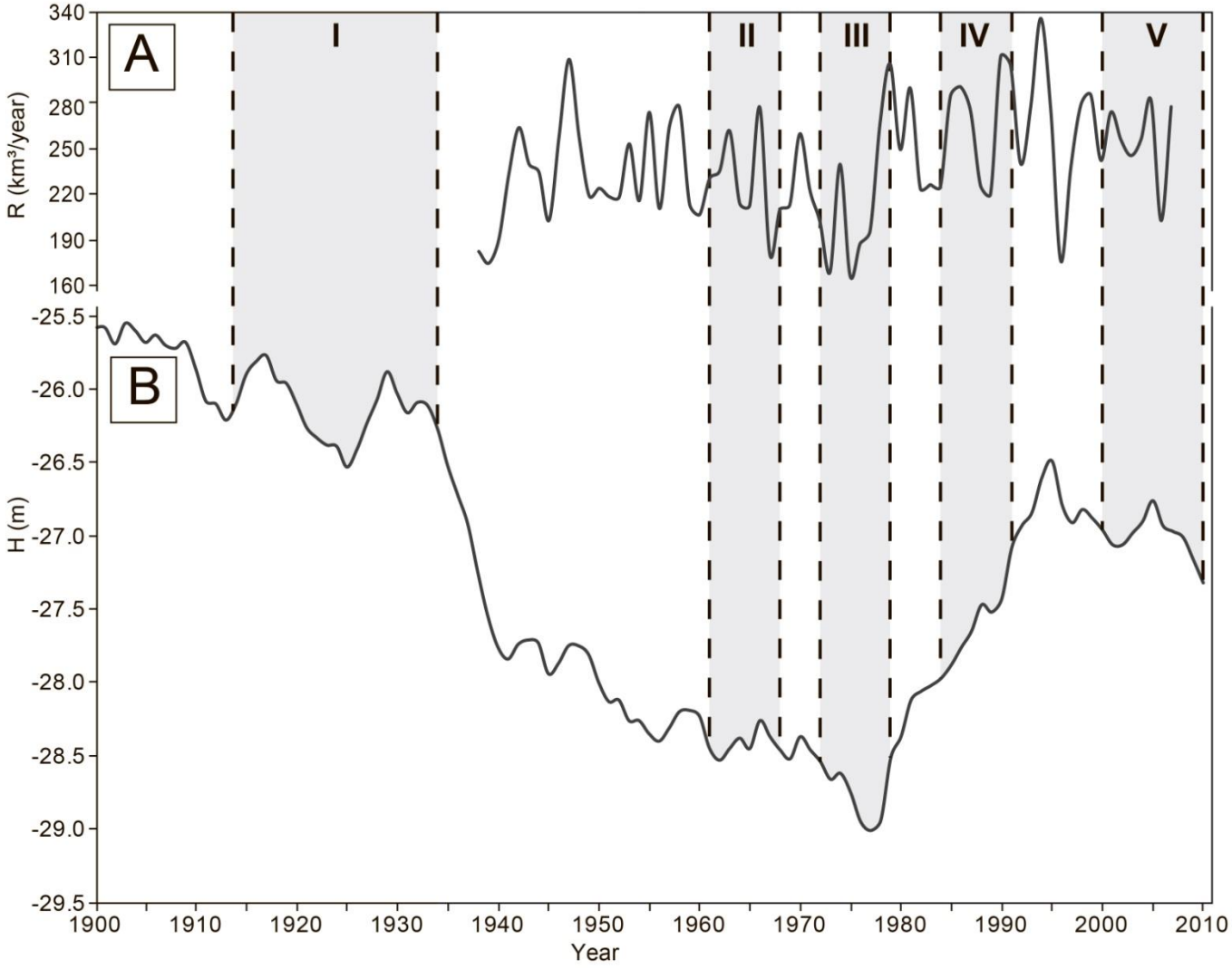

Figure 3.22. The change of the river runoff (R) (A) and sea level (H) of the Caspian Sea LME (B) for the period of 1900-2010.

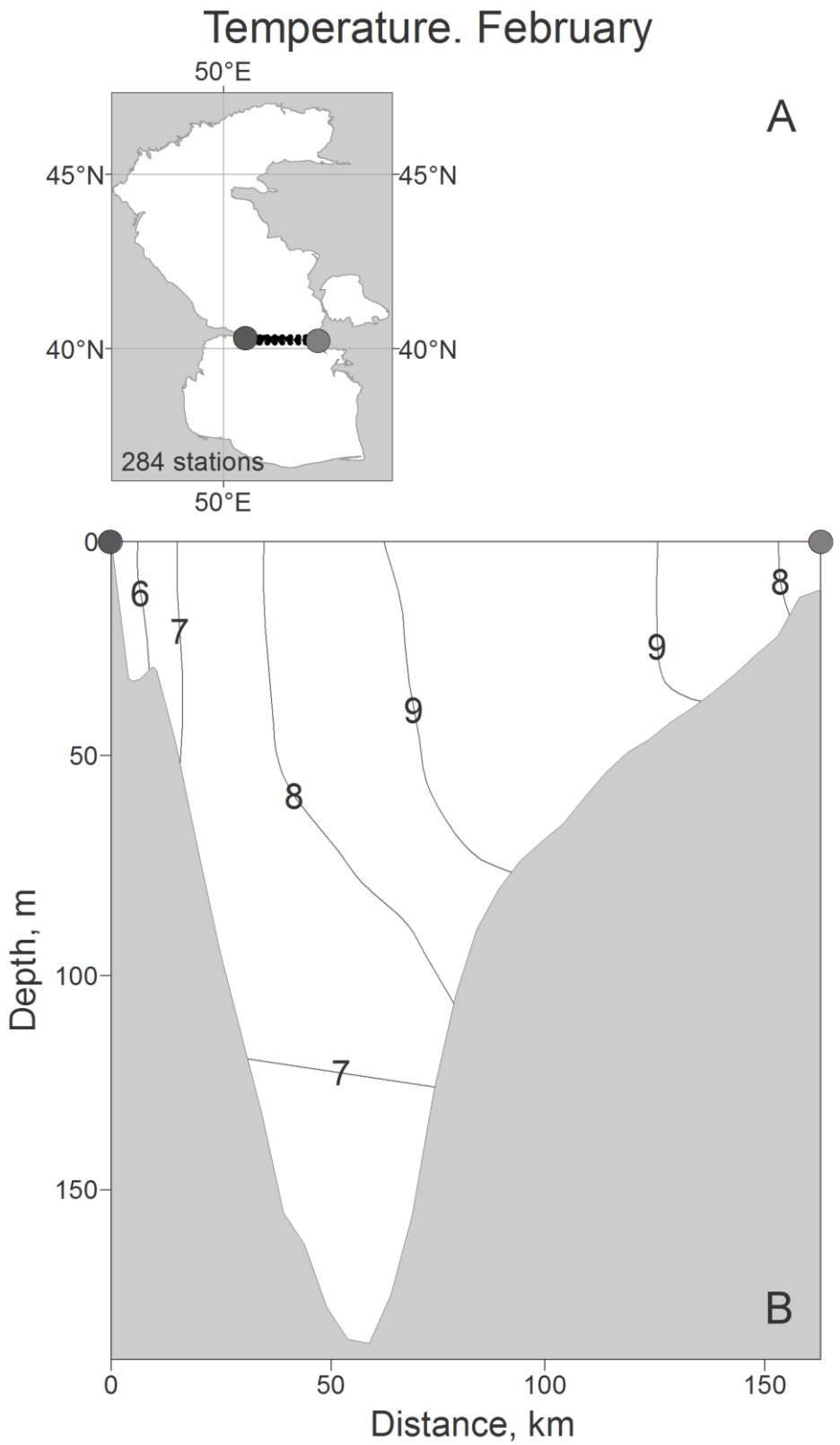

Figure 3.23. A sample construction of the mean long-term vertical distribution of average water temperature in February for Transect No. 6.

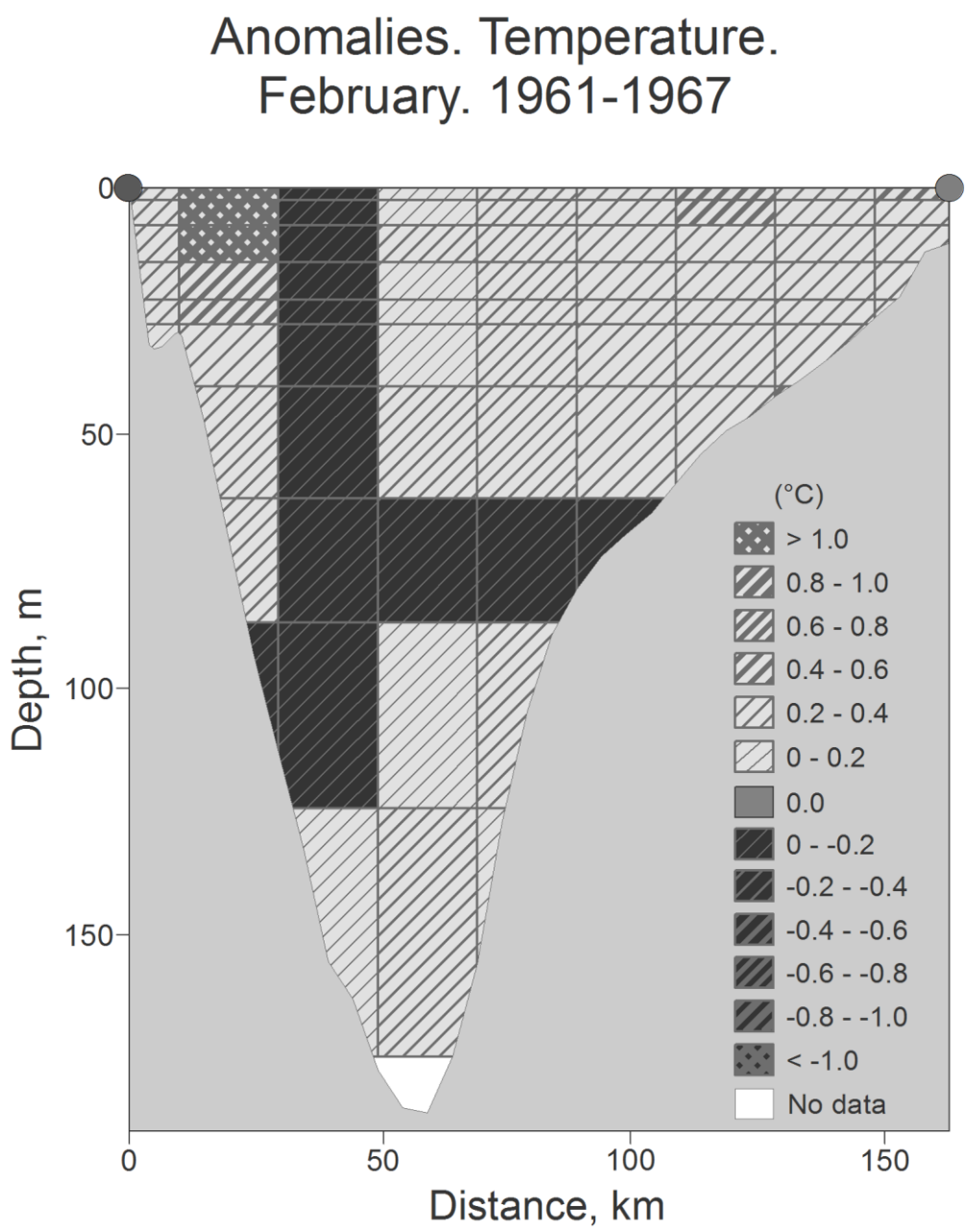

Figure 3.24. An example of calculated water temperature anomaly at Transect No. 6 in February of 1961-1967.

Time series of ice conditions

The ice cover in the Caspian Sea LME is formed each year in the northern region. The present Atlas contains observation data collected at the coastal hydro-meteorological sites (Figure 3.25). These observations are used to characterise the ice conditions of the Northern Caspian Sea, which is organized by the date of the first registration of ice in the coastal zone and the date when the entire water area becomes ice free.

These data are generalized and presented as graphs that illustrate the climatic dynamics of the Caspian Sea LME ice conditions. Figure 3.26 is an example of a hydro-meteorological station located on the Island of Seal (Tyuleniy).

.

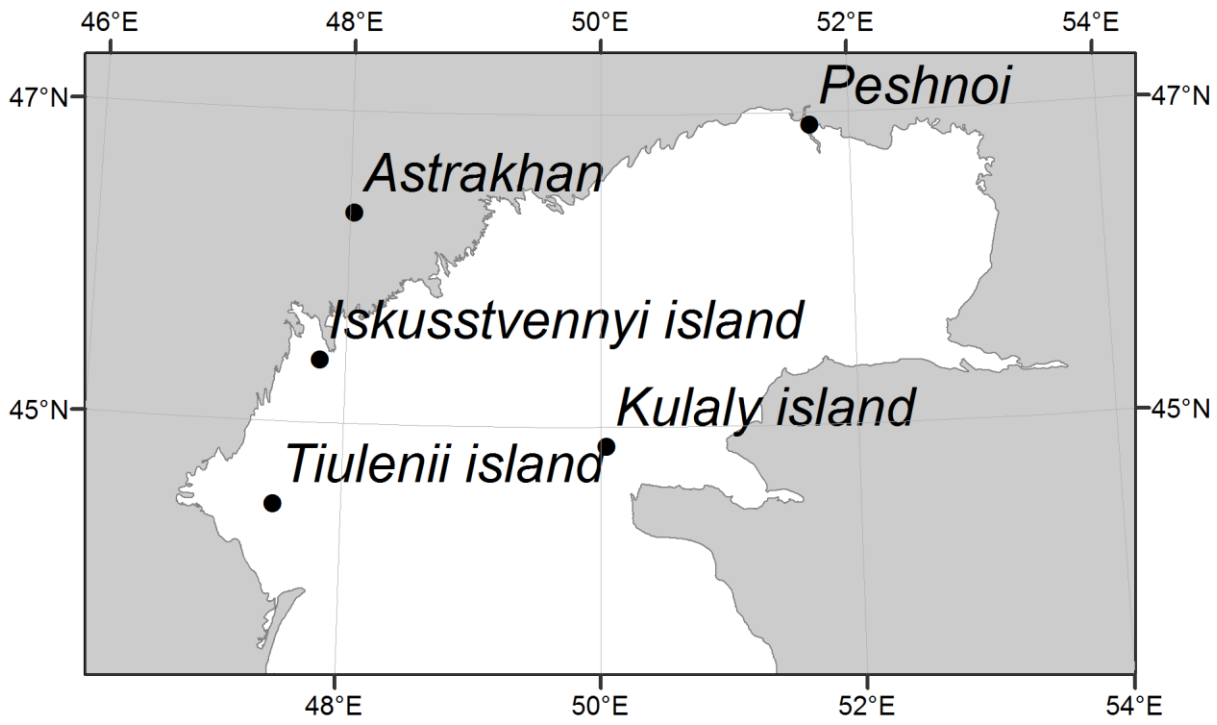

Figure 3.25. Coastal hydro meteorological stations with ice condition observation data in the Caspian Sea LME.

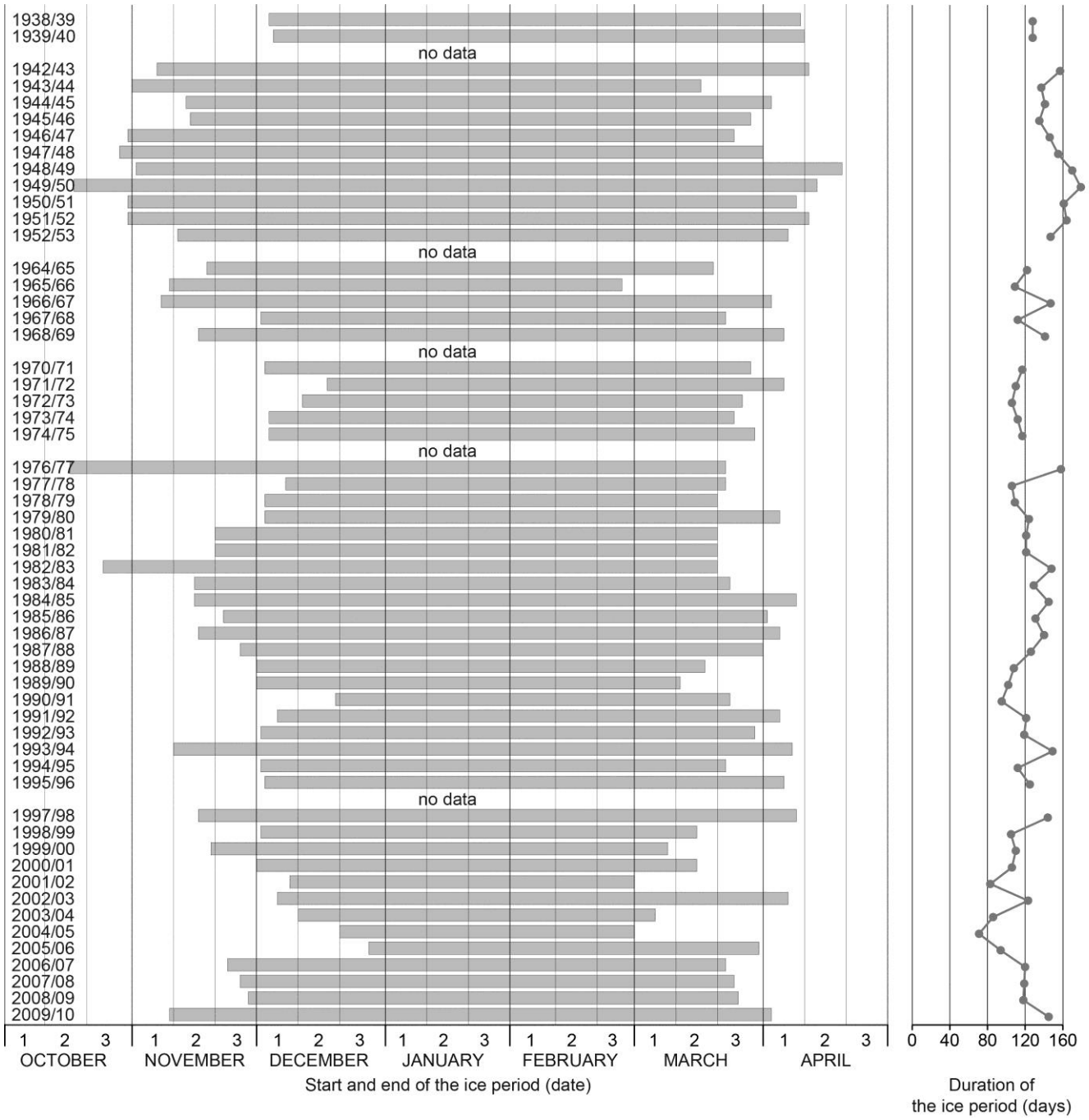

Figure 3.26. Long-term dynamics of the duration of ice conditions of the Island of Seal (Tyuleniy).

3.4. Plankton database of the southern seas

The plankton database contains the results of expeditions carried out by the Azov Branch of MMBI KSC RAS, SSC RAS, and IAZ SSC in 2003 – 2011 in the areas of the Sea of Azov, Black Sea, and the Caspian Sea.

When carrying out the activities, the focus was sampling plankton organisms including micro plankton and zooplankton following the protocols of research institutions of the former USSR (Guidelines, 1980).

Other parameters were sampled at the same time such as alien species, jelly plankton, micro-zooplankton, pico- and nanophytoplankton, and chlorophyll-A concentrations (Shiganova et al. 2001, Moses et al. 2012). Also, the role of micro-heterotrophic components in the cycle of carbon in the seas was examined (Azam et al. 1983).

Characteristics of the sampling and sample processing methods for different groups of plankton that were followed are described below.

Micro-phytoplankton

Traditional methods of studying phytoplankton were used in the Sea of Azov, Black Sea, and the Caspian Sea. Data was gathered on species composition, abundance, and biomass of microplankton organisms (Morozova-Vodianitskaya 1954). Sampling was by bathometer and fixed either by formalin or Lugol's solution. Samples were obtained from the surface (the Sea of Azov subarea), by standard horizons (0, 10, 25, 50, 100 m), or by the location of seasonal thermocline (the Black and Caspian Seas LMEs). In the latter case, three bathometric samples were collected above, inside, and below the thermocline using operational CTD-probing data (Guidelines, 1980).

Samples were concentrated by a settling method to a final volume of 50–100 ml. To quantify the phytoplankton, concentrated samples were examined with the help of the light microscope in the Nageotte chamber (0.1 ml) with magnification of 400x (Abakumov 1983). Large forms of microalgae are registered in the Nageotte chamber, in two-three repeated fillings. Other species are calculated in several lines of the chamber (up to 400 cells). The biomass calculation is by actual size of cells applying the geometric similarity method to calculate the volume of cell. These methods were used to obtain information on micro-phytoplankton during 2005 – 2011, and were included into the database.

Results from processing of 184 micro plankton samples from the Sea of Azov subarea have been added to the database. Results from 80 samples from the Black Sea LME were also added. Only fragmented data from the Volga Delta area were included (Figure 3.27 and Table 3.7).

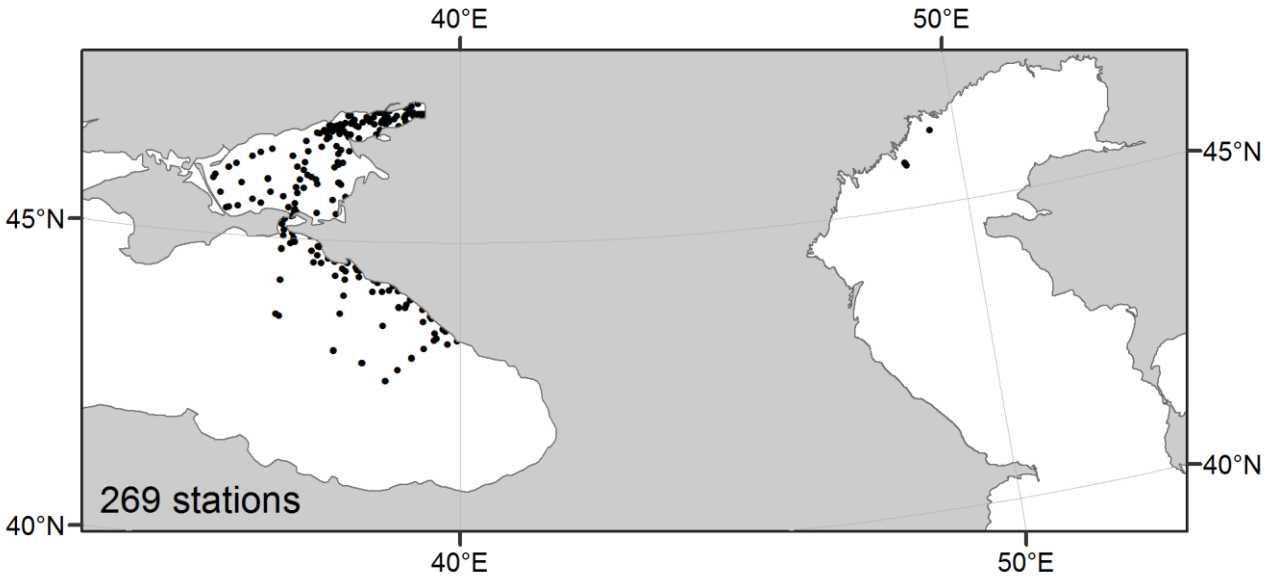

Figure 3.27. Distribution of stations with phytoplankton samples (2005-2011).

Table 3.7. Inventory of stations with phytoplankton samples (2005-2011).

Year	Months												
	1	**2**	**3**	**4**	**5**	**6**	**7**	**8**	**9**	**10**	**11**	**12**	**Total**
Sea of Azov													
2006	7	8		12	5	11	3	9					55
2007		6		11									17
2009	1			15				5		3		8	32
2010		14			6	9	25		13	3			70
2011						10							10
Total	**8**	**28**	**0**	**38**	**11**	**30**	**28**	**14**	**13**	**6**	**0**	**8**	**184**
Black Sea													
2007				1									1
2008				16		23				13			52
2009				13									13
2010							14						14
Total	**0**	**0**	**0**	**30**	**0**	**23**	**14**	**0**	**0**	**13**	**0**	**0**	**80**
Caspian Sea													
2005					2			3					5
Total	**0**	**0**	**0**	**0**	**2**	**0**	**0**	**3**	**0**	**0**	**0**	**0**	**5**
Total by seas	**8**	**28**	**0**	**68**	**13**	**53**	**42**	**17**	**13**	**19**	**0**	**8**	**269**

Pico- and nanoplankton

Despite the fact that the Sea of Azov subarea has a long-term record of hydrobiological research, the current state of phytoplankton community of the Sea of Azov subarea remains insufficiently studied. For many decades, phytoplankton studies were reduced to the research on

the quantitative and qualitative characteristics of algae over 20 µm. Microalgae under 20 µm – ultraphytoplankton, which can be further categorized into pico- (0.2–2 µm) and nanoplankton (from 2–10 to 20 µm), escaped the attention of researchers. Notably, these microorganisms may compose up to 59-69% of primary production and total phytoplankton biomass. (Azam et al. 1983).

Once collected from the surface profile, the samples of phytoplankton of pico- and nano-fractions are fixed by a glutaraldehyde solution. The samples are processed using epifluorescence microscope after filtration to black membrane filters and fluorochrome colouring. The indicated method also allows obtaining data on the total number of bacterioplankton cells (Sukhanova, 1983; Makarevich and Druzhkov, 1989).

Results from 178 pico- and nanoplankton samples (including bacteria) from the Sea of Azov have been added to the database. Results from 3 samples from the Black Sea were also added. There was no data available from the Caspian Sea for pico- and nanoplankton. (Figure 3.28 and Table 3.8).

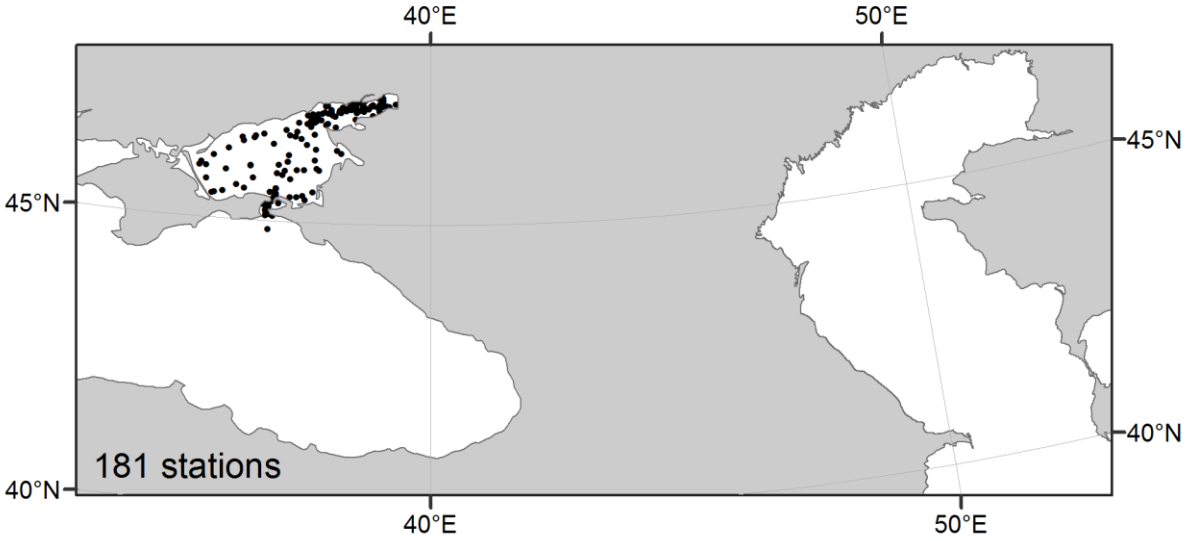

Figure 3.28. Distribution of stations with pico- and nanoplankton samples (2008-2011).

Table 3.8. Inventory of stations with pico- and nanoplankton samples (2008-2011).

Year	**Months**												
	1	**2**	**3**	**4**	**5**	**6**	**7**	**8**	**9**	**10**	**11**	**12**	**Total**
Sea of Azov													
2008		3		8		11	5						27
2009	10	6	8	14		7			11	7			63
2010		12			6	3	24		18	6			69
2011						19							19
Total	**10**	**21**	**8**	**22**	**6**	**40**	**29**	**0**	**29**	**13**	**0**	**0**	**178**
Black Sea													
2008				2		1							3
Total	**0**	**0**	**0**	**2**	**0**	**1**	**0**	**0**	**0**	**0**	**0**	**0**	**3**
Total by seas	**10**	**21**	**8**	**24**	**6**	**41**	**29**	**0**	**29**	**13**	**0**	**0**	**181**

Micro-zooplankton

Micro-zooplankton sampling methods are similar to standard micro-phytoplankton sampling methods. To fix samples, Lugol's acid solution was applied. Calculation of micro-zooplankton abundance and biomass is possible following cell settling. Determination of taxonomic (e.g. species) composition of unicellular organisms is also in the non-fixed samples.

Individual weights were obtained for some groups and species (Mordukhai-Boltovskoi 1954, Chorik 1968, Mamaeva 1979). Results presented in the database are of the Sea of Azov micro-zooplankton studies (Figure 3.29 and Table 3.9).

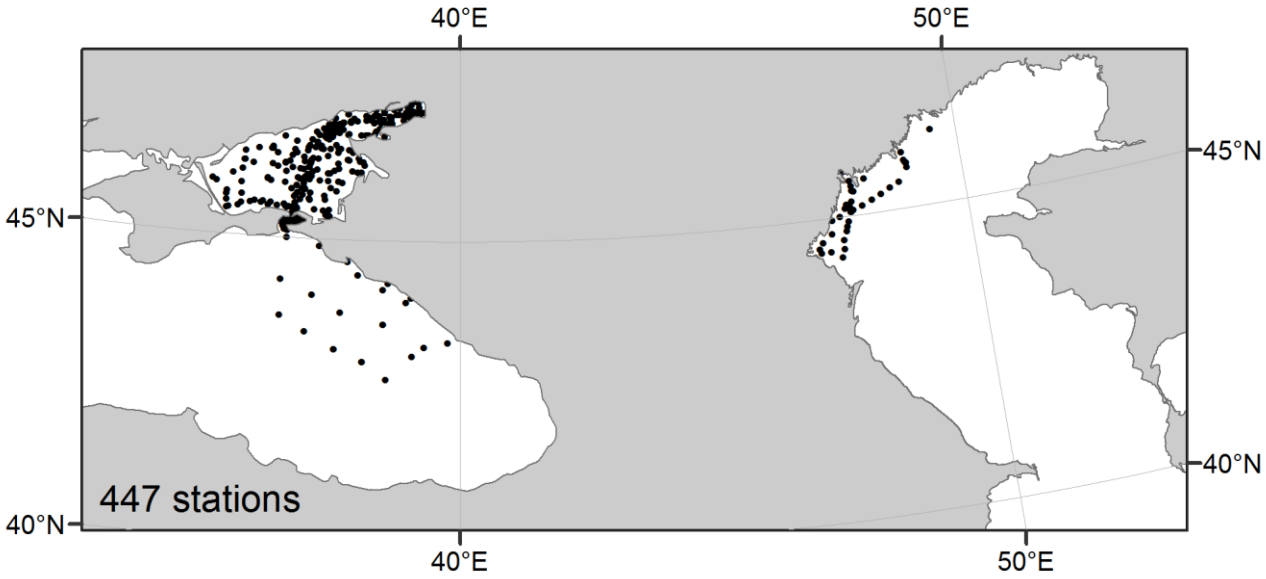

Figure 3.29. Distribution of stations with micro-zooplankton samples (2004-2011).

Table 3.9. Inventory of stations with micro-zooplankton samples (2004-2011).

Year	**Months**												
	1	**2**	**3**	**4**	**5**	**6**	**7**	**8**	**9**	**10**	**11**	**12**	**Total**
Sea of Azov													
2004			3		7	63	9						82
2005						16							16
2006	8	7		8	11	11	1					9	55
2007				6			10		1	10	22		49
2008		13		6		8	5	13		20			65
2009	10	6		6		17				4			43
2010		12					13						25
2011						21			13	4			38
Total	**18**	**38**	**3**	**26**	**18**	**136**	**38**	**13**	**14**	**38**	**22**	**9**	**373**
Black Sea													
2004						1							1
2007				4									4
2008										1			1

2009				5									5
2011						13							13
Total	**0**	**0**	**0**	**9**	**0**	**14**	**0**	**0**	**0**	**1**	**0**	**0**	**24**
Caspian Sea													
2004								33					33
2005					3			14					17
Total	**0**	**0**	**0**	**0**	**3**	**0**	**0**	**47**	**0**	**0**	**0**	**0**	**50**
Total by seas	**18**	**38**	**3**	**35**	**21**	**150**	**38**	**60**	**14**	**39**	**22**	**9**	**447**

Net zooplankton.

The sampling of net plankton was performed with a Juday net, which was first used in the Sea of Azov subarea in the late 1930s (Okul, 1940). This net has an opening diameter of 20 cm and a mesh size of 125 μm. While a relatively large mesh size prevents «blocking» of mesh by phytoplankton colonies in the summer period, this also leads to incomplete samples young copepods, copepods nauplius, and rotifers. These groups of zooplankton are counted in microplankton samples. When sampling zooplankton, the entire water column is towed vertically from the bottom to the surface (the Sea of Azov LME) and the layer of 0-50 m (the Black Sea). The determination of volume filtrated by the net is by the length and the slope angle of a loosened rope. To sample in the shallow water area of the Sea of Azov subarea, the Apstein net is used from time to time with which a definite volume of water is filtrated.

Determination of net plankton abundance is according to standard methods accepted and adopted in the USSR and Russia in the Bogorov's chamber (Guidelines, 1980). Determining the biomass of zooplankton was determined by linking the length and volume of specimens, which is an acceptable method for some species and groups such as Cladocera, rotifers, and meroplankton (Povazhniy, 2009).

The database contains the results of the Sea of Azov subarea net plankton studies. There are fragmented data for the summer period for the Black Sea LME (Figure 3.30 and Table 3.10).

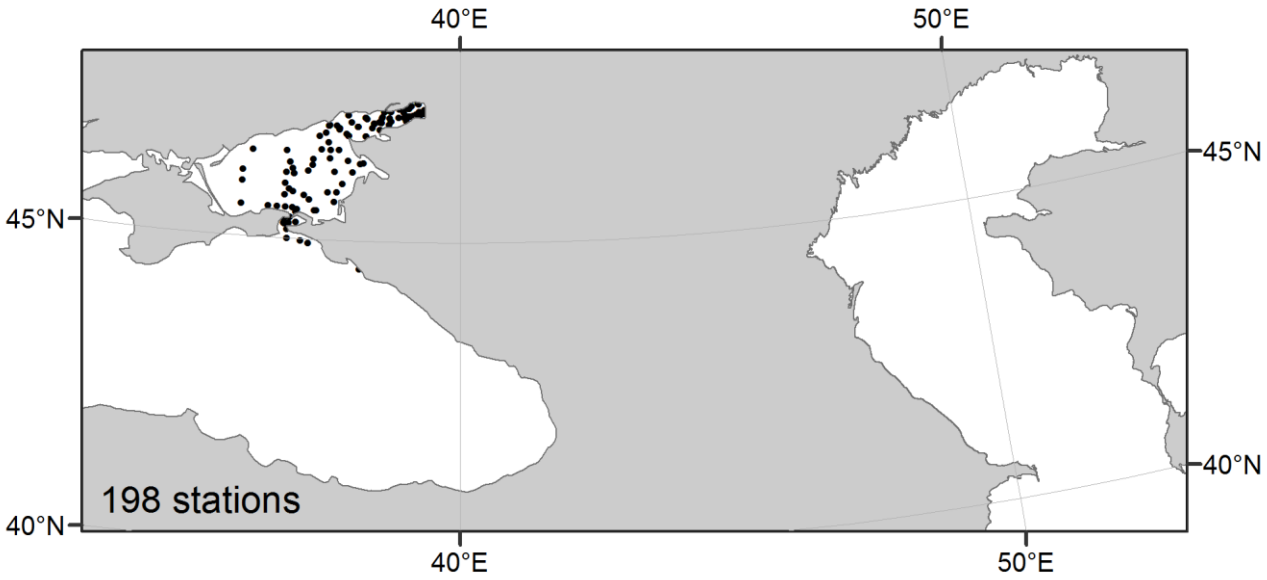

Figure 3.30. Distribution of stations with net zooplankton samples (2003-2008).

Table 3.10. Inventory of stations with net zooplankton samples (2003-2008).

Year	Jan	Feb	Mar	Apr	May	Jun	Jul	Aug	Sep	Oct	Nov	Dec	Total
Sea of Azov													
2003				2	3	2	1	8					16
2004	4		2		13	34	9		3	11			76
2005	7			14	7	23	1	1					53
2006	5			12	8			7	6			5	43
2008				1		4	1						6
Total	**16**	**0**	**2**	**29**	**31**	**63**	**12**	**16**	**9**	**11**	**0**	**5**	**194**
Black Sea													
2004						1							1
2005						3							3
Total	**0**	**0**	**0**	**0**	**0**	**4**	**0**	**0**	**0**	**0**	**0**	**0**	**4**
Total	**16**	**0**	**2**	**29**	**31**	**67**	**12**	**16**	**9**	**11**	**0**	**5**	**198**

Jelly Plankton

Mass numbers of alien comb-bearing jelly-fishes *Mnemiopsis leidyi* and *Beroe ovata* in the Sea of Azov, Black Sea, and the Caspian Sea is a focal point of current research. To monitor the jelly plankton, the IKS-80 net is used with the opening diameter of 80 cm and mesh size of 500 µm, similar by construction to the Bogorov-Rass (BR) net for horizontal catch. Sampling occurs in summer by vertical towing from the bottom to the surface (the Sea of Azov) and in the layer of 0 – 50 m (the Black and Caspian Seas LMEs). The net does not have a meter of filtrated water. The determination of volume filtrated by the net is by the length and slope angle of a loosened rope. Measuring of jelly plankton wet biomass by species with the use of a graduated cylinder (volume method) once organisms are separated from the water. Hydroid and scyphozoan jelly-fishes, as well as comb-bearing jelly-fishes, are considered in the samples.

The database contains data from 12 expeditions that sampled jelly plankton in the Taganrog Bay of the Sea of Azov subarea and in the Russian sector of the Caspian Sea LME for the summer period (Figure 3.31 and Table 3.11).

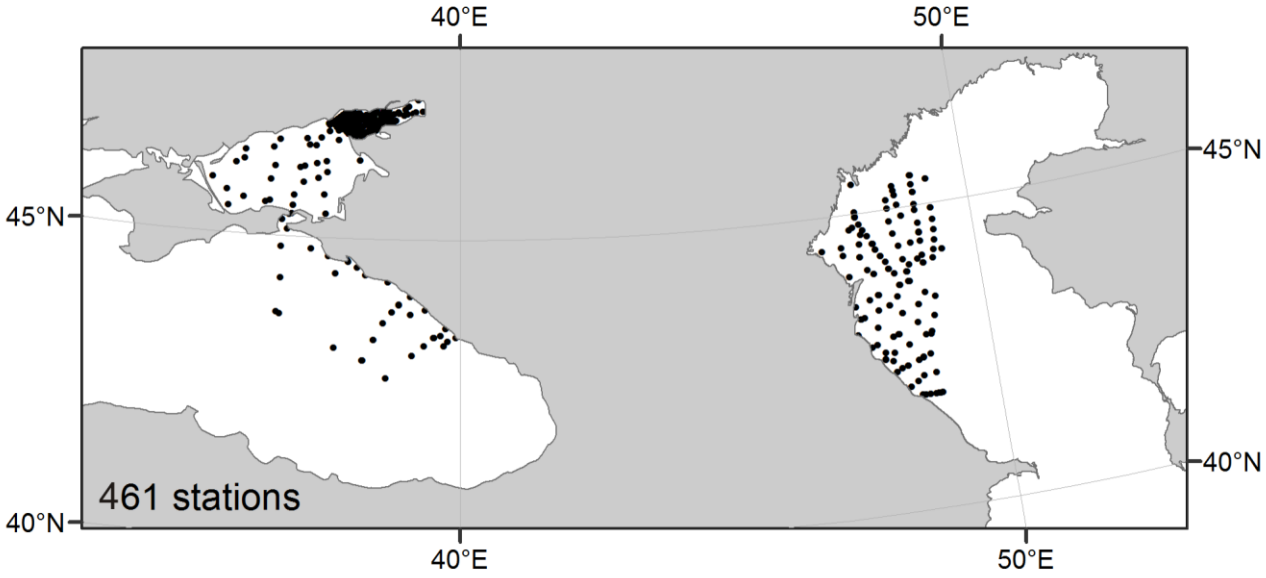

Figure 3.31. Distribution of stations with jelly plankton samples (2003-2011).

Table 3.11. Inventory of stations with jelly plankton samples (2003-2011).

Year	**Months**												
	1	**2**	**3**	**4**	**5**	**6**	**7**	**8**	**9**	**10**	**11**	**12**	**Total**
Sea of Azov													
2003								30					30
2004									7	9			16
2005									153				153
2007									2	32			34
2008									11	21			32
2009									19				19
Total	**0**	**0**	**0**	**0**	**0**	**0**	**0**	**30**	**192**	**62**	**0**	**0**	**284**
Black Sea													
2008										22			22
2009				12									12
Total	**0**	**0**	**0**	**12**	**0**	**0**	**0**	**0**	**0**	**22**	**0**	**0**	**34**
Caspian Sea													
2004								2					2
2008							45						45
2009								49					49
2011								47					47
Total	**0**	**0**	**0**	**0**	**0**	**0**	**45**	**98**	**0**	**0**	**0**	**0**	**143**
Total (all seas)	**0**	**0**	**0**	**12**	**0**	**0**	**45**	**128**	**192**	**84**	**0**	**0**	**461**

4. List of tables and figures

List of Tables

List of Figures

5. References

Abakumov, V. 1983. Rukovodstvo po metodam gidrobiologicheskogo analiza poverkhnostnykh vod i donnykh otlozheniy. L.: Gidrometeoizdat.

Azam, F., T. Fenchel, J. Field, J. Gray, L. Meyer-Reil, and F. Thingstad. 1983. The ecological role of water-column microbes in the sea. Marine ecology progress series. Oldendorf **10**:257-263.

Azumaya, T., and K. Ohtani. 1995. Effect of winter meteorological conditions on the formation of the cold bottom water in the eastern Bering Sea shelf. Journal of Oceanography **51**:665-680.

Boyer, T., J. Antonov, O. Baranova, H. Garcia, D. Johnson, R. Locarnini, A. Mishonov, D. Seidov, I. Smolyar, and M. Zweng. 2009. World Ocean Database 2009, vol. 1, Introduction, NOAA Atlas NESDIS, vol. 66. NOAA, Silver Spring, MD.

Chorik, F. 1968. Free-living ciliates in Moldavian water basins. Akademia Nauk MSSR, Kischinev:25.

Coachman, L. 1986. Circulation, water masses, and fluxes on the southeastern Bering Sea shelf. Continental Shelf Research **5**:23-108.

Coachman, L., and R. Charnell. 1979. On lateral water mass interaction-a case study, Bristol Bay, Alaska. Journal of Physical Oceanography **9**:278-297.

Coachman, L., T. Kinder, J. Schumacher, and R. Tripp. 1980. Frontal systems of the southeastern Bering Sea shelf. Pages 917-933 *in* Second International Symposium on Stratified Flows.

Ingleby, B., and M. Huddleston. 2007. Quality control of ocean temperature and salinity profiles—Historical and real-time data. Journal of Marine Systems **65**:158-175.

Ivanov-Frantskevich, G. 1953. Vertical stability of water layers as an important oceanographic characteristic. Trudy IO Akad. nauk SSSR **7**.

Karamushko, O. 2008. Species composition and structure of the ichthyofauna of the Barents Sea. Journal of Ichthyology **48**:277-291.

Kinder, T. H. 1981. Hydrographic structure over the continental shelf of the southeastern Bering Sea. The eastern Bering Sea shelf: oceanography and resources **1**:31-52.

Koto, H., and T. Maeda. 1965. On the movement of fish shoals and the change of bottom temperature on the trawl-fishing ground of the eastern Bering Sea. Bull. Jap. Soc. Sci. Fish **31**:769-780.

Levermann, A., J. L. Bamber, S. Drijfhout, A. Ganopolski, W. Haeberli, N. R. Harris, M. Huss, K. Krüger, T. M. Lenton, and R. W. Lindsay. 2012. Potential climatic transitions with profound impact on Europe. Climatic Change **110**:845-878.

Levitus, S., J. Antonov, and T. Boyer. 2005. Warming of the world ocean, 1955-2003. Geophysical Research Letters **32**:L02604

Levitus, S., J. I. Antonov, T. P. Boyer, R. A. Locarnini, H.E. Garcia, and A. V. Mishonov. 2009. Global ocean heat content 1955-2008 in light of recently revealed instrumentation problems. Geophysical Research Letters **36**:LO7608.

Liu, J., J. A. Curry, H. Wang, M. Song, and R. M. Horton. 2012. Impact of declining Arctic sea ice on winter snowfall. Proceedings of the National Academy of Sciences **109**:4074-4079.

Luchin, V., A. Kruts, O. Sokolov, V. Rostov, T. Perunova, E. Zolotukhin, V. Pischalnik, L. Romeiko, V. Hramushin, and V. Shustin. 2010. Climatic Atlas of the North Pacific Seas 2009: Bering Sea, Sea of Okhotsk, and Sea of Japan. NOAA Atlas NESDIS **67**:380 pp.

Luchin, V., I. Semiletov, and G. Weller. 2002. Changes in the Bering Sea region: Atmosphere—ice—water system in the second half of the twentieth century. Progress in Oceanography **55**:23-44.

Luchin, V. A., V. A. Menovshchikov, V. M. Lavrentiev, and R. K. Reed. 1999. Thermohaline structure and water masses in the Bering Sea. Dynamics of the Bering Sea:61-91.

Maeda, T., T. Fujii, and K. Masuda. 1967. On the oceanographic condition and distribution of fish shoals in 1963. Part 1. Studies on the trawl fishing grounds of the Eastern Bering Sea. Bull. Jpn. Soc. Sci. Fish **33**:713-720.

Maeda, T., T. Fujii, and K. Masuda. 1968. On the annual fluctuation of oceanographical conditions in summer season. Part 2. Studies on the trawl fishing grounds of the Eastern Bering Sea. Bull. Jap. Soc. Sci. Fish **34**:586-593.

Mamaeva, N. 1979. Protozoa (*Sarcodina, Ciliata, Suctoria*). The River Volga and its life. Junk, The Hague:232-234.

Matishov, G. 2010. Quality control of oceanographic data with the Sea of Azov database being exemplified. Pages 13-14 *in* International Marine Data and Information Systems Conference Ifremer, Plouzane, Paris, March 29-31.

Matishov, G., L. Dashkevich, and V. Kulygin. 2009. Atlases of oceanographic observations as the tool of climatic analysis. 6th European Congress on Regional Geoscientific Cartography and Information Systems. Pages 105-107 *in* EUREGEO. Landesamt fur Vermessung und Geoinformation, Munich, June 9-12.

Matishov, G., S. Dzhenyuk, V. Denisov, A. Zhichkin, and D. Moiseev. 2012. Climate and oceanographic processes in the Barents Sea. Ber Polarforsch **640**:63-73.

Matishov, G., A. S. Gasanova, and G. Kovaleva. 2011. Effects of changes in the hydrological and hydrochemical regime of the Caspian Sea on the development of microalgae in the coastal zone. Pages 437-441 *in* Doklady Earth Sciences. Springer.

Matishov, G., P. Makarevich, S. Timofeev, L. Kuznetsov, N. Druzhkov, V. Lariono, V. Golubev, A. Zuyev, N. Adrov, V. Denisov, G. Iliyn, A. Kuznetsov, S. Denisenko, V. Savinov, A. Shavikyn, I. Smolyar, S. Levitus, T. O'Brien, and O. Baranova. 2000. Biological Atlas of the Arctic Seas 2000: Plankton of the Barents and Kara Seas. International Ocean Atlas Series. Murmansk Marine Biological Institute and World Data Center for Oceanography. US Government Printing Office, Washington, DC.

Matishov, G., D. Matishov, G. Gargopa, D. L, B. S, B. O, and I. Smolyar. 2006. Climatic Atlas of the Sea of Azov 2006. U.S. Government Printing Office, Washington D.C.

Matishov, G., D. Matishov, Y. Gargopa, L. Dashkevich, S. Berdnikov, V. Kulygin, O. Archipova, A. Chikin, I. Shabas, O. Baranova, and I. Smoylar. 2008. Climatic Atlas of the Sea of Azov U.S. Government Printing Office, Washington, D.C.

Matishov, G., and L. Pavlova. 1990. General Ecology and Paleogeography of Polar Oceans. Leningard: Naua.

Matishov, G., O. Stepan'yan, V. Povazhnyi, G. Kovaleva, and K. Kreneva. 2007. Functioning of the ecosystem in the Sea of Azov during winter. Pages 297-299 *in* Doklady Earth Sciences. Springer.

Matishov, G., A. Zuyev, V. Golubev, N. Adrov, V. Slobodin, S. Levitus, and I. Smolyar. 1998. Climatic Atlas of the Barents Sea 1998: Temperature, salinity, oxygen. U.S. Government Printing Office, Washington D.C.

Matishov, G., A. Zuyev, V. Golubev, N. Adrov, S. Timofeev, O. Karamusko, L. Pavlova, A. Braunstein, O. Fadyakin, A. Buzan, D. Moiseev, I. Smolyar, R. Locarnini, R. Tatusko, T. Boyer, and S. Levitus. 2004. Climatic Atlas of the Arctic Seas 2004: Part I. Database of the Barents, Kara, Laptev, and White Seas - Oceanography and Marine Biology. U.S. Government Printing Office, Washington, D.C.

Moiseev, D. V. G., V. V. Kulygin, and S. V. Berdnikov. 2012. Joint MMBI, SSC RAS and NODC NOAA approach to oceanographic and hydro-biological database organisation for

the Arctic and Southern Seas of Russia. Pages 137-151 *in* G. Hempel, K. Lochte, and G. Matishov, editors. Arctic Marine Biology: A workshop celebrating two decades of cooperation between Murmansk Marine Biological Institute and Alfred Wegener Institute for Polar and Marine Research, Berichte zur Polar- und Meeresforschung. Reports on polar and marine research, Bremerhaven, Alfred Wegener Institute for Polar and Marine Research.

Moore, G., and I. Renfrew. 2012. Cold European winters: Interplay between the NAO and the East Atlantic mode. Atmospheric Science Letters **13**:1-8.

Mordukhai-Boltovskoi, F. 1954. Materialy po srednemu vesu vodnykh bespozvonochnykh basseina Dona. Tr. Probl. Soveshch. ZIN **2**.

Moroshkin, K. 1966. Water masses of the Sea of Okhotsk. . US Department of Commerce; Clearinghouse for Federal Scientific and Technical Information, Joint Publication Research service. Translation of Vodnyye massy Okhostkogo Morya, Moscow.

Morozova-Vodianitskaya, N. 1954. Phytoplankton of the Black Sea. Tr. Sevastop. Biol. Stantsii **8**:11-99.

Moses, W. J., A. A. Gitelson, S. Berdnikov, V. Saprygin, and V. Povazhnyi. 2012. Operational MERIS-based NIR-red algorithms for estimating chlorophyll-a concentrations in coastal waters. The Azov Sea case study. Remote Sensing of Environment **121**:118-124.

Overland, J. E., and M. Wang. 2010. Large-scale atmospheric circulation changes are associated with the recent loss of Arctic sea ice. Tellus A **62**:1-9.

Plotnikov, V. 2002. Variability of ice conditions of Far Eastern Seas and their forecast. Dal'nauka, Vladivostok.

Privalsky, V. 1985. Climatic variability (stochastic models, predictability, and spectra). Moscow: Nanka (in Russian).

Shiganova, T., Z. Mirzoyan, E. Studenikina, S. Volovik, I. Siokou-Frangou, S. Zervoudaki, E. Christou, A. Skirta, and H. Dumont. 2001. Population development of the invader ctenophore *Mnemiopsis leidyi* in the Black Sea and in other seas of the Mediterranean basin. Marine Biology **139**:431-445.

Sukhanova, I. 1983. Concentrating phytoplankton in a sample. Sovremennye metody kolichestvennoi otsenki raspredeleniya morskogo planktona:97-108.

Takenouti, A. Y., and K. Ohtani. 1974. Currents and water masses in the Bering Sea: A review of Japanese work. Oceanography of the Bering Sea:39-57.

Tourpali, K., and P. Zanis. 2013. Anticyclonic blocking effects over Europe from an ensemble of regional climate models in recent past winters. Pages 773-778 Advances in Meteorology, Climatology and Atmospheric Physics. Springer.

Tuzhilkin, V. S. 2008. Thermohaline structure of the sea. Pages 217-253 The Black Sea Environment. Springer.

Voeikov, A. 1884. Klimaty zemnogo shara, v osobennosti Rossii.(Climates of the Earth, particularly of Russia). St. Petersburg.

Zadeh, L. A. 1975. Fuzzy logic and approximate reasoning. Synthese **30**:407-428.

Zhichkin, A. 2009. Atlas of the Russian cod fishery in the Barents Sea (1977–2006). Raditsa, Murmansk (in Russian).